Attenuation of Tides and Storm Surges in Coastal Mangroves

A thesis submitted in fulfilment

of the requirements for the degree of

Doctor of Philosophy in Earth Sciences

at

The University of Waikato

by

John M. Montgomery

2021

Abstract

Mangrove forests have been shown to provide coastal protection by reducing waves, moderating currents, stabilizing sediments, and lessening storm winds. However, the interaction between storm surge and mangroves is less understood with some studies showing substantive water level reductions across mangrove forests and other work demonstrating negligible flood reduction. Here, the relationship between mangrove forests and storm surge is investigated using a variety of techniques including a simplified analytic solution, water level observations in two contrasting mangrove forests (with and without channels), and a numerical model used to explore the importance of variations in vegetation density and complex bathymetry.

The analytic solution to flow through vegetation was based on the shallow water approximation to the equations of motion and predicts water level across a simplified mangrove forest during a flood event. The solution accurately reproduced observed peak water levels of a 10-year flood event in the Firth of Thames, New Zealand and in a forest during Hurricane Charley in Ten Thousand Island, Florida. The analytic solution demonstrated that in a simplified scenario vegetation density, forest size, flood amplitude, and flood duration determine peak water level reduction. Mangroves reduce flood levels by limiting the landward flow of water and acting as a water storage mechanism.

The variability in flood protection provided by coastal mangroves is demonstrated through the comparison of inundation events in two contrasting forests in New Zealand, channelized mangroves in Tauranga and a more homogenous forest in the Firth of Thames. New observations from Tauranga were collected to complement existing observations from the Firth of Thames. Both forests are ~1 km wide and populated by mono-specific cultures of grey mangroves and subjected to inundation events that reached a depth of ~0.6 m at the seaward edge of the forest. However, no reduction of water level occurred across the mangroves in Tauranga and the forest in the Firth of Thames provided quantifiable flood protection.

The influence of channels, variations in vegetation density, and forest slope on the flood protective services provided by mangroves was explored with a series of numerical "experiments" based on a depth integrated 2-D numerical model of a mangrove forest in Tauranga, New Zealand. Modelling results demonstrated that channelization and large-scale distribution of vegetation are more important to determining flood attenuation than detailed characterization of the vegetation.

Population densities in coastal areas are rapidly expanding; simultaneously, intertidal ecosystems that provide coastal protection are degrading resulting in an increased reliance on traditionally engineered solutions. Sea-level-rise and a projected increase in storm frequency and severity requires modifications to existing coastal defense strategies. Natural ecosystems, such as mangroves, may both protect coastlines and help shorelines adapt to climate change. Integrating natural ecosystems into coastal defense schemes requires a thorough understanding of the interaction between the coastal hazard and ecosystem. Here we show that the flood defense provided by mangroves is non-linear and strongly site specific

and that mangroves provide effective flood protection if vegetation properties, local bathymetry, and storm characteristics allow for vegetation to reduce the landward flow of water.

Acknowledgements

I would like to thank my supervisors for their input over the last years: Julia Mullarney, Giovanni Coco, Scott Stephens, and Heide Friedrich. Karin Bryan, my primary supervisor, has been particularly helpful and I am appreciative of her guidance and patience throughout this process.

Fieldwork assistance from Dave Culliford, Mike Tyler, and Ron Ovenden was much appreciated. Dean Sandwell was helpful throughout the fieldwork process and is deserving of thanks for his efforts.

I enjoyed my interactions with Erik Horstman during our time at University of Waikato and am thankful for his assistance providing data from the Firth of Thames experiment and his comments on our collaborations. I sincerely hope we will have the opportunity to work together in the future.

I am grateful for The Natural Hazards Platform for funding this work and providing the scholarship that allowed me to pursue my studies.

A special thanks to the staff at NIWA Christchurch for allowing me to pursue my studies from the "library". I am grateful for the community at NIWA and would not be submitting this work without their support.

Finally, I would like to thank my wife Kelsey for supporting me throughout this process. Your encouragement has been essential, I am lucky to have you in my life.

Table of Contents

List of Figures

List of Tables

1 Introduction

Coastal flooding is a major global hazard damaging to property, destroying infrastructure, and causing loss of life. Globally, storm surges are among the most costly and deadly global catastrophes killing an average of 13,000 people and causing billions of dollars in damage annually (*Needham et al.*, 2015). Devastation due to storm surges is expected to increase because of climate change driven sea level rise, an expected increase in the number of annual storms, greater storm intensity and continued development along coastlines (*Woodruff et al.*, 2013). Enhancing and retaining coastal vegetation as a shore protection solution has been proposed by Arkema et al. (2013) and Temmerman et al. (2013), in what has become commonly known as '*eco-defense'.* Vegetation can range over broad scales, from low-lying marsh grasses to tall mangrove trees. Because of their size and complex root structures, the latter is a particular focus of eco-defense strategies, and so was chosen as a focus of this research.

Mangroves are a salt-tolerant plant that dominate in many tropical and sub-tropical intertidal environments and provide ecosystem services including habitat and breeding grounds for a range of animal species, carbon sequestration (*McLeod et al.*, 2011), forestry, and nutrient uptake and transformation (*FAO*, 2007). Additionally, coastal mangroves provide shore protection by reducing wind waves, moderating currents, lessening potentially damaging winds, and limiting erosion (*Das and Crépin*, 2013; *Guannel et al.*, 2015; *Temmerman et al.*, 2013). However, the protection mangroves provide with respect to coastal flooding is less understood than other mangrove ecosystem services. Existing research can be separated into three categories: observations of water level, numerical simulations that simulate storm surge in the presence or absence of mangroves, and analysis of damage in environments with and without forests (*McIvor et al.*, 2016).

Detailed water level observations of flood protection provided by mangroves has been limited to hurricanes impacting the Gulf Coast of the United States of America (*Krauss et al.*, 2009). Krauss et al. (2009) described flood attenuation rates in Ten Thousand Islands, Florida during Hurricane Charley (2004) and near the Shark River, Florida during Hurricane Wilma (2005). Observed flood attenuation rates ranged from 4.2 to 15.8 centimetres per kilometre of forest. The wide variability of attenuation rates was attributed to variations in storm characteristics and the more open waters of the Shark river. Collecting high spatial and temporal resolution during large flood events in mangroves is inherently difficult; therefore, detailed observations of extreme flood events are limited. Additionally, the limited observations are from varying locations and storm events, extrapolating the protective benefit of mangroves to independent locations and events is inappropriate.

Numerical models an indispensable tool for evaluating the flood protection services provided by mangroves. Xu et al. (2010) and Zhang et al. (2012) investigated hurricanes impacting mangroves in Florida using a depth integrated numerical model with flow resistance parametrized by a Manning's coefficient representation of bottom friction. Xu (2010) selected a Manning's coefficient of 0.15 through a calibration process comparing model results to observations. Due to numerous bodies of water and discontinuous mangrove forests in the region of interest, Zhang et al. (2012) used a slightly reduced

Manning's coefficient of 0.14 to capture the flow resistance of mangroves. Zhang et al. (2012) found that surge reduction across mangroves varied from 23 to 48 centimetres per kilometre of forest with maximum attenuation occurring across the vegetation fringe and reduced flood attenuation rates in the landward portion of the forest. Additionally, Zhang et al. (2012) note that mangroves provide less flood protection from slow moving storms than faster events that are shorter in duration. However, the numerical modelling provides no understanding of the principle mechanisms that control storm surge attenuation in mangroves. Increasing Manning's coefficient is an efficient method to represent increased flow resistance, this bottom friction parametrization does not require vegetation measurements nor does this approach accurately capture flow resistance variations with depth. Therefore, extrapolating results to uncalibrated events or locations may be inappropriate.

The value of mangroves to coastal protection has been explored by statistical analysis based on the relationship of deaths in hundreds of villages in Orissa, India during a super cyclone in 1999 (*Das and Vincent*, 2009). Villages with wider mangroves along the coast experienced less deaths than villages with narrower forests. However, it is difficult to separate multiple correlated variables such as inundation water level, topographic gradient, proximity to coast, forest characteristics, etc. Also, the statistical analysis does not improve fundamental understanding of the interaction between storm surge and mangroves.

Current literature identifies a large range of flood attenuation rates but fails to adequately address the importance of key problem variables (forest size, vegetation density, flood amplitude and duration, sloping bathymetry, forest channelization, etc.) to account for that variability. Additional research is needed to understand the importance of both forest and storm characteristics on flood attenuation rates in mangrove forests to allow for informed decisions on mangrove management.

Much work has been done on the dynamics of tidal flows through mangrove swamps (*Horstman et al.*, 2015; *Mazda et al.*, 1995; *Mullarney et al.*, 2017; *van Maanen et al.*, 2015); however, existing research has had an emphasis on morphodynamics not flood dynamics. At low water levels, tidal flow through mangroves dissected by channels is dominated by creek flow (*Horstman et al.*, 2021). Flow across the vegetated regions is described as sheet flow and becomes increasingly important at higher water levels. Slow sheet flows promote sedimentation in highly vegetated areas and ebb-dominant higher velocity channel flows act to scour creeks and maintain channel integrity (*Horstman et al.*, 2015). Haughey (2017) found that the forest fringe tends towards ebb dominance, but within the vegetation tidal distortion becomes increasingly flood dominant. The impact of flow complexity on flood attenuation has not previously been explored.

1.1 Mangrove Flood Protection: A New Zealand Perspective

Detailed research on mangroves and storm surge interaction has primarily focused on hurricanes impacting the southern United States with reduction described as a linear decay rate of peak water level per kilometre of forest. The applicability of flood protection studies from the southern US in which wide forests of low topographic gradient are impacted by large

hurricane driven storm surge to other locations worldwide with varying forest structure, bathymetry, and storm types is unknown.

New Zealand storm surge heights tend to be an order of magnitude smaller (<1m) than in many other regions (*de Lange and Gibb*, 2000), with the inverse barometer effect and wind stress approximately equal contributors (*Bell et al.*, 2000). Local tidal variations in New Zealand are up to 2-2.4 m above MSL; total water level is generally dominated by tide. Therefore, inundation duration is often determined by M2 tidal period, not storm duration. Internationally, storm surge inundation duration can be on the order of days with tide signals being dominated by large flood events.

Mangrove forests in New Zealand differ from forests in the Southern United States due to plant diversity and tree configuration. New Zealand has a single mangrove species, *Avicennia marina* var. *australasica*, that is existing at the southern limit of the species' natural range. In New Zealand, the single mangrove species exhibits a variety of forms ranging from short shrub like dwarf mangroves to forests of trees several meters in height. In the Gulf Coast of the United States, mangrove forests consist of a complex array of species (black mangroves, red mangroves, white mangroves) that reach up to 9 m in height (*Pool et al.*, 1977). Mangrove species complexity and density may influence coastal flood protection provided by the vegetation.

Storm surge in New Zealand is an order of magnitude less than other regions worldwide. However, it is estimated that currently 1.5% of the population is exposed to a 1 in 100-year coastal flood event (*Paulik et al.*, 2020). The threat of water inundation is of particular importance along estuaries with low elevation, high-value manmade structures, and complex coastal processes. The combination of sea level rise and increased storm severity in the next century is expected to result in an increased threat of coastal inundation (*Bell et al.*, 2006). Mangroves offer an alternative to traditional engineered coastal flood protection; however, additional knowledge is required to quantify the protection of the coastal vegetation.

New Zealand mangroves are rapidly expanding, in contrast to much of the rest of the world in which mangroves are in steep decline and are shrinking faster than coral reefs and tropical forests (*Duke et al.*, 2007). It is estimated that ~35% of global mangrove forests were lost between 1980 and 2000 (*FAO*, 2007). Mangrove expansion in New Zealand has been linked with land use changes and the accumulation of fine sediments and the altering of estuarine ecosystems (*Horstman et al.*, 2018b). Consequently, mangrove expansion in New Zealand has resulted in negative public perception and led to intentional forest destruction.

The ability to accurately predict coastal dynamics and inundation patterns are essential to enact effective coastal policies and protect human developments. With comparatively small storm surge levels and short duration coastal floods relative to many international locations a fundamental understanding of the interaction between mangrove forests and storm surge is required to assess the importance of coastal mangroves to surge attenuation in New Zealand.

1.2 Method & Structure

This thesis explores the interaction of storm surge and mangrove forests and answers the following questions:

1. What characteristics of storm surges and mangrove forests determine flood attenuation?
2. What is the role of channels in flood attenuation?
3. How do complexities in vegetation and bathymetry influence flood attenuation?

These general research questions are addressed using separate techniques: a highly simplified analytic solution, observations of two contrasting environments, and numerical modelling of an idealized forest. The three research questions are presented in separate scientific articles, presented here as chapters 2, 3, and 4, respectively. These articles are all written to stand alone but address the same topic of flood attenuation through coastal mangroves and combine to form a cohesive message on the interaction of storm surge and mangroves. A summary and discussion of the conclusions is presented at the end of this thesis.

Inundation and vegetation parameters that determine flood reduction across a mangrove forest are explored through an analytic solution to friction dominated periodic flow through uniform emergent vegetation (Chapter 2). Mangroves are approximated as rigid vertical cylinders with flow resistance parameterized by frontal area. The solution assumes a no flow boundary condition at the landward edge of the forest and a simple relationship determining water level as a function of distance into the forest is obtained. The analytic model is compared to water level observations during a 10-year return period flood event in a mangrove forest in the Firth of Thames, New Zealand that has a stop bank at the landward edge of the vegetation. The solution is also compared with water level observations from Hurricane Charley impacting Ten Thousand Islands, Florida. The validated one-dimensional analytic solution is used to explain key parameters (of both the flood event and mangrove forest) that determine long wave attenuation in simple forests and two mechanisms by which vegetation provides flood protection are suggested.

The role of channels in flood attenuation through mangroves is demonstrated with observations in two contrasting mangrove forests in New Zealand: a forest bordering the southern Firth of Thames and a forest in Pahoia Domain, Tauranga (Chapter 3). Both sites are comprised of mono-specific cultures of grey mangroves with cross-shore forest widths of ~1 km and relatively flat topography within the vegetation. Also, peak flood levels at the seaward fringe of both forests reached a maximum of ~0.6 m during observed events. However, flood levels were dissipated at an average of ~0.24 cm per km distance into the forest in the Firth of Thames and no measurable flood attenuation occurred across the forest in Pahoia Domain. The variation in flood attenuation is attributed to the presence of an extensive channel network in Pahoia and the absence of channels through the Firth of Thames forest.

The influence of complexities in plant density, vegetation distribution, and bathymetry on coastal flood protection provided by mangrove forests is explored using a depth integrated Delft3D numerical model based on a forest in Pahoia, New Zealand (Chapter 4). A baseline

numerical model is created with bathymetry generated with a combination of LiDAR data for intertidal areas and limited RTK GPS data for subtidal areas. Vegetation flow resistance is parametrized by frontal area, but the shrub-like dwarf mangroves in Pahoia are poorly approximated by rigid vertical cylinders and required additional complexity to represent flow resistance. Vegetation properties are estimated using a Strahler ordering scheme based on the mechanical design of trees. The baseline model is validated using water level and velocity data collected during a 2017 field study. For simplicity, the initial model is simplified by removing vertical variations in vegetation density, simplifying forest bathymetry, and using sinusoidal water level forcing the model boundary. The importance of vegetation density and forest channelization are assessed by perturbing the baseline model by increasing vegetation density and separately removing channels from the environment. To isolate the importance of inundation amplitude on flood attenuation, the simplified unchannelized model is subjected to forcing at the open boundary varying from 1.0 m to 1.8 m amplitude. Similarly, the importance of forest slope on flood attenuation in mangroves is demonstrated by altering the bathymetry of the unchannelized forest and comparing rates of flood reduction.

2 Attenuation of Storm Surges by Coastal Mangroves

2.1 Contribution of Authors

Chapter 2 presents "Attenuation of Storm Surges by Coastal Mangroves", published in *Geophysical Research Letters* in February 2019 (*Montgomery et al.*, 2019). This article presents a simple analytic solution to demonstrate that mangroves reduce flood amplitude by both limiting the exchange of water and providing a water storage mechanism. Mangrove forest characteristics (width and vegetation density) and flood characteristics (inundation duration and amplitude) determine water exchange and storage and therefore flood attenuation rate.

The Firth of Thames dataset analysed in this article was collected by my co-authors prior to the start of my studies. Data from Ten Thousand Islands, Florida was obtained from publicly available information (*Krauss et al.*, 2009). I derived the solution, performed the data processing, prepared figures, and wrote the initial draft of the article. My co-authors collected data, edited drafts, provided advice on direction of work and content, and assisted with response to reviewer's comments.

2.2 Abstract

The interaction between mangroves and storm surges is explored using an analytical solution. A simplified momentum equation, balancing vegetation drag and pressure gradient, is combined with the continuity equation resulting in a diffusion equation. Assuming a simplified environment, a 1-dimensional analytical solution is obtained to predict peak surge level across a forest. The solution accurately reproduces peak water level of a 10-year return period flood event in mangroves in the Firth of Thames, New Zealand, and in Ten Thousand Islands, Florida, during Hurricane Charley. Vegetation properties that determine the capacity of mangroves to reduce surges are forest density and cross-shore extent. Storm characteristics–flood duration and peak water level at the forest fringe–also influence surge attenuation. Mangroves are shown to be an effective form of coastal flood protection if forests are sufficiently wide/dense, relative to the surge decay length scale, to restrict water exchange during a storm.

2.3 Plain Language Summary

Storm-driven flooding is a major hazard in low-lying coastal areas. Mangroves have previously been shown to provide effective coastal protection from storm waves. However, there is sparse evidence that mangroves reduce storm surge, which is the temporary increase in water level resulting from the combination of high winds and low atmospheric pressure during a weather event. Here, we demonstrate that mangroves can reduce water flow and store water, thus helping to reduce peak surge water levels. We show that if forests are sufficiently wide, water levels within (and landward of) the mangroves are substantially lower than for a scenario in which mangroves are absent. The density of the vegetation, cross-shore extent of the forest, and characteristics of the surge (duration and amplitude) all influence water level reduction in the forest.

2.4 Introduction

Tropical cyclones can be destructive and deadly events in which coastal flooding is one of the primary causes of damage and casualties. Climate-change-driven sea level rise, increased storm frequency, and greater storm intensity are expected to enhance devastation due to storm surges (*Woodruff et al.*, 2013). Coastal mangroves have been shown to lessen the impact of coastal storms by reducing wind-generated waves, dissipating currents, stabilizing sediments, and decreasing storm surge levels (*Guannel et al.*, 2015; *Temmerman et al.*, 2013). Existing documentation of the protective services mangroves provide with respect to storm surge attenuation can be separated into three categories (*McIvor et al.*, 2016): observations of water level (*Krauss et al.*, 2009), numerical simulations (*Zhang et al.*, 2012), and analysis of damage caused by storm surges at coasts with and without mangroves (*Das and Vincent*, 2009). Numerical models are not always well validated (*Zhang et al.*, 2012), and are sensitive to the way in which vegetation is represented (*Horstman et al.*, 2013). Conversely, field observations of flood attenuation through mangroves are limited in location and events (primarily describing hurricane impacts on the gulf coast of the United States). Without a clear theoretical framework, applying observed flood attenuation rates to other sites is problematic. Given the loss of lives and infrastructure associated with coastal flooding (*Costanza et al.*, 2008) and the potential for vegetation to reduce flooding, better understanding of the interaction between storm surge and mangroves is critically needed.

Environmental characteristics, such as vegetation density, root and stem diameter, bathymetry, and inundation characteristics influence the capacity of mangroves to reduce flood water levels (*Alongi*, 2008), but interaction between parameters has not been well quantified. Previous numerical experiments have shown that the influence of mangrove forest width (cross-shore extent) on storm surge attenuation is non-linear (significant attenuation of water levels occurred across the forest fringe but little attenuation occurred at further distances into the forest), and surges from slow moving long-duration storms were less effectively attenuated than those from faster-moving shorter duration events (*Zhang et al.*, 2012). However, the physical mechanisms to explain the above results were not provided.

Storm surge propagation in mangrove forests is friction-dominated and is reasonably well described as a "zero-inertia" diffusive wave (*Carl T. Friedrichs and Madsen*, 1992; *LeBlond*, 1978). We develop a simplified analytic approximation to the non-linear diffusion equation to describe the interaction between storm surge and emergent vegetation. Here, the analytic solution is applied to two extreme surge events in contrasting mangrove forests, a 10-year return period flood event in the Firth of Thames, New Zealand, and Hurricane Harvey in Ten Thousand Islands, Florida. Such analytical solutions provide efficient and accurate predictions of surge levels across a forest.

2.5 Study Sites

2.5.1 Firth of Thames, New Zealand

The Firth of Thames (FoT) is a shallow ~800 km^2 basin in the North Island of New Zealand with a monoculture of grey mangroves (*Avicennia marina* var. *australasica*) occupying much of the southern shore. Mangrove colonization began in the mid-1950s, with trees currently varying in height from 0.5 m to 3.5 m. The site is relatively uniform in the

longshore direction, allowing for the hydrodynamics to be reasonably simplified to a 1-dimensional problem. The mangrove forest extends ~1 km seaward of a stop bank, designed to prevent flooding of the low-elevation farmland behind the mangroves (*Lovelock et al.*, 2010). The mesotidal estuary is a moderately wave exposed area (typically <1 m) with a spring tidal range of 2.8 m and neap range of ~2 m. The upper vegetated flat (Figure 2-1c) is 0.1-0.2 m above mean high water spring tide resulting in infrequent inundation of the forest (*Swales et al.*, 2015). Storm surges in the region rarely exceed 0.5 m (*Bell et al.*, 2000). The forest has no significant channels and therefore we can assume that fluid transport is dominated by flow through the vegetation. Additionally, the low slope of the vegetated portion of the upper intertidal supports a zero-slope simplification (Figure 2-1c).

2.5.2 1.2.2. Ten Thousand Islands, Florida

Located on the Gulf of Mexico coast in Florida, Ten Thousand Islands (TTI) is part of a large mangrove estuary with multiple mangrove species (red, white, and black mangroves) up to 9 m in height (*Pool et al.*, 1977). (No pneumatophore information is provided.) The study site is located landward of the outer islands and is comprised of ~3 km of mangrove forests before transitioning to salt marsh (*Krauss et al.*, 2009). Tides influence the outer portion of the forest, but do not penetrate the salt marsh.

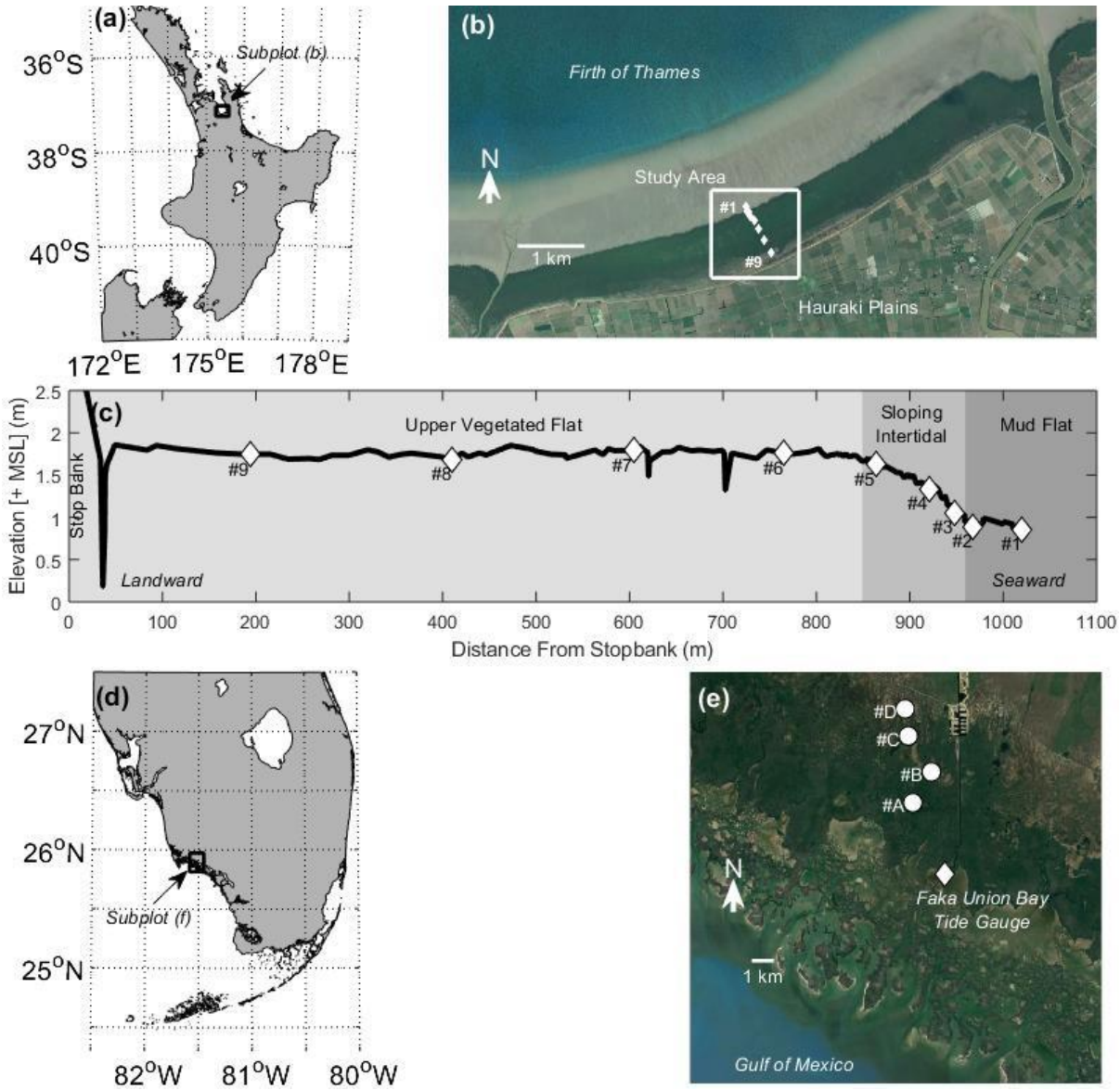

Figure 2-1: (a) North Island of New Zealand with the southern Firth of Thames (FoT) outlined in black. (b) FoT field study area (white) with instrument locations identified. (c) Location of instruments relative to stop bank in the FoT. (d) Florida with Ten Thousand Islands (TTI) study area (black). (e) Aerial image of TTI study site with instrument locations identified (Photo sources: Google Earth).

2.6 Field Observations

2.6.1 Firth of Thames, November 2016 Event

Observations of extreme water levels across the mangroves in the FoT were collected in November 2016. A series of nine pressure sensors were deployed along a cross-shore transect extending from the stop bank to the vegetated intertidal (Figure 2-1b/c). Station 1 is located just seaward of the vegetation. Stations 2-5 are in the first ~100 m of the mangrove forest and provide a high degree of spatial resolution across the gently sloping (1:125) mangrove fringe. The remaining stations are roughly equally spaced across the vegetated tidal flat between the fringe and the stop bank. A small channel exists just seaward of the stop bank and may influence the inundation pattern towards the back of the mangrove forest. A long-term water level gauge was located to the northeast of the study area. Additional

details on the instrumentation and data processing are presented in Montgomery et al. (2018).

In November 2016, unusual astronomical conditions combined to create the largest spring tide in 70 years. On November 17, a storm contributed to the abnormal tidal amplitude to generate a local peak water level 2.36 m above MSL, which corresponds to a 10-year return period flood at the long-term water level gauge near the study site. As the surge propagated across the study site, a decrease in amplitude as well as a temporal delay in peak water levels was evident (Figure 2-2a).

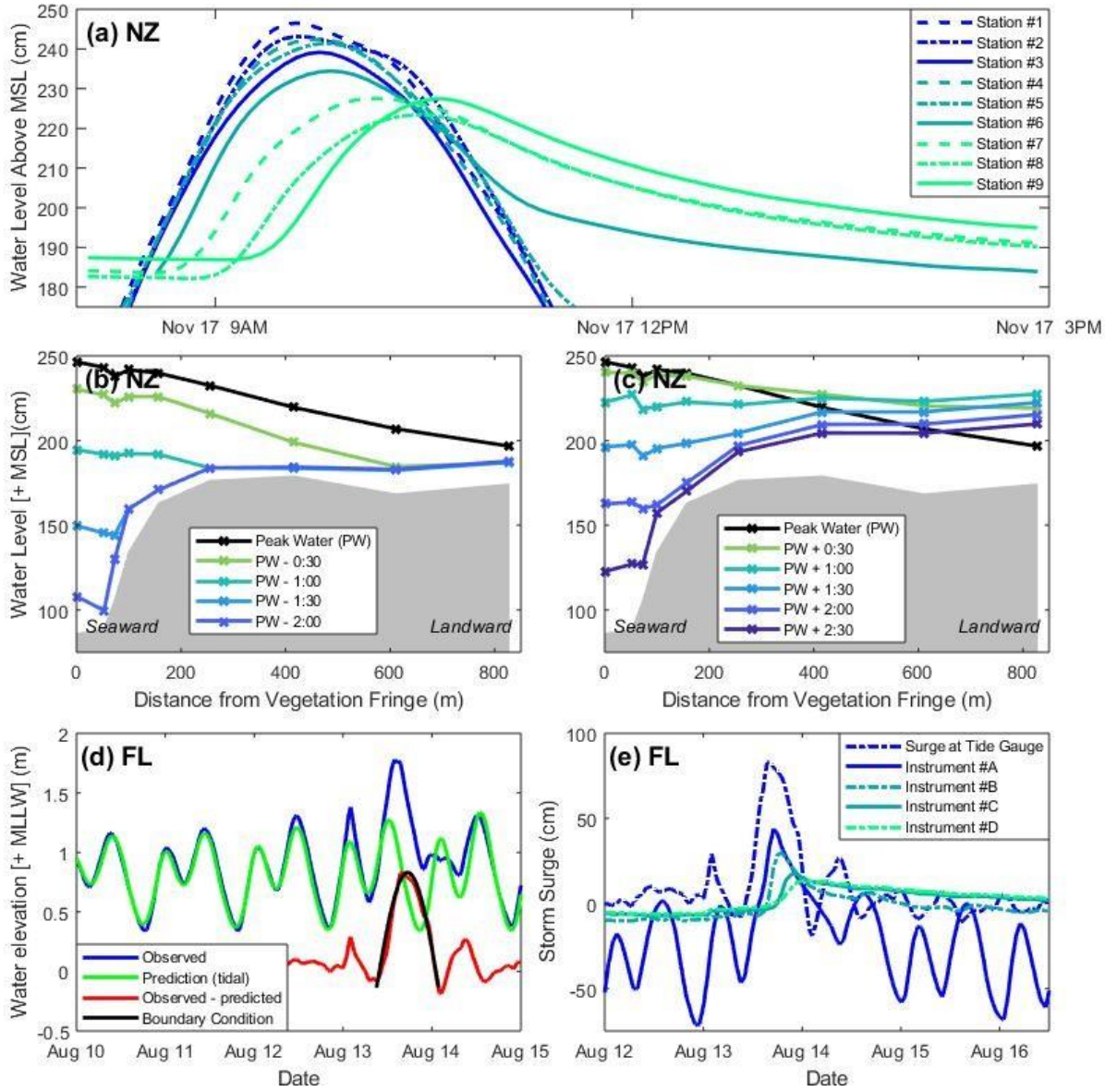

Figure 2-2. (a) Water levels at all nine instrument locations for surge event in the Firth of Thames (FoT). (b) Water levels along the FoT transect every 30 minutes (colors) before peak water level at the seaward boundary of the forest (black), data from surge event in panel (a). (c) Ebb water levels along the FoT transect every 30 minutes (colors) following the peak water level at seaward boundary of the forest (black). Note that maximum water level at the most landward station occurred 1 hour after peak water at the open boundary. (d) Ten Thousand Islands (TTI) Florida 2004 Faka Union Tide Gauge data (blue), tidal water level prediction (green), difference between actual water level and predicted (red), and half sinusoid fit to represent boundary condition used in diffusion equation (black). (e) Storm surge water levels at instrument locations in TTI (colors). For the tidally influenced location (#A) storm surge is the difference between measured water level and average high

tide level. For non-tidal locations (#B, #C, #D) storm surge is calculated as the difference between measured water level and mean water level for the 5 hours prior to the surge event.

2.6.2 Ten Thousand Islands, Hurricane Charley

Hurricane Charley impacted South West Florida in August 2004. Water level data were collected at: a permanent tide gauge positioned in Faka Union Bay just outside the mangrove forest (Figure 2-2d), site #A in the mangrove forest ~2.3 km from the bay, site #B at a transition from mixed mangrove to salt marsh at a distance of ~3.2 km, site #C in a marsh 4.5 km from the bay, and site #D 5.5 km from Faka Union Bay in a marsh (locations shown in Figure 2-1e). Note that no instrument elevations were recorded and therefore water levels cannot be related to a vertical datum; additional details on data collection and processing can be found in Krauss et al. (2009). The three most landward instrument sites were not influenced by tidal fluctuations and therefore storm surge height was determined by the difference between the 5-h mean water level prior to the storm surge event and peak water level (Figure 2-2e). For tidally influenced instrument sites, storm surge height was determined as water level above predicted high tide.

2.7 Theoretical Model

Sheet flow over an intertidal platform with uniform vegetation cover contrasts with creek flow in which flow dynamics are dominated by transport through channels, and the higher elevation vegetated regions primarily act as water storage. A simple analytic solution to creek flow was previously developed (*Carl T. Friedrichs and Madsen*, 1992). In contrast, the new formulation presented here characterizes a regime in which flux through flat vegetated areas dominates over flux through channels.

Sheet flow hydrodynamics through mangroves can be separated into 3 depth-dependent regimes imposed by the submerged portion of the plant. In shallow flows, friction is dominated by the high density pneumatophores (aerial roots) which are typically between 5 and 25 cm in height (*Horstman et al.*, 2018a) . At intermediate water depths, flow interacts with trunks and pneumatophores. In sufficiently deep water, flow interacts with the canopy in addition to the trunks and pneumatophores. In the present work, flow past trunks and pneumatophores is examined, as water levels during the high-water events were not sufficient to be significantly influenced by the leafy canopy at these sites.

Long-period storm surge (~O(hours)) through uniform emergent vegetation is reasonably described by a simplified 1-D conservation of momentum equation (3-dimensional turbulence is parameterised by vegetation drag, which is balanced by the pressure gradient). Combining momentum and continuity equations (see S1) yields a diffusion equation:

$$\frac{\partial \eta}{\partial t} = \frac{\partial}{\partial x}\left(D \frac{\partial \eta}{\partial x}\right), \tag{2-1}$$

where D is a nonlinear diffusion coefficient $D = h\sqrt{\frac{2g}{a_v C_D \frac{\partial \eta}{\partial x}}}$, which relates the temporal and spatial gradients of sea surface (η) - similar to Friedrichs & Madsen (1992), but assuming sheet

flow (not channel flow) and that frictional drag is dominated by vegetation and not the seabed. Mangrove trunks are modelled as rigid emergent cylinders spaced sufficiently far apart for inter-element interactions to be negligible (as suggested by Nepf (2004)). The diffusion coefficient *D* is a function of: gravity *g*; drag coefficient C_d; water depth h, varying in both time and space; vegetation frontal area density a_v, varying in space and vertically with water depth; and spatial sea surface gradient $\frac{\partial \eta}{\partial x}$, varying in both time and space (*Bedient and Huber*, 1992). Note that larger water depths and lower vegetation density result in a larger diffusion coefficient and a greater rate of fluid exchange.

2.7.1 Constant Diffusion Coefficient Solution

An approximate analytic solution to (2-1) can be obtained by treating the diffusion coefficient *D* as a constant $\overline{\langle D \rangle}$ equal to the spatial and temporal average of the variable quantities (note that overbar designates a time average and angle brackets a spatial-average). The open boundary condition (*x=L)* is set by assuming a sinusoidally varying sea surface $\eta = a\ sin\ (\omega t)$, with amplitude *a* and angular frequency $\boldsymbol{\omega}$ computed from fitting a half sine wave to the inundation event at the mangrove/open water interface. At the landward side of the basin (x=0), a zero sea surface gradient boundary condition is assumed (associated with no flow through the boundary), providing the solution (following Friedrichs and Madsen (1992)):

$$\eta = a\ \frac{cosh\left(\frac{x}{L_{Decay}}\right)}{cosh\left(\frac{L_{Forest}}{L_{Decay}}\right)} e^{i\omega t}\ ; L_{Decay} = \left(\frac{\overline{\langle D \rangle}}{i\omega}\right)^{1/2} = \left(\frac{\overline{\langle h \rangle} g^{1/2}}{i\omega\pi \left[2\langle a_v \rangle C_D \overline{\langle \frac{\partial \eta}{\partial x} \rangle}\right]^{1/2}}\right)^{1/2} \quad (2\text{-}2)$$

where sea surface elevation is dependent on the position in the basin *x* relative to the landward end of the forest, and the relationship between decay length scale $\boldsymbol{L_{Decay}}$ and width of the mangrove forest $\boldsymbol{L_{Forest}}$.

Evaluating the decay length scale requires an estimate for average sea surface slope (averaged in both time and space), which was obtained by taking the time-averaged partial derivative of Eq. (1-2) evaluated at the open boundary (*x*=L_{Forest}) (*Carl T. Friedrichs and Madsen*, 1992) to yield

$$\left|L_{Decay}\right| = \left(\frac{\pi g \overline{\langle h \rangle}^2}{\omega^2 \langle a_v \rangle C_D a \left| tanh\left(\frac{L_{Forest}}{L_{Decay}}\right)\right|}\right)^{1/3} . \quad (2\text{-}3)$$

Eq. (2-3) can be solved iteratively and requires an estimate for inundation period to obtain a value for angular frequency ω. To accommodate exposure at low tide in a solution that assumes a sinusoidal water level boundary condition at the seaward end of the vegetation, a wave period of double the inundation duration was assumed. Amplitude *a* was set as the maximum water elevation above the seabed at the open boundary and average depth $\overline{\langle h \rangle}$ as half that amplitude. Forest width L_{Forest} and average vegetation frontal density a_v are

assigned from field observations. Coefficient of drag C_d is ~1 for Reynolds numbers ≥ 200, with an average stem diameter of ~2 cm this corresponds to velocities greater than 1 cm/s and indicates that flow through mangroves is often turbulent (*Mullarney and Henderson*, 2018). A more direct equation for decay length scale is obtained by rearranging Eq. (2-3), substituting, and simplifying, to obtain

$$\left|L_{Decay}\right| = \left(\frac{gT^2 a}{16\pi \langle a_v \rangle tanh\left(\frac{L_{Forest}}{L_{Decay}}\right)} \right)^{1/3} . \quad (2\text{-}4)$$

LeBlond (1978) originally proposed a diffusion equation to describe bottom friction-dominated tidal flows. A formulation for drag due to rigid emergent vegetation (suggested by Nepf (2004)) results in a different formulation for the diffusion coefficient compared to bottom friction dominated flows. The new equation presented here uses representative values to approximate variable quantities in the diffusion coefficient (similar to the methods of Friedrichs & Madsen (1992)) for bottom friction dominated environments) to obtain an analytic solution to the non-linear diffusion equation describing flooding through mangrove vegetation.

Depth-averaged flow velocities *u* can be found from the combination of the continuity equation and the time derivative of the solution to the diffusion equation (2-2) (*Carl T. Friedrichs and Madsen*, 1992):

$$u = -\frac{ia\omega L_{Decay}}{h_0} \frac{\sinh\left(\frac{x}{L_{Decay}}\right)}{\cosh\left(\frac{L}{L_{Decay}}\right)} e^{i\omega t}. \quad (2\text{-}5)$$

Flow speeds (not shown) are therefore greatest at the seaward edge of the vegetation (x=L_{Forest}) and approach zero at the landward boundary (x=0).

Alternative analytic approximations to friction-dominated flow such as Dronkers' (2005) linearization of the friction term are not appropriate in this case as, in strongly dissipative environments, drag is highly non-linear (*Lanzoni and Seminara*, 1998).

2.7.2 Importance of Flow through Pneumatophores

Baptist et al. (2007) described the time-averaged flow over submerged vegetation as being comprised of 4 zones: a zone influenced by the bottom, flow through vegetation, a transition region at the top of the vegetation, and logarithmic flow above the vegetation. Our situation is reasonably described as a zone influenced by the bottom and two layers of vegetation: a submerged pneumatophore layer, and an emergent trunk layer. Pneumatophore heights are variable and the gradual decline of vegetation density along the vertical diffuses the transition layer (*Horstman et al.*, 2018a). Bed roughness is insignificant compared to the roughness provided by the dense pneumatophore cover (*Horstman et al.*, 2018a) and therefore influence of the bottom on water flux is ignored.

The relative importance of water flux through the pneumatophore and trunk layers can be examined by considering the ratio of discharge per unit width. Vegetation surveys in the FoT showed average pneumatophore densities ~2 m^{-1} with an average height of 0.1 m. Additionally, an average value for trunk frontal area density of 0.13 m^{-1} was found, although with substantial variability (values from 0.03-0.35 m^{-1}).

The ratio of the discharge through the pneumatophore zone and through the remainder of the water column can be obtained by solving for water velocity in Eq. (2-5) and using a simple formula for discharge per unit width $Q = u*h$. The relative flow through pneumatophores is expressed as Eq. (2-6) below, with height of the pneumatophore layer and remaining water column (above the pneumatophores) denoted by h_P and h_T, respectively and frontal area of the pneumatophores and trunks as a_P and a_T,

$$\frac{Q_P}{Q_T} = \frac{{a_T}^{1/2} h_P}{(a_T + a_P)^{1/2} h_T}. \quad (2\text{-}6)$$

The relative contribution of volume transported through the pneumatophore layer depends on total water depth and vegetation characteristics. FoT peak water depths reached 72 cm above the intertidal flat; therefore, for average vegetation parameters in the FoT, water flux through the pneumatophore layer is at least an order of magnitude lower than through the trunk zone, and so can reasonably be neglected. In the absence of further data, the same assumptions are applied to the TTI site.

2.8 Comparison of model predictions to Field observations

2.8.1 Firth of Thames

Predicted maximum water levels across the FoT intertidal (Eq. (*2-2)*) were compared to observations (Figure 2-3a). Root Mean Square (RMS) error between the theoretical model and observations is 2.7 cm. Flood duration and amplitude, used to establish the open water boundary condition, were selected from inspection of the flood signal of the most seaward instrument and estimated with respect to the top of the pneumatophore layer. Inundation duration of the flood event was 3 hrs 5 mins and amplitude 0.62 m (above pneumatophore layer at ~1.85m + MSL). Note that due to the sinusoidal forcing assumption, the period of the boundary condition signal is double the measured inundation duration. Mangrove properties were averaged over the study site and a vegetation frontal area density of 0.13 m^{-1} was used for model computations, the real component of the resultant decay length scale is 812 m. Maximum flood water level decays most rapidly across the outermost vegetated region where maximum sea surface slope and therefore maximum flow speeds occur.

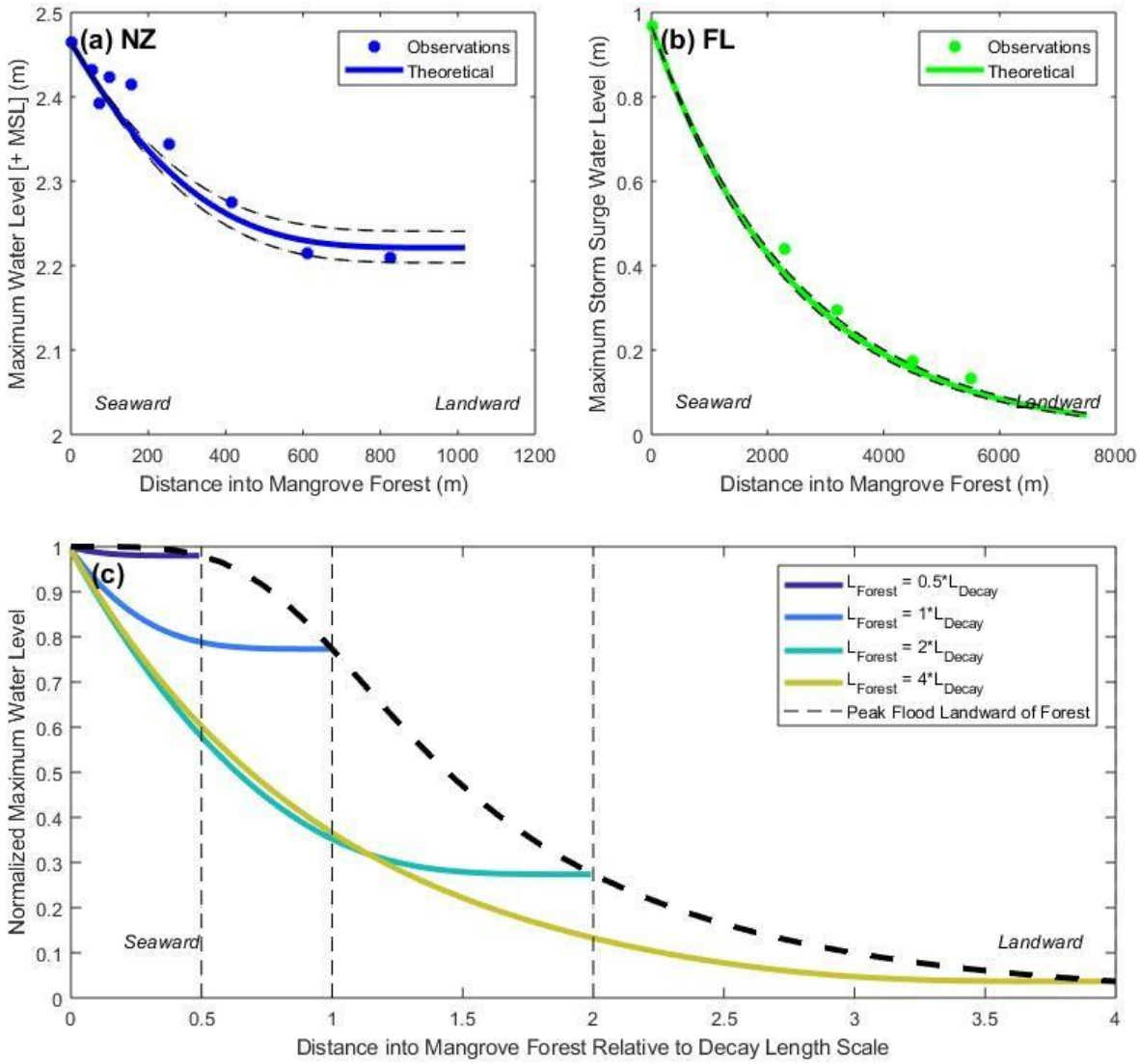

Figure 2-3. (a) Maximum water level predicted by the diffusion model (solid) and measured maximum water levels (dots) across the mangrove in FoT for November 2016 flood event shown in Figure 2-2a/b/c. (see text for details). (b) Maximum water level predicted by the diffusion model (solid) and measured maximum water levels (dots) across the mangrove forest in TTI for Hurricane Charley (Figure 2-2 d/e). Black dashed lines in panels a and b show the sensitivity to ± 10% in α_v. (c) Decay of normalized maximum inundation level for different widths of mangrove forests (L_{Forest}), normalized by inundation decay length scale (L_{Decay}) (solid). Dashed line shows total water level decay across mangrove forest widths.

2.8.2 Ten Thousand Islands

Maximum water levels in the TTI mangroves predicted by the diffusion method showed strong agreement with observed peak water levels during Hurricane Charley (Figure 2-3b), with RMS error between the theoretical model and observations of peak water level of 3.6 cm. Forest fringe boundary conditions were selected from fitting a half sinusoid to the skew surge at the Faka Union tide gauge (Figure 2-2d), an inundation duration of 16 hours, 48 minutes and peak elevation of 0.97 m was identified. Due to a small local topographic gradient, no limit on forest width was imposed when calculating decay length of the flood signal (Eq. (*2-4*) $tanh\left(\frac{L_{Forest}}{L_{Decay}}\right) \sim 1$). Mangrove frontal area of 0.19 m^{-1} was used in the diffusion model and was calculated from vegetation data presented by Pool et al. (1977) for

the TTI site. The real component of the inundation decay length L_{Decay} of Hurricane Charley through the TTI site is 2460 m.

2.9 Discussion

Our solution to friction-dominated surge propagation through uniform mangroves has two parts: the formulation of decay length scale, and the relationship between decay length scale and forest width. Decay length (Eq. (*2-4)*) increases with longer surge duration, deeper surge events and less dense vegetation. Surge durations typically vary from a few hours, for fast-moving storms or tidally dominated inundation (as in FoT), to several days for large slow-moving events (Hurricane Harvey elevated water levels off the Gulf Coast of Texas for ~4 days). The variation in surge period is the dominant influence on decay length scale (changing by ~1 order of magnitude). Pool et al. (1977) presented mangrove density data for a variety of mangrove species in around 20 forests. Frontal area density of trunks and stems varied by ~1 order of magnitude (0.07 – 0.62 m^{-1}), influencing surge decay length by a factor of ~2. Observations by Zhang et al. (2012) showed peak water levels of longer duration hurricanes in South Florida were attenuated less than shorter duration surges. Mangroves restrict the flow of water through the forest, therefore, shorter period storms are unable to transport water through the forest as efficiently as longer period storms, resulting in greater surge attenuation of shorter duration events. In sufficiently long duration floods, no attenuation of water level occurs and flood levels across the forest are uniform (e.g. narrow forest in Figure 2-3c).

The dynamics of storm surge through coastal mangroves are dependent on the relationship between inundation decay length and mangrove forest width (Eq.(2-3*)*, Figure 2-3c), as derived from the diffusion equation. Figure 2-3c shows the rate of decay of water level for a series of forests of varying relative length. Peak water level decays more rapidly in wider forests than in narrower, a result which can be attributed to additional water storage within the wider forest and the associated water flux through the vegetation. Although water level is not reduced as effectively in narrow forests, these results were generated assuming no water was transported landward of the inner forest boundary (further attenuation could occur if water storage exists landward of the vegetation). In the simplified environment assumed for this study, the outer portion of the vegetation acts to limit water exchange and the inner portion of the forest primarily serves as water storage, rendering the presence/properties of vegetation in the landward portion of the forest irrelevant. The forest in TTI was ~3.2 km wide with marsh landward of the mangroves. The rigid vegetation diffusion model with constant vegetation density (which only represents the front region of the wetland) accurately predicted water levels because the marsh landward of the mangroves acted only as water storage. Examining overall water level reduction across mangrove forests shows that total attenuation of water level increases most rapidly (with additional forest width) when the decay length scale and forest width are approximately equivalent (slope of dashed line, Figure 2-3c). With sufficient forest width relative to the decay length of the surge event, mangroves effectively attenuate water levels by limiting fluid exchange across the forest.

Rigid emergent vegetation, dominated by sheet flow, is assumed in our new adaptation of (*Carl T. Friedrichs and Madsen*, 1992), and therefore our method is not applicable to a wider array of coastal vegetation or geomorphology. The flexibility of saltmarsh grasses invalidates the assumption that the drag coefficient is independent of velocity and that vegetation frontal area is only proportional to depth (reviewed in Nepf (2012); Mullarney and Henderson (2018)). Saltmarshes are likely to be fully submerged during extreme events and the dominant water transport mechanism will either be through channels or skimming above the submerged vegetation. Application of the diffusion method requires a single frontal area value to be representative of the flow impeding effect of vegetation. Therefore, model application depends on mangroves being distributed such that flow routing through channels, around patches, or over submerged vegetation is insignificant, and sufficiently rigid to not deflect in flow. Moreover, the method assumes the momentum balance is characterised by sea surface gradient and friction due to emergent vegetation. Tsunamis and very large/short duration storm surges may require additional terms in the momentum equation.

2.9.1 Variations in the Diffusion Coefficient

The assumption of a constant diffusion coefficient facilitated an analytic solution to the diffusion equation, but results in symmetrical surge waves. The diffusion coefficient (Eq. (*2-3)*) contains three sources of variation: linear dependence on water depth (η), non-linear dependences on sea surface slope $\left(\frac{\partial \eta}{\partial x}\right)$ and dependence on vegetation characteristics (a_v). The emergent vegetation assumption provides a linear relationship between the diffusion coefficient and depth (Eq. (*2-1)*). The upper portion of the surge propagates at higher velocity than the lower portion resulting in a flood-dominant asymmetry, shorter flood stage and longer ebb stage (*Parker*, 1984), which is not captured by a constant diffusion coefficient. Although vegetation reduces peak surge levels due to limiting water exchange, vegetation also reduces the rate at which water returns to the seaward boundary, increasing ponding time (Figure 2-2a & Figure 2-2e and Rodríguez et al., (2017)). The constant diffusion coefficient solution produces a decaying, temporally shifted sine wave that overpredicts the rate of the receding water levels. The depth-dependence of the diffusion coefficient is of greater importance in a traditional bottom friction-dominated environment ($D \sim \eta^{5/3}$ (*Carl T. Friedrichs and Madsen*, 1992)), than for the linear dependence in emergent vegetation presented here.

Vertical and horizontal variations in vegetation induce complexity in flow that is not captured by the present approach. Mangrove trunk densities varied up to an order of magnitude throughout the FoT study area. Despite this variation, the simplified solution assuming uniform mangrove density well matched observations (Figure 2-3a). The vegetation variations were not organized in patches and did not cause significant flow routing; therefore, averaging mangrove characteristics resulted in a representative value for estimating drag due to vegetation. Highly channelized and creek dissected mangroves do not attenuate surge water levels as effectively as more uniform forests without creeks (*Krauss et al.*, 2009; *Montgomery et al.*, 2018).

2.10 Conclusions

Surge propagation in a friction-dominated mangrove environment is well described as a diffusive phenomenon. Mangrove forests have been conceptualized here as a buffer limiting water exchange and providing water storage. Our new analytic solution derived from the linearized diffusive model compared well with field observations of extreme surges in two contrasting mangrove environments. Mangroves have been shown to provide effective coastal flood protection if forests are sufficiently wide with respect to the decay length scale of the surge wave. The newly derived simplified equations that isolate the dominant physics, can be helpful in both qualitatively and quantitatively understanding surge attenuation in mangrove forests and provide an easily accessible solution without the need for advanced computing resources. Such formulae can help with planning for sea-level rise and flooding scenarios in the vulnerable low-lying areas that characterize many tropical and sub-tropical coastlines.

2.11 Acknowledgments, Samples, and Data

The research presented was supported by the Natural Hazards Platform (contract C05X0907). KRB, JCM, EMH and the field work were funded by the Marsden Fund (grant number 14-UOW-011). The authors acknowledge the field help provided by Caitlyn Gillard, Hieu Nguyen, Dave Culliford and Rex Fairweather.

Montgomery, John. (2018). Mangrove Field Study, Firth of Thames New Zealand, November 2016 (Version 1) [Data set]. Zenodo doi: 10.5281/zenodo.1323413

Montgomery, John. (2018). Mangrove Water Level Study, Tauranga New Zealand (Version 1) [Data set]. Zenodo. doi: 10.5281/zenodo.1323417

2.12 Supplementary Materials

2.12.1 Introduction

An analytic approximation to frictionally dominated flow through emergent rigid vegetation is presented below to describe storm surge propagating through coastal mangroves. A simplified 1-D momentum equation, balancing vegetation flow resistance and pressure gradient, and a 1-D continuity equation are combined to obtain a diffusion equation. The presented approach is similar to the derivation for tidal flow in embayments dominated by bottom friction (*Carl T. Friedrichs and Madsen*, 1992); however, in the present case, the bottom friction term is replaced by a vegetation drag term.

2.12.2 Solution

The stiff nature of mangrove trunks allows for the vegetation to be characterized as rigid emergent cylinders. Drag per unit volume (F_c) of rigid emergent vegetation, sufficiently spaced as to avoid inter-element interactions is given as a function of water density (ρ), frontal area density (a_v), coefficient of drag (C_D), and velocity (u) (*Nepf*, 2004):

$$F_C = \frac{1}{2}\rho a_v C_D |u| u. \tag{S1}$$

Note that for emergent vegetation a_v, the frontal area density, is the plant area perpendicular to the flow (per unit volume) and is estimated as a function of the number of elements (n) per unit area and diameter of each emergent element (d), and water depth (h): $a_v = \sum_{i=1}^{n} h d_i$. Although the drag coefficient is a function of Reynolds number, for turbulent flows, C_D is reasonably approximated as unity (*Williamson*, 1992).

The one-dimensional shallow water (depth-averaged) momentum equation including the term for vegetation drag is:

$$\underset{\text{(I)}}{\rho \frac{\partial u}{\partial t}} + \underset{\text{(II)}}{\rho \frac{\partial u^2}{\partial x}} + \underset{\text{(III)}}{\rho g \frac{\partial \eta}{\partial x}} + \underset{\text{(IV)}}{\frac{\rho C_B u^2}{h}} + \underset{\text{(V)}}{\frac{1}{2}\rho a_v C_D |u| u} = 0, \tag{S2}$$

where g is acceleration due to gravity, C_B is bottom drag coefficient, and η is sea surface elevation. Note water depth h is the sum of mean water level h_0 and surface elevation η ($h = \eta(x,t) + h_0$). The terms in Eq. (S2) correspond to acceleration (I), momentum flux (II), pressure gradient (III), bottom drag (IV), and vegetation drag (V). Assuming length scale $L \sim O$(km), velocity scale $U \sim O$(cm/s), time scale $T \sim O(T_{M2})$, wave amplitude $A \sim O$(m), and gravitational acceleration $g \sim O$ ($10 ms^{-2}$), we can neglect lower order terms to obtain the leading order balance between vegetation-induced viscous drag and pressure gradient (*Carl T. Friedrichs and Madsen*, 1992; *LeBlond*, 1978):

$$-\rho g \frac{\partial \eta}{\partial x} = \frac{1}{2} \rho a_v C_D u|u| \tag{S3}$$

Combining the simplified conservation of momentum equation (Eq. S3) with the 1D depth-integrated continuity equation,

$$\frac{\partial \eta}{\partial t} = -\frac{\partial hu}{\partial x} \tag{S4}$$

yields a diffusion equation with a non-linear diffusion coefficient (*D*):

$$\frac{\partial \eta}{\partial t} = \frac{\partial}{\partial x}\left(D \frac{\partial \eta}{\partial x}\right). \tag{S5}$$

The diffusion coefficient

$$D = h \sqrt{\frac{2g}{a_v C_D \left|\frac{\partial \eta}{\partial x}\right|}} \tag{S6}$$

depends on water depth h (varying in both time and space), vegetation frontal area density a_v (varying in space and across the water depth), and spatial sea surface gradient ($\frac{\partial \eta(x,t)}{\partial x}$) (varying in both time and space) (*Bedient and Huber*, 1992). Note that larger water depths and a lower vegetation density result in a larger diffusion coefficient and therefore a higher rate of fluid exchange.

2.12.3 Constant Diffusion Coefficient

An analytic solution can be obtained by treating the diffusion coefficient (Eq. S6) as a constant ($D=\overline{\langle D \rangle}$) equal to the space-time average:

$$\overline{\langle D \rangle} = \overline{\langle h \rangle} \sqrt{\frac{2g}{\langle a_v \rangle C_D \overline{\langle \frac{\partial \eta}{\partial x} \rangle}}} \tag{S7}$$

Note that the overbar designates a time average and angle brackets a spatial average. We assume constant vegetation density and no bottom slope. The open boundary condition ($x=L_{Forest}$) is set by assuming a sinusoidally varying sea surface $\eta = a\, sin\,(\omega t)$, with amplitude ($a$) and angular frequency (ω) computed from the inundation period T ($\omega = 2\pi/T$). At the landward side of the basin ($x=0$), a no sea surface gradient boundary condition is assumed (associated with no flow through the boundary). A solution is:

$$\eta = a \frac{cosh\left(\frac{x}{L_{Decay}}\right)}{cosh\left(\frac{L_{Forest}}{L_{Decay}}\right)} e^{i\omega t}, \tag{S8}$$

where $L_{Decay} = \left(\frac{\overline{\langle D \rangle}}{i\omega}\right)^{1/2} = (1+i)\left(\frac{2\overline{\langle D \rangle}}{\omega}\right)^{1/2}$ (*Carl T. Friedrichs and Madsen*, 1992). The decay length scale is therefore:

$$L_{Decay} = \left(\frac{T\overline{\langle h \rangle} g^{1/2}}{i\pi \left[2\langle a_v \rangle C_D \overline{\langle \frac{\partial \eta}{\partial x} \rangle} \right]^{1/2}} \right)^{1/2} . \tag{S9}$$

Evaluating the constant diffusion coefficient $\overline{\langle D \rangle}$ requires an estimate for average sea surface slope (averaged in both time and space), which is obtained by taking the partial derivative of Eq. (S8) and evaluating at the open boundary (x=L_{Forest}) (*Carl T. Friedrichs and Madsen*, 1992).

$$\overline{\langle \frac{\partial \eta}{\partial x} \rangle} = \left| \frac{1}{L_{Decay}} \right| a \left| tanh\left(\frac{L_{Forest}}{L_{Decay}}\right) \right| \frac{2}{\pi}. \tag{S10}$$

The constant diffusion coefficient becomes:

$$\overline{\langle D \rangle} = \frac{(\pi g)^{1/2} \langle \bar{h} \rangle}{\left[\langle a_v \rangle C_d^{1/2} |L_{Decay}| a \left| tanh\left(\frac{L_{Forest}}{L_{Decay}}\right) \right| \right]^{1/2}}. \tag{S11}$$

Decay length scale can be written as:

$$|L_{Decay}| = \left(\frac{\pi g \langle \bar{h} \rangle^2}{\omega^2 \langle a_v \rangle C_d a \left| tanh\left(\frac{L_{Forest}}{L_{Decay}}\right) \right|} \right)^{1/3} . \tag{S12}$$

Eq. (S12) can be solved iteratively and requires an estimate for inundation period to obtain a value for angular frequency (ω). To accommodate exposure at low tide in a solution that assumes a sinusoidal water level boundary condition at the seaward end of the vegetation, a wave period of double the inundation duration is assumed, and the solution calculated for only the crest of the flood wave moving across the vegetation. Amplitude a is set as the maximum water elevation above the seabed at the open boundary and average depth $\overline{\langle h \rangle}$ as half the amplitude. Forest width L_{Forest} and average vegetation frontal density a_v are assigned from field observations. A more direct equation for decay length is obtained by arranging Eq. (S12), substituting, and simplifying, to obtain:

$$\left|L_{Decay}\right| = \left(\frac{gT^2a}{16\pi\langle a_v\rangle tanh\left(\frac{L_{Forest}}{L_{Decay}}\right)}\right)^{1/3} . \quad \text{(S13)}$$

Sea surface gradient drives flow in the diffusion equation, and therefore peak water velocity coincides with maximum sea surface gradient. LeBlond (1978) commented that when the sea surface slope is zero at slack water, the diffusion relationship is invalid and water velocity and drag forces disappear. The balance between frictional and gravitational forces is no longer appropriate and additional terms would need to be included to accurately describe the flow dynamics. Nonetheless, the diffusion model is valid through most of the inundation event, over which the majority of the water transport occurs.

3 Attenuation of Tides and Surges by Mangroves: Contrasting Case Studies from New Zealand

3.1 Contribution of Authors

Chapter 3 presents "Attenuation of tides and surges by mangroves: Contrasting case studies in from New Zealand", published in *Water* in August 2018 (*Montgomery et al.*, 2018). This article demonstrates the importance of channels to water conveyance and long wave attenuation by a comparison of water level observations in two New Zealand mangrove forests: a forest bisected with channels near Pahoia in Tauranga and a forest in the southern Firth of Thames.

The Firth of Thames dataset analysed in this article was collected by my co-authors in November 2016 prior to the start of my studies. I planned and led the field work in Pahoia, performed the data processing, generated figures, and wrote the initial draft of the article. My co-authors assisted with data collection, edited drafts, provided advice on direction of work, and assisted with response to reviewer's comments.

3.2 Abstract

Mangroves have been suggested as an eco-defense strategy to dissipate tsunamis, storm surges and king tides. As such, efforts have increased to replant forests along coasts that are vulnerable to flooding. The leafy canopies, stems, and aboveground root structures of mangroves limit water exchange across a forest, reducing flood amplitudes. Attenuation of long waves in mangroves was measured using cross-shore transects of pressure sensors in two contrasting environments in New Zealand, both characterized by mono-specific cultures of grey mangroves (*Avicennia marina*) and approximate cross-shore widths of 1 km. The first site, in the Firth of Thames, was characterized by mangrove trees with heights between 0.5 and 3 m, and pneumatophore roots with an average height of 0.2 m, and no substantial tidal drainage channels. Attenuation was measured during storm surge conditions. In this environment, the tidal and surge currents had no alternative pathway than to be forced into the high-drag mangrove vegetation. Observations showed that much of the dissipation occurred at the seaward fringe of the forest, with an average attenuation rate of 0.24 m/km across the forest width. The second site, in Tauranga harbor, was characterized by shorter mangroves between 0.3 and 1.2 m in height and deeply incised drainage channels. No attenuation of the flood tidal wave across the mangrove forest was measurable. Instead, flow preferentially propagated along the unvegetated low-drag channels, reaching the back of the forest much more efficiently than in the Firth of Thames. Our observations from sites with the same vegetation type suggest that mangrove properties are important to long wave dissipation only if water transport through the vegetation is a dominant mechanism of fluid transport. Therefore, realistic predictions of potential coastal protection should be made prior to extensive replanting efforts.

3.3 2.1 Introduction

Mangroves are the dominant species of vegetation in many tropical and sub-tropical intertidal environments. These salt-tolerant trees provide valuable habitat for a range of animal species, reduce hydrodynamic forces, promote sedimentation, and provide protection

from floods (*FAO*, 2007). Additionally, mangroves are significantly more efficient than many terrestrial ecosystems at sequestering carbon (*McLeod et al.*, 2011). Mangroves thrive in the zone between mean sea-level and high water and thus are sensitive to changes in inundation regime. Their zonation and ability to prevent erosion or increase sedimentation may provide a mechanism for mangroves to adapt to sea level rise and alleviate the threat of coastal retreat (*van Maanen et al.*, 2015). Despite the diverse array of valuable services, world-wide mangrove populations are in steep decline, with the loss of over one-quarter of global mangrove cover since 1980 (*FAO*, 2007; *Giri et al.*, 2011).

Extreme flooding events are projected to increase with sea level rise (*Kroeker et al.*, 2016; *Wahl et al.*, 2017). Additionally, coastal populations and infrastructure are increasing (*Small and Nicholls*, 2003), driving demand for effective coastal protection. Conventional engineering solutions are often costly, and may have a limited life span, destroy or fragment sensitive habitat, and have been associated with enhanced erosion (*Airoldi et al.*, 2005; *Plant and Griggs*, 1992). Coastal vegetation has been proposed as an alternative to hard engineering solutions. Mangroves can provide coastal protection by reducing storm waves, dissipating currents, and stabilizing sediments (*Guannel et al.*, 2015; *Temmerman et al.*, 2013). Additionally, sedimentation in mangrove forests may provide a mechanism to maintain present coastlines with respect to sea level rise (*Alongi*, 2008).

The reduction in wave height of short period wind-generated waves due to interaction with mangroves is well established (*Guannel et al.*, 2015; *Henderson et al.*, 2017; *Massel et al.*, 1999). Less well established are the protective benefits of mangroves with respect to storm surge (*House Document*, 1965; *Krauss et al.*, 2009; *Zhang et al.*, 2012). Mangroves reduce peak flood levels by limiting fluid exchange across the forest (*McIvor et al.*, 2012). Dissipation of storm surge through coastal vegetation has previously been quantified as a reduction in peak water level (cm) per distance of flood propagation (km) with values categorized by vegetation type (*House Document*, 1965; *Krauss et al.*, 2009; *McIvor et al.*, 2012; *Zhang et al.*, 2012). Although providing an easily accessible solution, using fixed dissipation rates over wide-ranging sites may over simplify flood protection provided by coastal vegetation.

Alongi (2008) noted that flood protection provided by coastal vegetation is dependent on vegetation properties, local bathymetry, and storm parameters. At forest-wide scales applicable to coastal inundation issues, obtaining mangrove properties is problematic. Vegetation can be heterogeneously distributed (*Chen and Twilley*, 1998) and quantifying the drag-inducing elements (leaves, stems, trunks, and pneumatophores) unwieldy. Several different summary statistics are used for large scale hydrodynamics, including frontal area density, proportion of volume occupied by the solid canopy, and blockage factor (*Mullarney and Henderson*, 2018; *Nepf*, 2012). However, Nepf (2012) comments that at reach scales in vegetated rivers, the patch distribution plays a larger role in determining flow resistance than individual plant geometry. Typically, vegetation drag is large relative to bed drag and therefore in heterogeneously vegetated environments, flow is channelized and deflected away from vegetation/high-drag patches (*Folkard*, 2011; *Nepf*, 2012).

The influence of channelization on mangrove flood attenuation is explored through comparison of high water events in two contrasting New Zealand mangrove forests. The study sites are similar in length, with the forest extending ~1 km in the direction of flood propagation, and both sites are comprised of the same mangrove species, *Avicennia marina* var. *australasica* (*Horstman et al.*, 2018b). The key distinction is that the Tauranga mangrove forest is highly channelized in comparison with the Firth of Thames site.

3.4 2.2. Materials and Methods

3.4.1 Study Sites

3.4.1.1 Firth of Thames

The Firth of Thames (FoT) is a ~800 km^2 estuary on New Zealand's North Island (37° 12' S, 175° 27' E) (Figure 3-1b). The mesotidal estuary has a spring tidal range of 2.8 m and due to a shallow bed slope and plentiful fine-sediment supply, a large intertidal mud flat has developed (*Swales et al.*, 2007). The basin is bounded to the east and west by mountain ranges and the Hauraki plains to the South. A stop bank (visible as a diagonal track on Figure 3-2a) prevents inundation of the Hauraki plains to the south of the Firth. The basin is exposed to moderate waves from the North and subject to a high terrigenous sediment supply from the Waihou and Piako rivers. The southern boundary of the Firth is colonized by a 1 km wide forest of grey mangroves (*Avicennia marina* var. *australasica*).

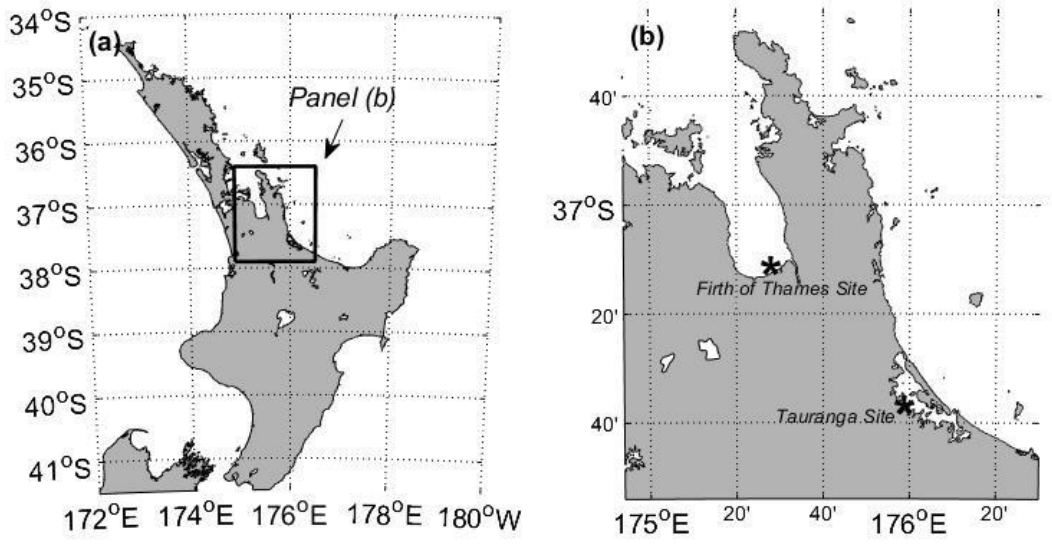

Figure 3-1. (a) North Island of New Zealand with panel (b) outlined; (b) Section of North Island of New Zealand showing proximity of Firth of Thames and Tauranga mangrove sites.

The cross-shore profile of the vegetated region (Figure 3-3a) consists of a level mangrove forest ~1.7-1.9 m above MSL extending ~800 m seaward of the stop bank (*Swales et al.*, 2007). The sloping vegetation extends an additional ~100 m seaward to the mud flat. The topography and forest characteristics are relatively homogenous in the longshore direction. The elevation of the seaward fringe of the forest is close to mean high water neap tide level (0.98 m MSL), so the tidal prism within the forest is relatively small and no substantial creeks have developed (Figure 3-3a) (*Swales et al.*, 2015).

Mangrove characteristics vary throughout the forest. Along the forest fringe, trees are characterized by open spreading forms (Figure 3-4 a/b). Within the forest trees tend to have straight vertical trunks (Figure 3-4c). Tree height ranges from 0.5m to 3.5m. Dense pneumatophores, as many as ~500 m^{-2}, emerge from the bed up to 25 cm in height and ~1 cm in diameter (Table 3-1).

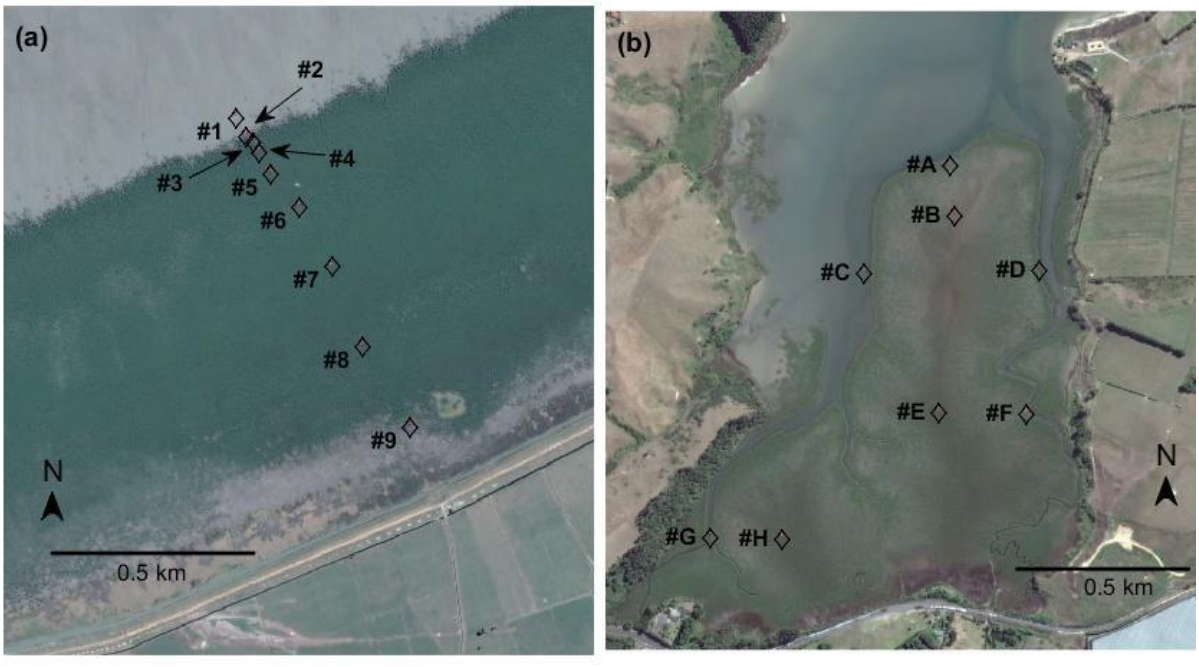

Figure 3-2. (a) Firth of Thames study site with 9 (#1 seaward - #9 landward) instrument locations noted. Station #1 is on the unvegetated mudflat, station #2 is in the vegetation fringe, stations #3-#5 are in the gently sloping intertidal, and stations #6-#9 are on the intertidal flat. (b) Tauranga study site with 8 instrument locations noted. Station #A is on the vegetation fringe on the seaward boundary, stations #C & #D are in the western channel, stations #B #E & #H are in the central mangrove forest, stations #D & #F are in the eastern channel. Note that length scales are similar in both panels.

In November 2016, a supermoon and low-pressure event occurred to produce an unusually large flood event in the Firth of Thames (Figure 3-4d, Figure 3-5 a/b). Water levels reached 2.36 m above MSL, corresponding to an event with a ~10-year return period for the Firth of Thames. The study area was flooded for several tidal cycles prior to peak high water and remained flooded for several tidal cycles after peak water level.

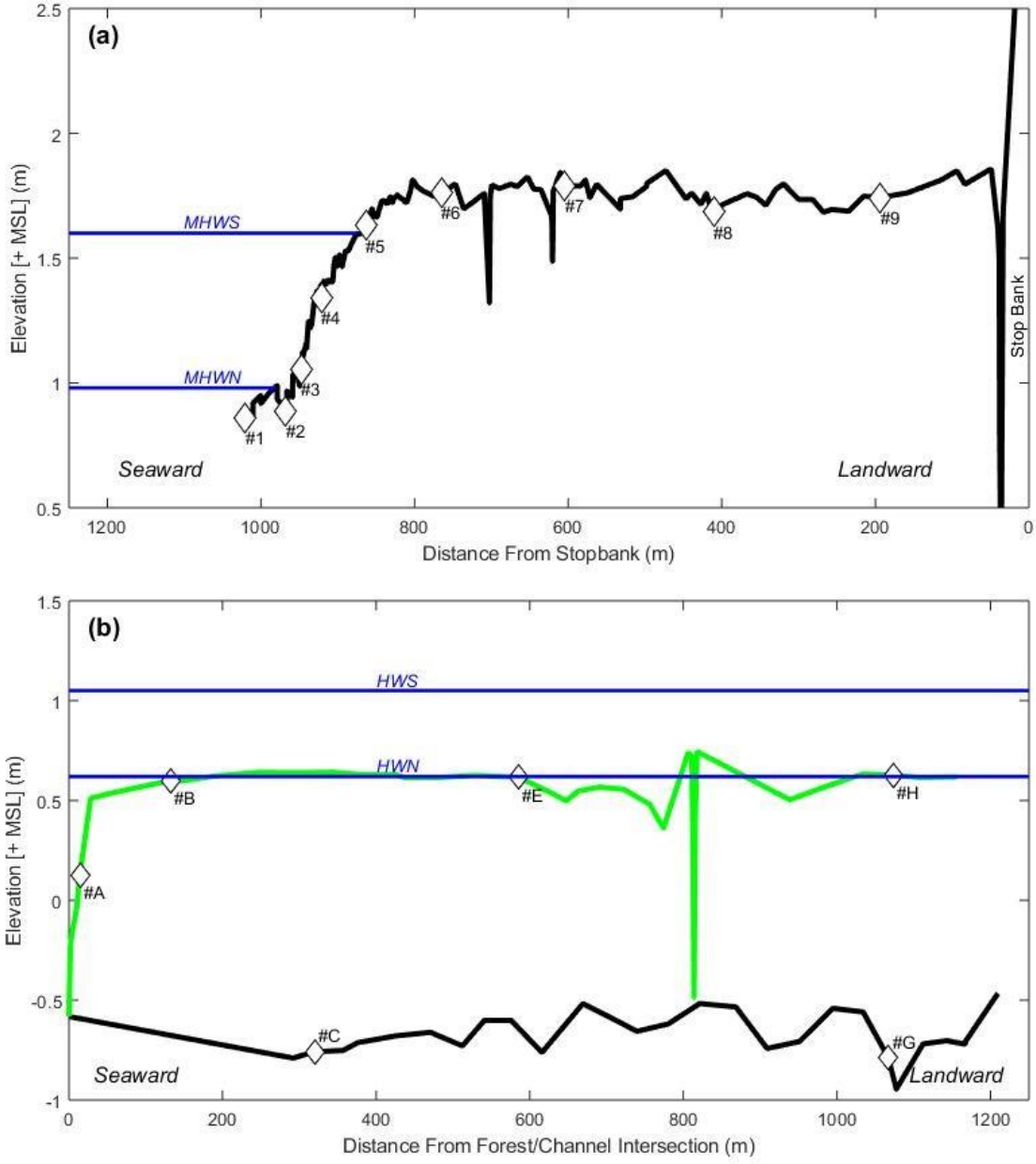

Figure 3-3. (a) Elevation profile along the instrument transect in the Firth of Thames. Mean High Water Spring (MHWS) and Mean High Water Neap (MHWN) are noted. The main forest is higher than normal tidal levels and therefore no drainage channels have been scoured by tidal water flow. (b) Tauranga RTK survey of transect through central mangrove forest (green) and thalweg (black). High Water Spring (HWS) and High Water Neap (HWN) are marked (blue). The semi-diurnal tidally driven flow through forest are responsible for channelization at the site.

Figure 3-4. Images of Firth of Thames study site. (a) Forest fringe at low tide. (b) Fringe at mid tide, trees are characterized with open spreading branches. (c) Interior mangrove forest with two researchers for scale. Trees are tall with vertical trunks. (d) Two researchers in the mangrove forest during flood event.

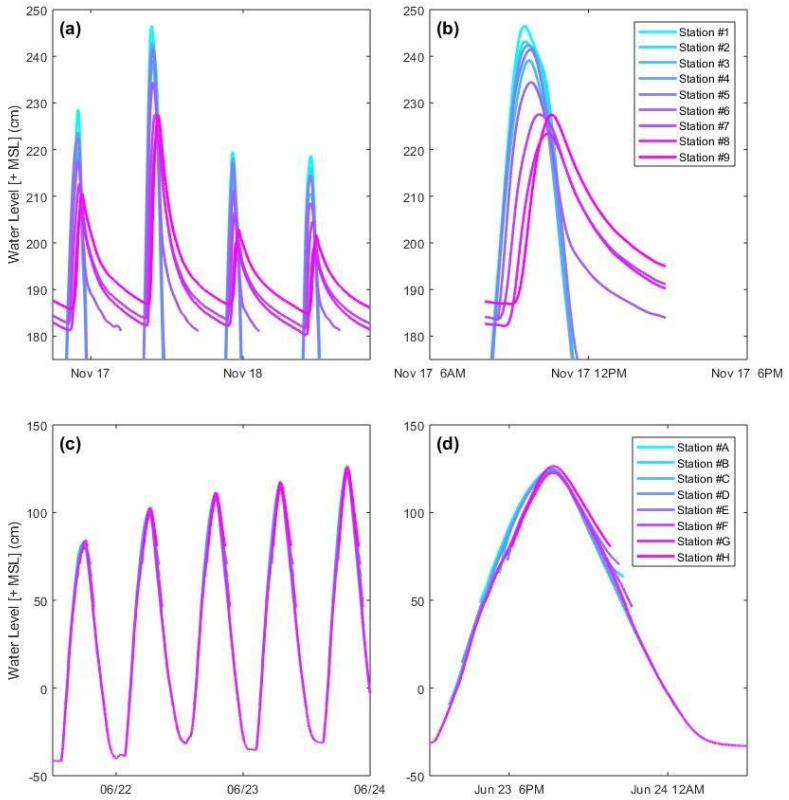

Figure 3-5. (a) Firth of Thames water level at each instrument station for five consecutive spring tidal cycles. The upper intertidal flat (stations #6-#9) did not fully drain for several tidal cycles. (b) Firth of Thames water level during maximum inundation event. (c) Tauranga water level for five consecutive spring tidal cycles. Note that only station #G was submerged at low tide. (d) Tauranga water level during largest tidal cycle.

3.4.1.2 Tauranga Site

Tauranga harbor is a 200 km^2 barrier-enclosed lagoon on the North Island of New Zealand (37° 39' S, 176° E) (Figure 3-1). The mesotidal estuary has an average spring tidal range of 1.62 m and neap range of 1.24 m (*Heath*, 1985). Due to the complexity of the estuary, exact tidal ranges are location-dependent (*Tay et al.*, 2013). The shallow lagoon, with an average depth of 3 m at low tide, has extensive intertidal areas that make up nearly 2/3 of estuary area (*Healy et al.*, 1996). The estuary has two entrances and is comprised of many sub-estuarine basins. Mangroves in Tauranga have expanded rapidly, from 13 hectares in the 1940s to 168 hectares in 1999 (*Park*, 2004). Mangroves in Tauranga are at the southern boundary of their latitudinal range, which causes the forests to be less productive and the trees to be shorter (*Horstman et al.*, 2018b). The focus of the presented work is a basin north of Pahoia (Figure 3-1) that nearly drains at low tide.

The Pahoia field site is comprised of a ~1 km long intertidal mangrove forest that occupies ~2/3 of the basin surface area (Figure 3-2b). Two unvegetated steep-sided channels, along the eastern and western sides of the forest, maintain a near-uniform depth throughout the study site and dominate water flow into the area (Figure 3-3b, Figure 3-6b). The western channel bifurcates around a ~300-400 m wide central mangrove platform. The vegetated regions are at the same elevation as high-water neap tidal levels and are approximately flat. A small creek drains into the western channel and further divides the central mangrove forest. The significant tidal prism in the forest is likely responsible for creating the channel network (*van Maanen et al.*, 2015).

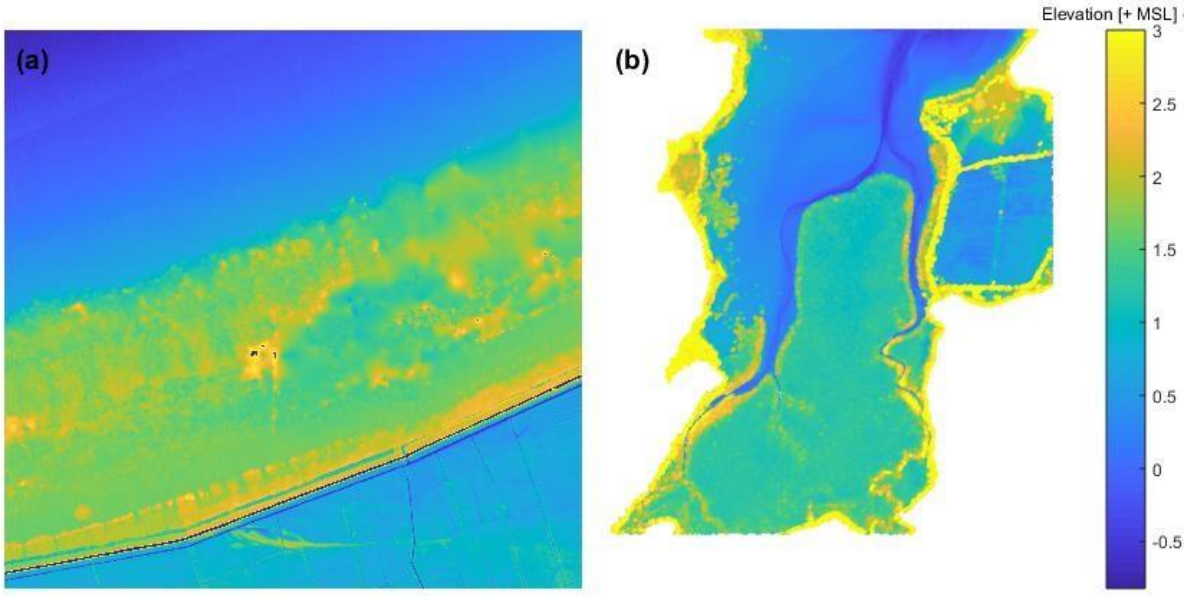

Figure 3-6. (a) Firth of Thames LiDAR devoid of a channel network. Patchy higher elevations likely indicate vegetation canopy. (b) Tauranga LiDAR data. Deep, incised channels and a level vegetated intertidal characterize the site. High elevation along channels displays dense mangrove canopy. The colour bar shows elevation scale for both subplots.

The forest is comprised of small shrub like grey mangroves less than 1.2 m in height (average 0.41 m). Individual trees have complex geometry (Figure 3-7a) and present a low dense canopy (Figure 3-7b). The pneumatophore density averages 75 per square meter, with individual pencil-roots of similar dimension to the pneumatophores in the Firth of Thames (Table 3-2).

Figure 3-7. Images of Tauranga study site. (a) Example mangrove tree. Vegetation is characterized by complex trunk structure and low canopy height. (b) Mangrove forest at mid tide. (c) Mangrove lined channel with steep densely vegetated banks. (d) Weather station recording barometric pressure and wind speed during high spring tide with canopy almost submerged.

Typical spring tides nearly fully submerge the Pahoia mangrove forest (Figure 3-7d). Figure 3-5c/d displays data from a series of spring tides in June 2017. Peak water level reached ~1.25 m above MSL. Note that the study site nearly drained at low tide, leaving most of the instruments exposed.

3.4.2 Field Data Collection

Field observations were collected during two experiments conducted in November 2016 in the southern Firth of Thames and in April 2017 in Pahoia sub-estuary of Tauranga Harbor. In each case, arrays of water level sensors were deployed, along with RTK-GPS surveying and manual vegetation surveys. Details of surveys and deployments are given below.

3.4.2.1 Vegetation Survey

Vegetation surveys were conducted to quantify the rigid vegetation at the study sites. The heterogeneous distribution of vegetation, large study area, and diverse mangrove properties necessitated a unique approach to measure vegetation. The survey objective was targeted at the two types of structure that characterize the flow-reducing properties of *Avicennia marina*: (1) the pneumatophores and seedling which comprise small, but dense structures near the sea bed, and (2) the trees and branches which are much less dense but can form a large blocking mechanism at high tide and surge levels. Flexible leafy canopies were not quantified. Although the canopies contribute drag, flexible vegetation has reduced flow resistance compared to rigid vegetation due to reconfiguration by currents both reducing frontal area and becoming more streamlined (*de Langre*, 2008; *Nepf*, 2004).

Due to the different growth forms of the mangroves at the two sites, slightly different strategies were employed. In the Firth of Thames, mangrove trees in some areas were nearly impenetrable, 5 m by 5 m quadrats were established along the cross-shore instrument transect. In Pahoia, where the mangroves were generally less than a meter tall, a cross-shore

and an along-shore transect were established, and vegetation properties measured every 10 m.

In the Firth of Thames, the number of trees was counted in each quadrat. The height and width of the canopy, and the stem diameter at 0.3 m from the seabed were measured for 5 trees closest to pre-defined coordinates within the quadrat. To quantify pneumatophores, five 0.5 by 0.5 m quadrats were selected, one at each corner and one at the center of the large quadrat. Within these small quadrats, all the pneumatophores and seedlings were counted. In addition, the height, top diameter, and bottom diameter of five pneumatophores were measured.

In Pahoia, a transect through the central mangrove forest was established. Along the transect canopy height was measured at 5-m intervals. Pneumatophore and seedling characteristics were measured in 0.5 by 0.5 m quadrats every 5 m using the same method as that used at the Firth of Thames site.

3.4.2.2 Bathymetry

Manual RTK GPS surveys were conducted to obtain bathymetry at both study sites. In the Firth of Thames an RTK survey of the instrument transect was conducted (Figure 3-3a). In Tauranga, RTK elevations were obtained for the western channel and a transect through the central mangrove forest (Figure 3-3b). Additionally, LIDAR data was provided by local government organizations for both sites (Figure 3-6).

3.4.2.3 Water level

Pressure sensors were deployed at each of the study locations (Figure 3-2, Table 3-1, and Table 3-2). The array of water level sensors deployed in the Firth of Thames in November 2016 consisted of a single transect of 9 instruments, extending from the stop bank to the mud flat (Figure 3-2a): Station 1 was seaward of the vegetation on the mud flat, stations 2-5 were located across the sloping forest region and stations 6-9 were spread across the forest platform (Figure 3-3a). A man-made channel is located just seaward of the stop bank and is evident in the transect survey (Figure 3-3a). At Pahoia in Tauranga, the central mangrove forest and both the east and west channels were instrumented with pressure gauges (Figure 3-2b). Station #A is at the seaward edge of the mangroves and at the intersection of the two primary channels. Three stations (#B, #E, and #H) were located at increasing distances into the vegetated intertidal platform. An additional two gauges were positioned in each of the two channels.

Pressure sensors were corrected for variations in barometric pressure and for temperature dependence and referenced to mean sea level using survey data. Pressure signals were smoothed using a low-pass filter and converted to water level using a constant water density of 1025 kg/m^3.

Table 3-1. Firth of Thames instrument array.

Station	Instrument	Sampling		Temperature Dependence
		Regime	Details	Correction applied
#1	Nortek Aquadopp	Burst	2^{12} samples at 8Hz Every 15 minutes	Y
#2	Nortek Vector	Burst	7.5 minutes sampling at 16 Hz Every 15 minutes	Y

#3	Nortek Aquadopp	Burst	2^{12} samples at 8Hz Every 15 minutes	Y
#4	Nortek Aquadopp	Burst	2^{12} samples at 8Hz Every 15 minutes	Y
#5	RBR Concerto	Continuous	4Hz	N
#6	RBR Duet	Continuous	8Hz	N
#7	Solinst Levelogger	Continuous	1/60 Hz	N
#8	Solinst Levelogger	Continuous	1/60 Hz	N
#9	Solinst Levelogger	Continuous	1/60 Hz	N
	Weather Station	Continuous	1/5 minutes	N

Table 3-2. Tauranga instrument array.

Station	Instrument	Sampling		Temperature Dependence
		Regime	Details	Correction applied
#A	RBR Solo	Continuous	8 Hz	N
#B	RBR Solo	Continuous	Every 2 minutes Average 1 min of data sampled at 4 Hz	N
#C	RBR Duet	Continuous	8 Hz	N
#D	RBR Duet	Continuous	8 Hz	N
#E	RBR Solo	Continuous	Every 2 minutes Average 1 min of data sampled at 4 Hz	N
#F	RBR Solo	Continuous	8 Hz	N
#G	RBR Solo	Continuous	8 Hz	N
#H	RBR Solo	Continuous	8 Hz	N
	Weather Station	Continuous	1/5 minutes	N

3.5 Results

Water levels across the Firth of Thames and Pahoia study sites for successive tidal cycles are displayed in Figure 3-5. The ~1 km wide mangrove forest in the Firth of Thames site reduced peak water levels and delayed the inundation signal, with the reduction and delay increasing with distance into the forest. The largest inundation wave in the Firth of Thames reached a maximum of 72 cm above the tidal flat at the seaward forest fringe and decayed to 53 cm above the tidal flat at the landward most station. This reduction of 19 cm water height across the 800 m separation between station 1 and station 9 corresponds to a dissipation rate of ~24 cm/km. The temporal delay in peak water between station 1 and 9 is evident in Figure 3-5 and estimated at 1 hour. The average velocity of peak inundation through the Firth of Thames mangrove forest is ~0.2 m/s.

At the Pahoia site, no measurable reduction in water level occurred over the ~1km separation between instruments. Dissipation of flood levels were of the same scale as the uncertainty of the elevation measurements (O(mm)). Additionally, no identifiable temporal delay in peak water occurred over the study site (Figure 3-7c/d).

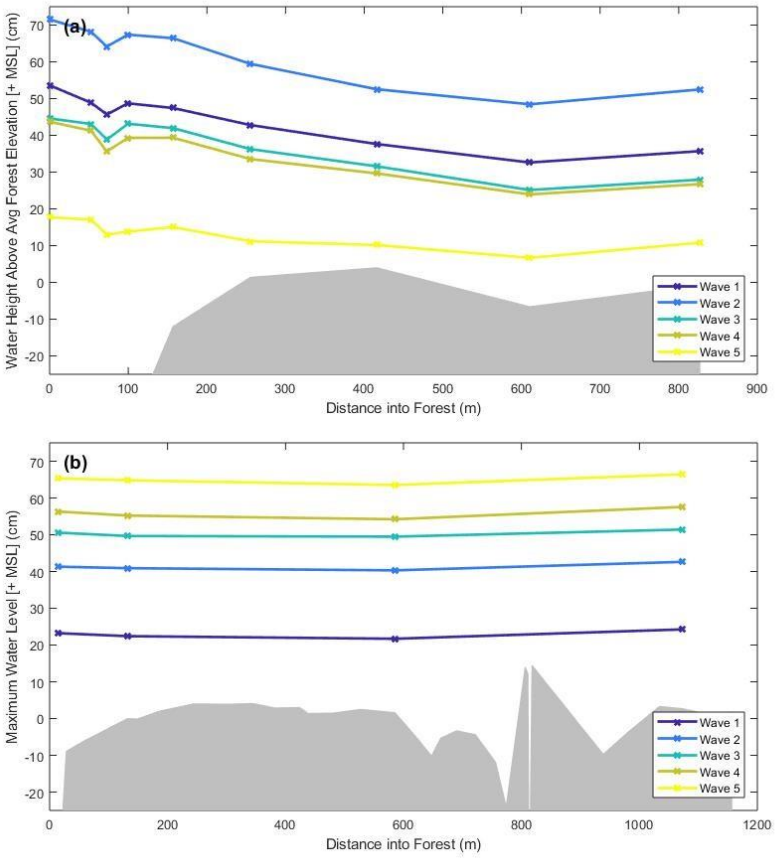

Figure 3-8. (a) Peak water level at each instrument station along transect in the Firth of Thames for 5 consecutive inundation events. (b) Peak water level at each instrument along central mangrove transect (#A, #B, #E, & #H). Elevations are with respect to average elevation of the forest floor, profiles of which are shown in grey.

The magnitudes of the inundation waves for the two locations are similar with respect to the elevation of the mangrove forest. The inundation waves for both sites range from ~20 cm to ~70 cm above average forest elevation (Figure 3-8). Nonetheless, the elevation of inundation relative to MSL was different between the two sites (Figure 3-5), with the Firth of Thames ranging from ~220 to ~245 cm above MSL at the seaward boundary of the mangrove forest, while the Tauranga inundation wave varied between 80 to 125 cm above MSL.

Table 3-3. Firth of Thames vegetation survey summary.

Location		Trees			Pneumatophores		
Description	Distance from Fringe (m)	Density (# per m²)	Avg. Height (m)	Avg. Diameter (cm)	Density (# per m²)	Avg. Height (cm)	Avg. Diameter (cm)
Mudflat	-49	0.1	1.6	0.6	0	0	0
Fringe (Front)	0	0.1	6.4	2.3	126	25.4	0.6
Fringe (Back)	22	1.0	4.8	1.9	385	22.9	0.6
Forest	36	1.0	5.8	2.9	386	17.0	0.5
Forest	114	6.4	3.0	2.3	322	12.5	0.6
Forest	166	11.4	2.8	1.5	357	7.7	0.6
Forest	262	12.2	1.9	1.2	481	8.3	0.6
Forest	376	6.4	3.6	3.0	342	8.7	0.5
Forest	476	1.4	4.2	3.8	330	10.5	0.6
Forest	561	3.6	3.9	1.6	570	12.0	0.5
Forest	667	5	3.8	2.6	482	11.0	0.5

Table 3-4. Tauranga vegetation survey summary.

Location		Trees	Pneumatophores		
Transect	Distance from Fringe (m)	Canopy Height (cm)	Density (# per m²)	Avg. Height (cm)	Avg. Diameter (cm)
Along-shore	0	0	10	1.5	0.3
Along-shore	5	97	41	1.7	0.3
Along-shore	15	48	74	1.1	0.4
Along-shore	25	41	77	1.1	0.5
Along-shore	35	36	74	0.6	0.4
Along-shore	45	38	63	1	0.4
Along-shore	55	36.5	62	6	0.5
Along-shore	65	34	89	8.7	0.6
Along-shore	75	37	49	10.8	0.6
Along-shore	85	29	61	7	0.6
Along-shore	95	23	60	5.1	0.6
Along-shore	105	26	54	10.3	0.5
Along-shore	115	27	43	4.3	0.6
Along-shore	125	22	43	5.3	0.5
Along-shore	135	29	66	6.9	0.5
Along-shore	145	26	62	7.4	0.5
Along-shore	155	23	91	6.3	0.6
Along-shore	165	23	73	6.1	0.6
Along-shore	175	22	63	6.2	0.7
Along-shore	185	20	43	6.3	0.7
Along-shore	195	20	50	13.6	0.6
Along-shore	205	32	53	5.4	0.5
Along-shore	215	30	56	11.2	0.6
Along-shore	225	24	48	7	0.5
Along-shore	200	27	69	11.7	0.6
Along-shore	190	29	81	3.7	0.6
Cross-shore	180	33	86	8.2	0.6
Cross-shore	170	52	48	11.7	0.6
Cross-shore	160	36	85	14.2	0.6
Cross-shore	150	35	89	8.5	0.6
Cross-shore	140	47	87	12.9	0.6
Cross-shore	130	54	99	10.2	0.6
Cross-shore	110	59	101	15.1	0.6
Cross-shore	100	63	134	12.7	0.6
Cross-shore	90	64	100	10.7	0.5
Cross-shore	80	71	138	8.1	0.5
Cross-shore	70	93	142	7.4	0.5
Cross-shore	60	55	101	8.8	0.6
Cross-shore	50	56	116	15.9	0.6
Cross-shore	40	42	102	7.6	0.5
Cross-shore	30	44	111	8.9	0.6
Cross-shore	20	72	77	10.5	0.5
Cross-shore	10	130	108	5.4	0.5
Cross-shore	0	0	67	12.8	0.5

3.6 Discussion

Mangroves reduce peak water levels during a flood by limiting the exchange of water through the vegetation (*McIvor et al.*, 2012). Krauss et al. (2009) observed that the presence of channels decreased the efficacy of mangrove flood attenuation from 9.4 cm/km to 4.2 cm/km. Using a combination of observations and numerical simulations, Zhang et al. (2012) found that the amplitude of storm surge was reduced at a rate of 40-50 cm/km through

mangrove forests and ~20 cm/km through patchy regions consisting of a combination of mangrove islands and open water. Flood level reduction during the series of large inundation events in the non-channelized Firth of Thames averaged 24 cm/km, which agrees with rates previously published for unchannelized forests by Krauss et al. (2009) and Zhang et al. (2012). In contrast, the channelized New Zealand mangrove site in Tauranga had no measurable reduction of flood amplitude. The vegetation characteristics for both sites were similar (Table 3-3 & Table 3-4), and so are unlikely to account for the dramatic differences in attenuation.

The interaction of water and vegetation is complex and has been investigated at multiple length scales. At small scales (O(mm)) boundary layers and shear caused by individual stems, roots, and leaves cause turbulent eddies that shed off each individual stem (*Norris et al.*, 2017). Turbulence is also generated at the shear layer between the faster moving flow over submerged vegetation, and the damped flow within the canopy (*Horstman et al.*, 2018a). Intermediate scales (O(m)) comprise flow at the canopy or patch scale involving a community of vegetation. Larger length scale interactions (O(km)) occurs at the forest level (*Mullarney et al.*, 2017). To appropriately investigate a process of interest, a reasonable spatial scale, associated conceptual model, and relevant measurements and methods must be identified (*Nepf*, 2012). Vegetated regions produce high drag with respect to unvegetated areas and flow is diverted to the path of least resistance. In areas described as dense vegetation patches, most flow is directed around the patches and a forest-wide approach is required. In sparse or homogeneously distributed vegetation, smaller-scale resistance dominates and a smaller-scale approach is justified (*Green*, 2005a).

In mangrove forests, it is not just the vegetation geometry that controls water transport, the intertidal bathymetry and water level relative to the elevation of the vegetation also play a role (*Horstman et al.*, 2015; *Mazda et al.*, 1995). Flow through mangrove forests has been categorized into creek flow or sheet flow depending on the primary mechanism of fluid transport. Creek flow dominates in channelized mangroves at low water levels. Sheet flow, transport over the vegetated platform through the mangroves, becomes increasingly important with reduced channelization and at increasing water levels (*Horstman et al.*, 2015). Our results show that the Tauranga mangrove forest is dominated by creek flow, and the density of mangrove vegetation therefore only has minimal contribution to flow restriction; no evidence of reduced inundation level nor delay in the flood signal exists. In Tauranga, flow resistance is best described by the larger-scale distribution of vegetation and degree of channelization. Conversely, the Firth of Thames mangrove forest is not channelized, and the primary shoreward water transportation mechanism is sheet flow through the vegetation. Here, vegetation properties are important to impeding water exchange across the forest, reducing inundation levels and slowing the flood wave propagation. In the Firth of Thames, the flow resistance relates to the vegetation properties along the one-dimensional cross-shore transect. The cumulative influence of large quantities of individual stems, stalks, and leaves on fluid flows at forest wide scales necessitates simplifying vegetation summary statistics (*Mullarney and Henderson*, 2018). Several different statistical parameters have been used to describe the influence of vegetation on large scale flow resistance, including: solid volume fraction, vegetation porosity, and frontal area per bed area (*Nepf*, 2012).

Channelization in mangrove environments develops as the trees grow and create flow resistance and concentrate the flow into channels (*van Maanen et al.*, 2015). However, for initiation of the feedback process that allows the channels to develop, the intertidal platform must be at a sufficiently low elevation with respect to the tidal excursion that currents occur on the vegetated platform. In the case of a very high platform, inundation only occurs at slack water close to high tide, at which time conditions promote sediment deposition. The Tauranga mangrove forest is inundated during normal tidal levels. The drainage channels in the Tauranga study site have likely resulted from scouring by tidally driven water transport through the forest. The forest elevation in the Firth of Thames is higher than Mean High Water Spring (MHWS) water levels (Figure 3-3a) and therefore water is only infrequently transported through the forest and channels cannot develop.

During the study, water depths in the relatively flat mangrove forests in Tauranga and the Firth of Thames were of similar magnitude (Figure 3-8). The capacity of mangroves to provide coastal flood protection is ultimately related to water transport pathways. Extrapolating from our case study environments, we can expect that lower intertidal areas with channelization will be far less capable of protection than higher intertidal areas with little channelization. Krauss et al. (2009) and Zhang et al. (2012) found that reduction of flood levels along a river corridor were less than through unchannelized vegetation but still provided flood protection. Both previous investigations focused on hurricane-driven storm surge in the south east United States. The extreme water levels greatly exceeded the capacity of the channel networks, likely resulting in flow pathways through the vegetation and therefore the capacity to mitigate flood levels was apparent but reduced compared to unchannelized locations. Moreover, the sediment regime has been shown to contribute to the development of profile shape, with muddy profiles often associated with high convex intertidal geometries (*Bryan et al.*, 2017).

3.7 Conclusion

The influence of mangroves on long wave propagation is strongly dependent on flow routing. In highly channelized mangrove forests, such as our Tauranga case study area, water is preferentially transported via the channels and flood levels are not reduced substantially across the forest. In these cases, the vegetation does not contribute significantly to flow resistance, so specific plant properties are irrelevant with respect to limiting fluid transport. However, we hypothesise that for sufficiently large flood events, in which the conveyance capacity of the channels is exceeded, a proportion of the flow will be forced through the vegetation, which thus will provide an intermediate level of attenuation (still reduced relative to an unchannelized environment). Conversely, in homogeneously vegetated forests without channels, such as the Firth of Thames study site, water is transported through the mangroves and the trees reduce flood levels by limiting fluid exchange through the forest. In these cases, knowledge of vegetation characteristics is essential for prediction of the rate of flood level reduction.

The degree of channelization and therefore the capacity of mangroves to reduce flooding depends on the elevation of the vegetation. Mangrove forests that occur at relatively low, frequently inundated elevations are subjected to tidal currents that promote

channelization, which in turn reduces their capacity to mitigate flood water level. Higher elevation mangrove forests are inundated only at peak tide when currents are at a minimum and the sediment regime is depositional. No channel network is created nor maintained, and the capacity of the mangrove forest to reduce flood events is maximized.

4 The Role of Mangroves in Coastal Flood Protection: The Importance of Channelization

4.1 Contribution of Authors

Chapter 4 presents the article "The role of mangroves in coastal flood protection; the importance of channelization", resubmitted to *Estuaries and Coasts* in April 2021. This study investigates the influence of complex bathymetry and vegetation on the capacity of mangroves to provide coastal flood protection. A numerical model of a mangrove forest in Pahoia New Zealand is created and validated with water level and velocity measurements. A simplified numerical model of the Pahoia mangrove forest - removing vertical variations in vegetation density, assuming a sinusoidal M2 period water level boundary condition, and setting channels and vegetated intertidal areas to constant depth – was also developed and compared to water level and velocity data. A series of numerical "experiments" are then performed on the simplified model to investigate the effect of vegetation density, the presence of channels, and different forest slopes on changes in flood attenuation.

The Pahoia dataset was collected during a field experiment in June 2017 which I led as part of my PhD. I performed the data analysis, setup the numerical model, created all figures, and wrote the initial draft of the paper. Co-authors assisted with the field experiment, provided advice and direction with the modelling, and edited drafts.

4.2 Abstract

The historical, present, and projected future risk of coastal flooding necessitates measures to protect coastal communities and environments, including using natural defences such as mangroves. Estimates of extent of flood protection provided by mangrove forests range widely, probably because of differences in growth characteristic of trees combined with variations in local geomorphology in each case study site. Here we use a Delft3D model of a mangrove forest in Tauranga, Aotearoa New Zealand, with vegetation flow resistance parameterized by frontal area, as a basis of idealised scenarios designed to explore and generalise the impact of channels, vegetation density, and forest slope on long wave (surge/tide) attenuation. Previous models often parameterise the frictional effect of mangroves with high bottom friction, which we show using theoretical arguments, becomes increasingly problematic with increased amplitude flood events. However, the contorted forms of the shrubby *Avicenna* mangroves at the field site necessitate new ways to quantify vegetation density more accurately for modelling. Nevertheless, modelling experiments show that vegetation distribution and channelization have a greater impact on flood attenuation than vegetation density, with large events resulting in less attenuation than smaller events due to the increased hydraulic efficiency associated with increased water depth. Additionally, a forest with sloping topography reduces the rate at which long wave attenuation occurs. Implications are that mangroves can be only effective coastal flood protection if the larger scale (forest-scale) distribution of vegetation also contributes to reducing the landward flow of water.

4.3 Introduction

As our climate changes, coastal areas are increasingly threatened by rising water levels and more extreme storm events (*Emanuel*, 2005; *Nicholls and Cazenave*, 2010). Mangroves are salt tolerant plants that exist along sheltered tropical and subtropical coastlines. Positioned at the interface between land and sea, mangroves have been shown to provide shore-protection ecosystem services including stabilization of sediments, dissipation of wave energy, reduced storm winds, reduction of currents, and mitigation of coastal flooding (*Das and Crépin*, 2013; *Guannel et al.*, 2015; *McIvor et al.*, 2012; *Temmerman et al.*, 2013). Although many of the protective benefits of mangrove forests have been well demonstrated, a lack of clear evidence on the interaction between mangroves and storm surge limit the inclusion of management of mangroves in effective planning of coastal flood defence strategies. There are several observations of storm surge propagation in mangroves that show encouraging but varied coastal protection benefits (*Krauss et al.*, 2009; *Montgomery et al.*, 2018). Observed peak water level reduction rates in mangroves have ranged from ~0 to ~50 cm per km of mangrove forest width (*Krauss et al.*, 2009; *McIvor et al.*, 2012; *Montgomery et al.*, 2018). Extrapolating observed flood attenuation rates more widely without a full understanding of the drivers of such variations is problematic; local variations in vegetation, bathymetry, and storm characteristics (which can vary widely (*Alongi*, 2009)) likely play a greater role than assumed.

There are a wide range of laboratory, field and numerical studies to show that vegetation increases hydrodynamic resistance and influences flow across a wide spatial range from stem-scale (*Nepf*, 2012) to forest scale (*Montgomery et al.*, 2018). Individual stems and leaves generate eddies and turbulence resulting in significant temporal and spatial variations in flow. At larger scales, flow heterogeneity is introduced due to vegetation clumps and patches (*Green*, 2005b). At forest scales, flow variation is caused by channels (*Horstman et al.*, 2021) and variations in canopy density (e.g. associated with species distribution). In riverine environments, Nepf (2012) noted that at reach scales flow resistance is better represented by patch distribution than the geometry of individual plants. Similarly, flow resistance at large scales has been shown to primarily be determined by vegetation blockage factor – the proportion of a channel occupied by vegetation (*Green*, 2005b; *Luhar et al.*, 2008; *Nikora et al.*, 2008).

Compounded with these issues of understanding the appropriate scale to model vegetation resistance, is how to incorporate complexity in applied numerical modelling. Applied modelling efforts investigating water level attenuation in mangrove forests often have relied on a bottom friction parameterization for vegetation resistance using a fixed Manning's coefficient. For example, Xu et al. (2010) incorporated the effect of mangroves on numerical simulations of flood levels in Biscayne Bay, Florida during Hurricane Andrew by increasing friction parameterized by Manning's coefficient (set at 0.15) in regions containing vegetation, calibrated to match model results to field data. Similarly, Zhang et al. (2012) used a Manning's coefficient of 0.14 to model the Gulf Coast of Florida during Hurricane Wilma. Zhang et al. (2012) used a slightly reduced Manning's coefficient, compared to Xu et al. (2010), to account for the numerous lakes, rivers, and creeks inside the mangrove forest which provide lower resistance to flow. Although models were calibrated with observational data

and a bottom friction parameterization for flow resistance captures both the water storage and flow resistance of vegetation, using Manning's coefficient is only strictly appropriate when vegetation is a small fraction of water depth (*Gioia and Bombardelli*, 2001; *James et al.*, 2004).

The effect of vegetation drag on long period flow (tidal or storm surge) through mangroves can be explored by examining the balance between friction due to vegetation and pressure gradient. Do do this, the flow resistance is parameterized by frontal area a_v, coefficient of drag C_v, and velocity u_v balanced by sea surface slope $\frac{\partial \eta}{\partial x}$ and gravity g (*Bedient and Huber*, 1992)

$$-g\frac{\partial \eta}{\partial x} = \frac{1}{2}a_v C_v {u_v}^2. \tag{4-1}$$

Similarly, Friedrichs and Madsen (1992) described long period flow in unvegetated shallow channels as a balance between bottom friction and pressure gradient as

$$-g\frac{\partial \eta}{\partial x} = \frac{C_c {u_c}^2}{h_c}, \tag{4-2}$$

with drag as a function of channel velocity u_c, coefficient of drag C_c, and channel depth h_c. The simplified conservation of momentum equations for both regimes, combined with the continuity equation results in a diffusion equation:

$$\frac{\partial \eta}{\partial t} = \frac{\partial}{\partial x}\left(D\frac{\partial \eta}{\partial x}\right). \tag{4-3}$$

With diffusion coefficient for flow through emergent rigid vegetation as

$$D = \eta_v \sqrt{\frac{2g}{a_v C_v \left|\frac{\partial \eta}{\partial x}\right|}}, \tag{4-4}$$

a function of forest water depth (η_v), gravity (g), vegetation frontal density (a_v), coefficient of vegetation drag (C_v), and sea surface slope ($\frac{\partial \eta}{\partial x}$) (*Mullarney and Henderson*, 2018). For channelized flow, the diffusion coefficient

$$D = {\eta_c}^{1.5} \sqrt{\frac{g}{C_c \left|\frac{\partial \eta}{\partial x}\right|}}, \tag{4-5}$$

depends on channel water depth (η_c), gravity (g), dimensionless coefficient of bottom drag (C_c), and sea surface gradient ($\left|\frac{\partial \eta}{\partial x}\right|$) (*Carl T. Friedrichs and Madsen*, 1992).

The effect of drag by mangrove vegetation has previously been incorporated into applied numerical models by representing trees and roots as rigid vertical cylinders (*Mazda et al.*, 1997), with drag parameterized as a function of frontal area density. Simple formulas such as the Baptist method (*Baptist et al.*, 2007), allow a switch from submerged to emerged conditions as water levels change even when models are depth-integrated. In depth integrated models, vegetation resistance and bottom friction are combined to generate a depth varying equivalent Chezy coefficient to represent total flow resistance. Estimating frontal area density in this way assumes that the submerged portion of the tree is well represented by simple shapes (commonly vertical cylinders) which is challenging with more complex vegetation like some species of mangroves. Large variations in plant structure exist within a single mangrove species with plants allocating biomass to maximize uptake of growth limiting factors. Mangroves limited by competition for light are often characterized by relatively simple geometry with tall straight trunks allocating biomass to crown development. Dwarf mangroves are more likely to result from nutrient limitations (*Lovelock et al.*, 2004) and result in complex forms presenting difficulties in quantifying the momentum absorbing area of vegetation.

Mangrove coasts tend to be heterogeneous, with patches of different vegetation species, tidal drainage channels, differences in hypsometries and variations in growth form within the same species. Heterogeneous vegetation distribution in riverine environments has been shown to concentrate flow. Folkard (2011) commented that with vegetation occupying a significant portion of the water column, inside vegetated regions flow is retarded by drag and flow acceleration occurs around vegetation. Similarly, in mangrove forests, unvegetated channels dominate water conveyance relative to flow through the mangroves. The importance of vegetation distribution and channelization on flow resistance in mangrove environments has been demonstrated to play a role in tidal asymmetry and sediment dynamics (*Aucan and Ridd*, 2000; *Horstman et al.*, 2013; *Mazda et al.*, 1995; *Mazda et al.*, 2005; *van Maanen et al.*, 2015), and so should also play a role in surge propagation. Observations by Krauss et al. (2009) of hurricane driven storm surge in the Gulf Coast of the United States noted a larger flood attenuation rate in unchannelized mangroves relative to a site with unvegetated channels. The effect of mangroves on inundation is not attributed solely to the distribution of high–friction areas, the macro-scale features of the bathymetry can also influence flood attenuation, with mangrove forests acting as a water storage mechanism (*Montgomery et al.*, 2019).

Here, we explore the importance of vegetation density, complex bathymetry, and surge amplitude on flow and long wave (tide and surge) attenuation in mangrove forests using idealised numerical modelling. We hypothesize that the catchment-scale features of the drainage network outweigh the details of the vegetation structures on longwave attenuation. We use a depth-integrated validated Delft3D numerical model of a mangrove forest where mangrove form drag is represented within the model using the Baptist method (*Baptist et al.*, 2007). The Baptist formulation allows us to explore the relative differences of bottom versus vegetation drag, and how this may impact the longwave characteristics at higher water levels. One of the problems of idealised modelling is that the number of ways in which the configuration of a system can be manipulated are infinite, particularly when bathymetric

complexity is included. Therefore, our idealised model is based on a natural mangrove forest (Pahoia, Aotearoa New Zealand), where we have collected in situ data to verify our model. Applying the Baptist formulation in Delft3D to a natural setting can be a significant challenge due to the necessity of calculating the frontal area density of mangrove trees, which can be dissimilar to the vertical cylinders on which the method is based. Here we show how the depth-averaged frontal area density can be extracted using a set of easily-obtainable field measurements using a method based on the mechanical design of trees (*Järvelä*, 2004), and we demonstrate that the depth-averaged frontal area density provides acceptable modelling results. We present the model for the Pahoia site first, including a description of verification data and calculation of vegetation parameters, and the idealised modelling thereafter. Our idealised modelling provides critical insight into how the interplay between vegetation distribution and morphology will ultimately control how low-lying coastal environments might behave as sea levels rise and inundation hazard increases.

4.4 Materials and Methods

The idealised numerical modelling scenarios are based on simplified versions of a natural setting. To ensure that the model is based on real flows, the model is set up to replicate observations collected at the site. Therefore, initially, a depth-averaged numerical model of the Pahoia mangrove forest was developed and verified with water level and water velocity data (data collection and model validation discussed below). From this 'real' model ("the Pahoia model"), a simplified base case was created by removing small local complexities in the model such as flattening the forest floor, removing pneumatophores, and simplifying the water level boundary condition. This simplified base case numerical model is then manipulated by changing the vegetation density, removing channels, and changing the slope of the forest floor.

The series of idealised model "experiments" were designed to explore the importance of vegetation and channels on flow pathways. Scenarios were compared with respect to flow pathways and water level attenuation in mangrove forests. The importance of channels in water conveyance through mangrove forests was investigated by removing channels from the model and varying forcing amplitude. The model without channels was subjected to varying amplitude water level forcing to demonstrate the importance of water level on flow conveyance and flood attenuation capacity of the forest. Finally, we modified the bathymetry of the model without channels to a gradually sloping vegetated intertidal to show the interaction between water storage and water conveyance in the attenuation of long period waves in mangrove forests.

Tides and storm surges are long waves (long wavelength relative to water depth) are friction dominated in shallow nearshore environments (*C. T. Friedrichs and Aubrey*, 1988; *LeBlond*, 1978; *Montgomery et al.*, 2019). In Tauranga, tidal flow dominates storm driven flow as spring tides have a range of ~1.6 m and storm surge rarely exceed 0.5 m (*Bell et al.*, 2000; *Heath*, 1985). Therefore, we assume that vegetation and nearshore bathymetry will influence storm surge and tidal flow similarly. The numerical model is validated with data collected during typical tides and the hydrodynamic impact of changes in nearshore bathymetry,

vegetation characteristics, and inundation amplitude on flow routing and attenuation are assumed to be applicable to both tidal flows and storm surge.

4.4.1 Pahoia Study Site

The Tauranga estuary is located on the east coast of the North Island of New Zealand. The estuary is a mesotidal barrier-enclosed lagoon with two inlets and is comprised of many smaller sub-estuarine basins (*de Ruiter et al.*, 2017). The estuary is primarily intertidal with ~2/3 of the estuary above the low tide waterline (*Healy et al.*, 1996). Mangroves in Tauranga are at the edge of their latitudinal range and are typically short dwarf shrub-like plants. They have recently expanded from 13 hectares in 1940 to 168 hectares in 1999 (*Park*, 2004). Here we focus on a sub-estuarine basin to the north of Pahoia in the central area of Tauranga harbour (Figure 4-1), which is dominated by a single species of shrubby grey mangroves (*Avicennia marina*). Tides in Tauranga are mixed semi-diurnal dominated by the M2 constituent. Tidal range varies throughout the estuary, but mean spring tidal range is ~1.62 m and neap tide range is ~1.24 m (*Heath*, 1985). Storm surges in Tauranga are relatively small compared to international events and have never exceeded 1 m (*de Lange and Gibb*, 2000).

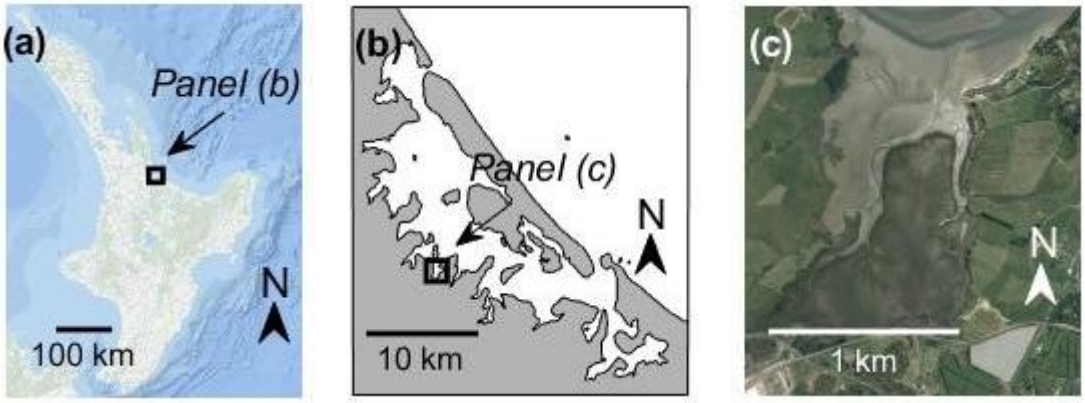

Figure 4-1: (a) The North Island of New Zealand. (b) Tauranga harbour. (c) Pahoia sub estuary (photo source: Google Earth).

The Pahoia sub-estuary is dominated by a ~1km long central mangrove forest. The topography of the forest was compiled from LiDAR flown in 2015, provided by the Bay of Plenty Regional Council, and a RTK-GPS survey undertaken in 2017 (Montgomery et al., 2018). The vegetated regions have nearly constant bathymetry and are at approximately the same elevation as peak neap tide (0.6 m above mean sea level datum). Steep-sided unvegetated channels exist on both the east and west sides of the main central forest. An unvegetated tidal flat exists northwest of the main forest (Figure 4-1c). The western channel has multiple branches that extend partially into the central mangroves. The elevation of all the channels is nearly constant at -0.6 m relative to mean sea level datum and channel width gradually decreases with distances into the forest (Figure 4-2).

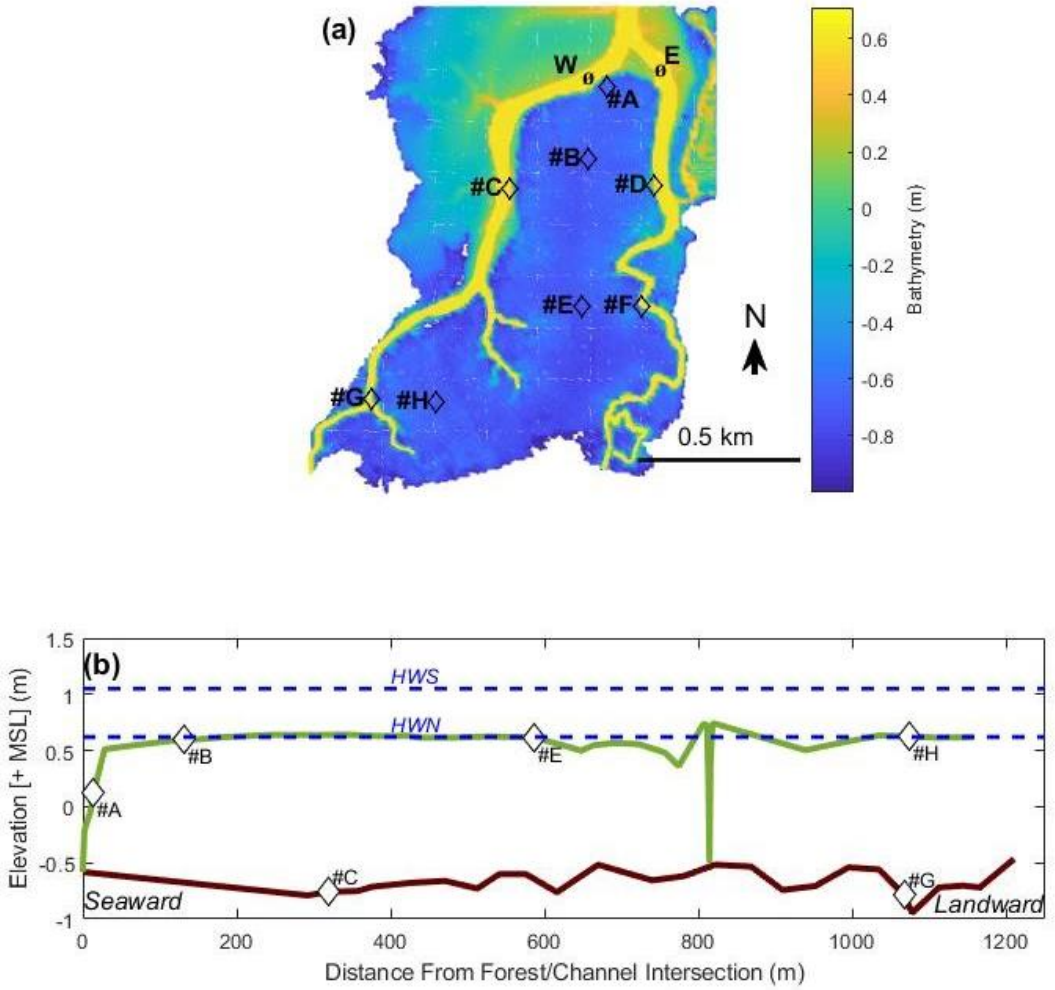

Figure 4-2: (a) Pahoia bathymetry developed from LiDAR data and RTK GPS survey for subtidal channels. Location of pressure sensors (#A-#H) and velocimeters (W and E) are indicated. (b) Pahoia RTK survey of the west channel thalweg (brown) and central mangrove transect (green). Mean High Water spring (HWS) and Mean High Water Neap (HWN) tide elevations are detailed (dashed blue). Water pressure sensors locations are marked with diamonds.

4.4.2 Pahoia Model Development

A computational grid of 2 m × 2 m cells over the width of the area of interest and extending 1 km seaward of the forest was developed. Grid cell size was selected to facilitate resolution of the smallest channels bisecting the mangrove forest. Validation of the model was accomplished by comparing model outputs with water level and velocity data collected on June 22, 2017. The model boundary was forced with data from a water level sensor ~250 m seaward of the Pahoia mangrove forest.

4.4.2.1 Bathymetry

Model bathymetry was primarily generated with the 2015 LiDAR survey (Figure 4-2a). To remove erroneous elevation values, assumed to be false returns of the vegetation canopy, the area of interest was divided into 10 m by 10 m grids and assigned an elevation of the minimum value occurring within each grid cell. The creek channels are subtidal and therefore LiDAR data could not be used to determine channel depths. A limited RTK elevation survey was performed during a 2017 field effort using a Leica GS18 T GNSS system. The RTK survey consisted of an elevation profile along the western creek thalweg and a single transect

through the central mangrove forest (Figure 4-2b). In the RTK survey, the west creek thalweg was found to be of near constant depth (-0.66 ± 0.12 m +MSL) and the vegetated mangrove platform was at near constant depth (+0.60 ± 0.08 m +MSL). Observations indicated that channel/vegetation platform boundaries are near vertical; therefore, LiDAR data were used to identify channel locations and assigned a constant value of -0.6 m relative to mean sea level. The local topography outside of the mangrove forest and channels is relatively steep and therefore the modelled area of interest was not extended beyond the forest/channel environment that is wetted during typical high tides.

4.4.2.2 Vegetation Density

Mangroves are often modelled as rigid vertical cylinders (*Horstman et al.*, 2015; *Nepf*, 1999) with hydrodynamic drag force per fluid mass (F_c) estimated as a function of fluid density (ρ), vegetation reference area (A_p), drag coefficient (C_D), and fluid velocity (u) (*Nepf*, 2004):

$$F_C = \frac{1}{2}\rho A_p C_D |u| u. \tag{4-6}$$

When modelling vegetation as rigid vertical cylinders, Nepf (2004) assigned the vegetation frontal area density, the plant area perpendicular to flow per unit volume, as the reference area in Eq. 4-6. Determining the reference area for tall straight trees (where the vegetation emerges from the flow) can be approximated using measurements of stem diameter and tree count for a representative area. The complex vegetation of the dwarf mangroves at the study site (Figure 4-3) made estimating vegetation density highly challenging. Here, we use a method developed by Järvelä (2004) based on the mechanical design of trees to estimate the momentum absorbing area of mangrove trees at our study site.

Flow resistance of vegetation was parameterized in the depth integrated Delft3D numerical model as increased bed roughness using a modified Chezy value (*Baptist et al.*, 2007) and updated every time step. An equivalent Chezy (C_{eq}) value was calculated to capture the combined flow resistance of emergent trees, submerged pneumatophores, and bed roughness – parameterized as a Chezy coefficient (C_b, set as 65 $m^{1/2}/s$):

$$\frac{1}{C_{eq}} = \frac{1}{\sqrt{\frac{1}{C_b^2} + \frac{C_{d_p} A_p h_p}{2g} + \frac{C_{d_T} A_T h}{2g}}}. \tag{4-7}$$

Pneumatophores are modelled as rigid vertical cylinders with drag parameterized by coefficient of drag C_{d_p} (set as 1), gravity (g), and frontal area density (A_P=nd). Frontal area density is estimated as the product of pneumatophore density (n) and average pneumatophore diameter (d) (*Klaassen and Van der Zwaard*, 1974). Pneumatophore density is the average number of pneumatophores per square meter in the survey area. Note that h_p is the lesser of pneumatophore height and water level (h). Average pneumatophore height is 7.9 cm, with average diameter of 0.6 cm, and density of 278 per m^2, resulting in a frontal area density of 1.67 m^{-1}. Flow resistance of emergent trees is parameterized by depth averaged frontal area density (A_t, selected from Table 4-2) and a coefficient of drag (C_{d_T}) set as 1. The

coefficient of drag for both pneumatophores and branches are set to 1, as both structures are approximated as rigid cylinders. Cheng (2013) determined that coefficient of drag for cylinders is ~1 across a wide range of Reynolds numbers. Bottom friction in the absence of vegetation was parameterized with a fixed Manning's coefficient, set at 0.02 s/$m^{1/3}$.

Pneumatophores, small aerial roots extending vertically from the ground, are reasonably approximated as rigid cylinders for hydrodynamic purposes. Pneumatophore characteristics were measured in 0.25 m $\times$ 0.25 m quadrats every 5 metres along one lengthwise and one width wise transect. In each quadrat, all pneumatophores were counted, and the length and width of the top, middle and bottom of 5 pneumatophores were measured (see Montgomery et al., (2018)) .

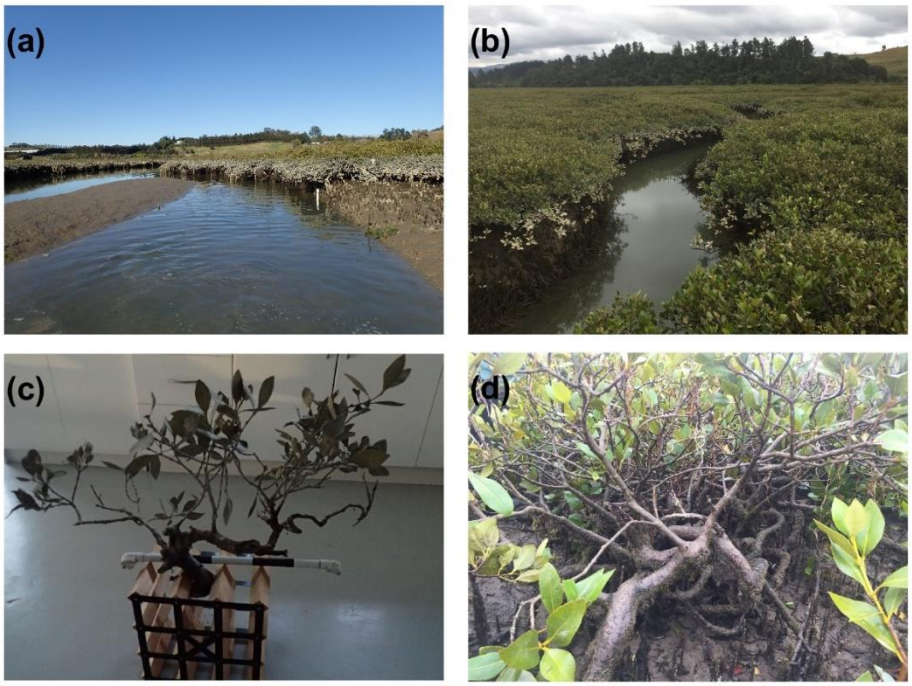

Figure 4-3: (a) Large channel in Pahoia displaying lack of vegetation and steep sided banks. (b) Small unvegetated Pahoia channel. (c) Individual dwarf mangrove tree removed from the site (graduations on the scale are ~10cm). (d) Image of Pahoia mangroves taken in situ below the canopy.

For the trees, the Järvelä (2004) method uses the dimensions of the main stem to calculate the frontal area of the tree by summing over the contribution of each order, where the smallest order are the branches with leaves, and the largest order is the main trunk of the tree. The method relies on the trees being self-similar and having consistent changes in branch diameter *D*, length *L*, and number *N*, between branch orders. The Strahler (1957) stream ordering scheme is used to describe the branching structure of trees (*McMahon and Kronauer*, 1976). The smallest leaf supporting branches are given order 1. The junction of two branches of order *m* results in a branch of order *m+1*. The junction of two branches of unequal order does not alter the order of the larger branch. In this method a tree species can be described by four tree structure parameters (*McMahon and Kronauer*, 1976): branching ratio R_B (number of order *m* branches supported by a branch of order *m+1*) , diameter ratio R_D (ratio of *m+1* diameter branch to *m* branch), length ratio R_L (ratio of *m+1* branch length to *m* branch length), and average diameter of the smallest (leaf bearing) branches D_{min}.

$$R_B = \frac{N_m}{N_{m+1}} \quad (4\text{-}8)$$

$$R_D = \frac{d_{m+1}}{d_m} \quad (4\text{-}9)$$

$$R_L = \frac{L_{m+1}}{L_m} \quad (4\text{-}10)$$

McMahon and Kronauer (1976) demonstrated that trees maintain elastic similarity and the branching pattern within any tree species is self-similar and can therefore be used to describe any tree (or part of the tree) of that species. Trees have been shown to follow the principle of elastic similarity, in that the distance any branch deflects under its own weight is a constant fraction of the branch length (*McMahon*, 1975; *McMahon and Kronauer*, 1976). Therefore, longer branches are proportionally thicker than short branches and maintain a constant safety factor against buckling under their own weight (*Norberg*, 1988).

The tree structure parameters (branching ratio, diameter ratio, length ratio, and minimum branch diameter) were determined by measuring six individual mangrove trees in each of three separate regions of the study site (interior, creek fringe, and tall creek fringe plants) (Table 4-1). Mangrove branch diameters displayed a relatively consistent ratio between consecutive branch orders and little variation of diameter for a given order (Figure 4-4a). Although branch order number generally decreased with elevation above sediment, large variability in elevation for a given branch order is evident. Branch angle relative to vertical was highly variable but increased locally at around 100 mm above the sediment level (Figure 4-4b). Additionally, the length between consecutive branch orders had large variation but decreased with height after reaching a local maximum at ~200 mm from the sediment level (Figure 4-4c). The local increase in length and orientation at around 100-200 mm off the bed level is likely due to the effect of 'canopy plasticity' that occurs in mangroves, which causes canopies to be displaced sideways to enhance competition for light (*Peters et al.*, 2014). For elastically similar beams, McMahon (1975) determined that $R_L \sim R_D^{2/3}$. Due to the high variability of the length ratio in our measurements (standard deviation ~ length) we use a length ration (R_L) based on a function of diameter ratio in our estimate of vegetation density.

Table 4-1: Tree structure parameters used in Equations 4-8 to 4-10.

Location	Branching ratio R_B	Diameter Ratio R_D	Length Ratio R_L	MINIMUM BRANCH DIAMETER D_{MIN} (MM)
Interior Forest	3.4	1.6	1.5	4.1

Fringe	3.0	1.6	2.0	3.3
Tall Fringe	2.8	1.6	1.6	3.4
Average	3.0 (+/- 1.0)	1.6 (+/-0.3)	1.7 (+/-1.6)	3.6 (+/-0.4)

Describing the structure of an individual plant requires the measurement of diameter and length of the highest order tree segment (trunk). An iterative process is then used to calculate the number, length, and diameter of subsequently lower order tree segments until further reducing segment diameter results in a branch that is smaller than the minimum diameter tree structure parameter D_{min}. The total momentum absorbing area of the tree is computed by summing up the cross-sectional area of all tree sections. Due to the high variation in vertical distribution of vegetation and small tree heights, we assumed the momentum absorbing area was evenly distributed over the height of the tree.

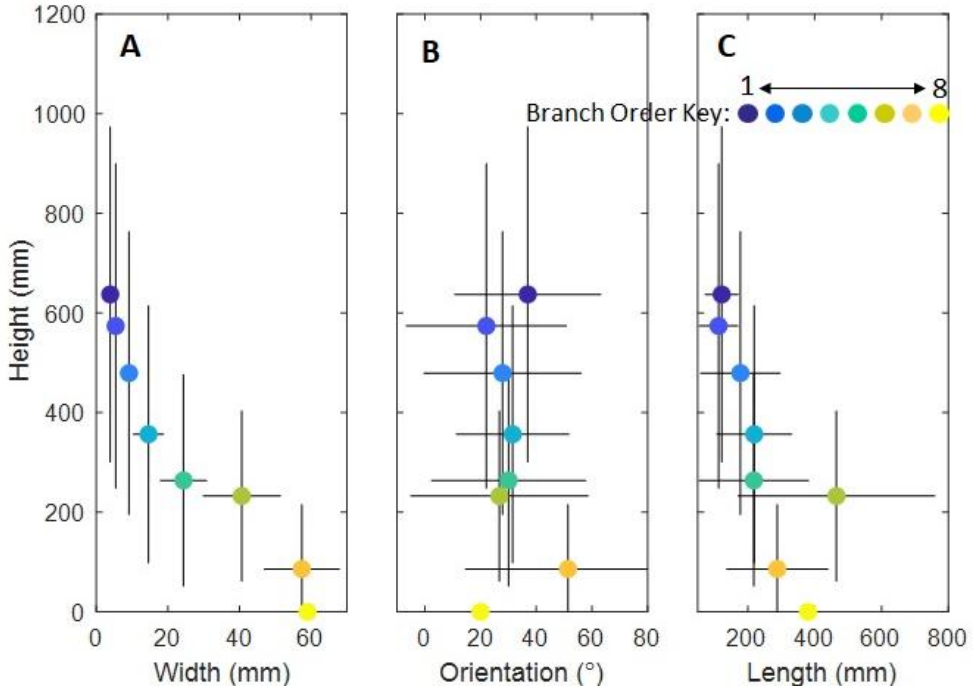

Figure 4-4: (a) Width and elevation above sediment for all branch orders (shown with standard deviations). (b) Angle of orientation (with respect to vertical) and elevation of branches. (c) Length and elevation of mangrove branch orders. Bars indicate the standard deviation of the 18 samples (6 for each of 3 regions).

The iterative process described above was performed for every tree in a 10 m^2 area at each of the three locations used to generate the tree structure parameters (interior, creek fringe, and tall creek fringe), and a summary of the results is presented in Table 4-2. Note that the depth averaged frontal area density displayed in Table 4-2 was computed by normalizing the frontal area by the canopy height and represents an average value over the height of trees, excluding pneumatophores. Canopy height is the average elevation of the foliage above the ground, approximated with a graduated staff. Pneumatophores are reasonably approximated as vertical rigid cylinders; therefore, measuring and estimating frontal area density was straightforward. Details of the pneumatophore survey is presented in Montgomery et al. (2018). Västilä and Järvelä (2014) estimated the total flow resistance of vegetation using linear superposition of the flexible foliage and rigid stalks. However, for

flexible vegetation the relationship between drag force and velocity is better represented by a linear relationship than a squared relationship (as in Eq. 4-6) (*Armanini et al.*, 2005; *Wilson et al.*, 2008). Additionally, Jalonen and Järvelä (2014) determined that at low flow velocities the drag of foliated vegetation can be less than the same vegetation in a defoliated condition due to reconfiguration of the branches caused by leaf mass. Due to complexity in estimating flow resistance of flexible vegetation and uncertainty in the interaction between flexible and rigid vegetation, here flow resistance of the flexible leafy tree components was ignored for simplicity. If model verification proved that our approach to characterise vegetation was unsuccessful, we would have explored the contribution of leaves in more detail. Vegetated locations were identified by inspection of satellite images (Figure 4-5a) and modelled as in Figure 4-5b.

Table 4-2: Tree statistics for each 10 m^2 survey area.

LOCATION	TREE CANOPY HEIGHT	NUMBER OF TREES	AVG. TRUNK DIAMETER	AVG. TRUNK LENGTH	DEPTH AVERAGED FRONTAL AREA DENSITY (A_T)
	(cm)		(mm)	(mm)	(m^{-1})
INTERIOR FOREST	43	43	24 (+/- 13.4)	152 (+/- 55.7)	0.41
FRINGE	78	13	52 (+/- 24)	164 (+/- 231)	0.29
TALL FRINGE	124	17	55 (+/- 16)	437 (+/- 307)	0.50
AVERAGE					0.40

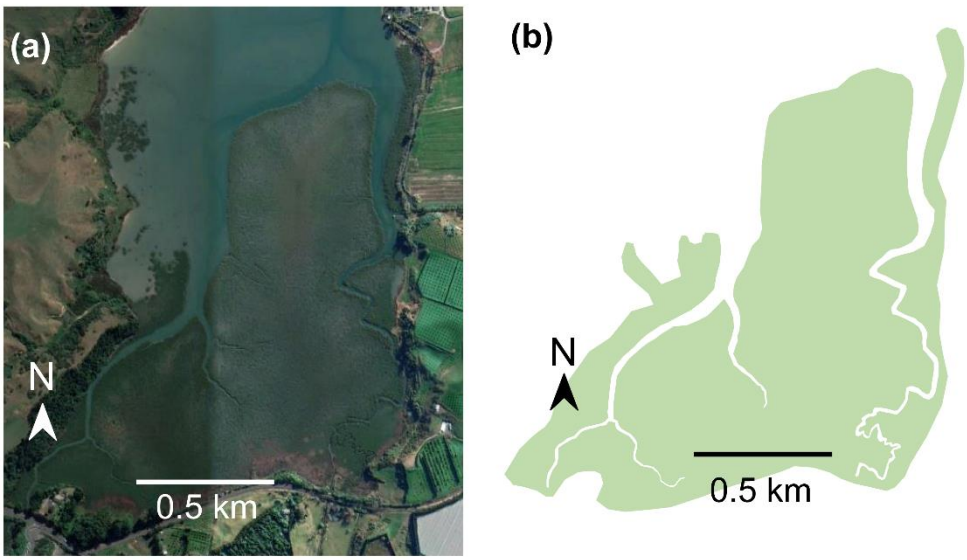

Figure 4-5: (a) Satellite image of Pahoia showing vegetation distribution and unvegetated channel network (Google Earth). (b) Modelled vegetation distribution (green shading).

4.4.3 Observations

An array of pressure sensors was deployed in the Pahoia basin in June 2017 (Figure 4-2). Station #A is at the northern edge of the mangrove forest with stations #B, #E, and #H located in a transect along the mangrove platform. Two additional gauges (#C and #G) were

deployed in the western channel and two gauges in the eastern channel (#D and #F). Data were corrected for variations in barometric pressure and sensor temperature dependence and smoothed using a low-pass filter. Pressure data was converted to water level assuming a constant water density of 1025 kg/m^3, and water elevation was referenced to a mean sea level datum using RTK survey data. Additional details on instrument setup, data processing, and measurement uncertainty is provided in Montgomery et al. (2018).

Instruments were deployed during a two-week field study in June 2017. During the deployment, peak water levels varied from ~80 cm + MSL to 125 cm +MSL. Here we present data from June 22, 2017 during a 1m + MSL tidal cycle (Figure 4-6). Note that no reduction in amplitude nor temporal delay of the inundation wave occurred throughout the study site.

Nortek Vector velocimeters were deployed in both the east and west channel at the outer boundary of the mangrove forest (see Figure 4-2 for instrument locations). Instruments recorded at a sampling rate of 8 Hz and nominal velocity range of 1 m/s. Several tidal cycles are presented in a tidal stage plot in Figure 4-7. Note that due to Ulva (sea lettuce) fouling the velocimeter, the velocity data does not correspond to the time period as the water depth data in Figure 4-6. The tidal stage plots (Figure 4-7) depict water level and velocity measurements of three tidal cycles with a peak water level of 0.8, 1.0, and 1.2 m above mean sea level. Although the water level data displayed in Figure 4-6 does not correspond to the same tidal cycle in which the water velocity data was captured, hydrodynamic conditions for the 1.0 m amplitude tides used to generate the water level data and tide stage plots are similar.

4.5 Results

4.5.1 Pahoia Model Development

Water level data and model results are shown for comparison in Figure 4-6 with instrument locations shown in Figure 4-2a. The model accurately reproduces the lack of water level reduction along the channel and through the forest with an average of 0.064 m RMS error. Also, the model generally replicates the complex shape of the inundation signal at all instrument locations. The model does not fully replicate the inundation pattern at instrument #G (far up the western channel) with the model showing a slightly delayed inundation pattern relative to the data; however, the timing and amplitude of peak water level is accurately reproduced. Additionally, the model predicts slower decay at the end of the ebb tide for water level sensors in the mangrove forest (instruments #B, #E, and # H in Figure 4-6 panels b, e, and h respectively). The slower decay of the water level signature in the model is attributed to the grid resolution and the instruments recording data a finite distance above the bed (varying by instrument, but ~ order of centimetres). A constant elevation is assigned to each grid in the model (2 m x 2 m) and results in slow draining of cells as water level recedes and depth approaches the wet/dry threshold (set as 2 cm).

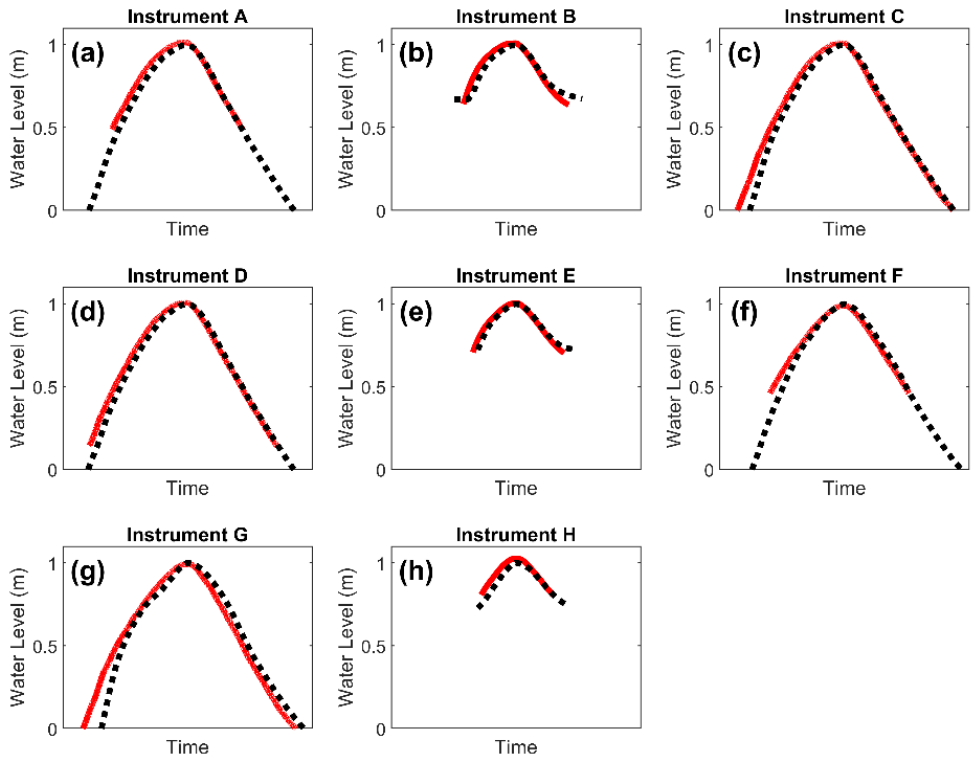

Figure 4-6: (a)-(h) Pahoia water level data (red line) and model results (black dashed line) for instruments A-H. Data is from a 1 m +MSL tide June 22, 2017. Model was forced with a water level boundary condition from an instrument located ~ 250 m seaward of the mangrove forest. Instrument locations correspond to locations identified in Figure 4-2a.

Water velocity data collected during the 2017 field study were used to generate tide stage plots to further validate the model (Figure 4-7). Water velocity data were only collected at two locations in the channels, marked in Figure 4-2a. The model accurately predicted the shape of the flood and ebb stages in the western channel (Figure 4-7a) with peak flood velocities occurring near mean water level and relatively constant flood velocities when water depth is above the mangrove forest elevation (0.6 m +MLS). The model accurately replicated that peak ebb velocities occur at slightly lower water levels; however, water velocities were under predicted by the model. The model did not reproduce the tide stage plot in eastern channel (Figure 4-7b) as accurately as the western channel. In the eastern channel the model reproduced that maximum flood and ebb velocities occurred at water levels below mean sea level; however, the model underpredicted the velocities and that velocities would be greatest at the lowest recorded water levels. The model reproduced that water velocity would be ~constant for much of the tide stage above 0.3 m; however, the model did not reproduce that water velocities approach zero near mean sea level during the flood tide stage. Note that due to the mounting configuration of the velocimeters, no data are available at water levels less than ~-0.4 m MSL.

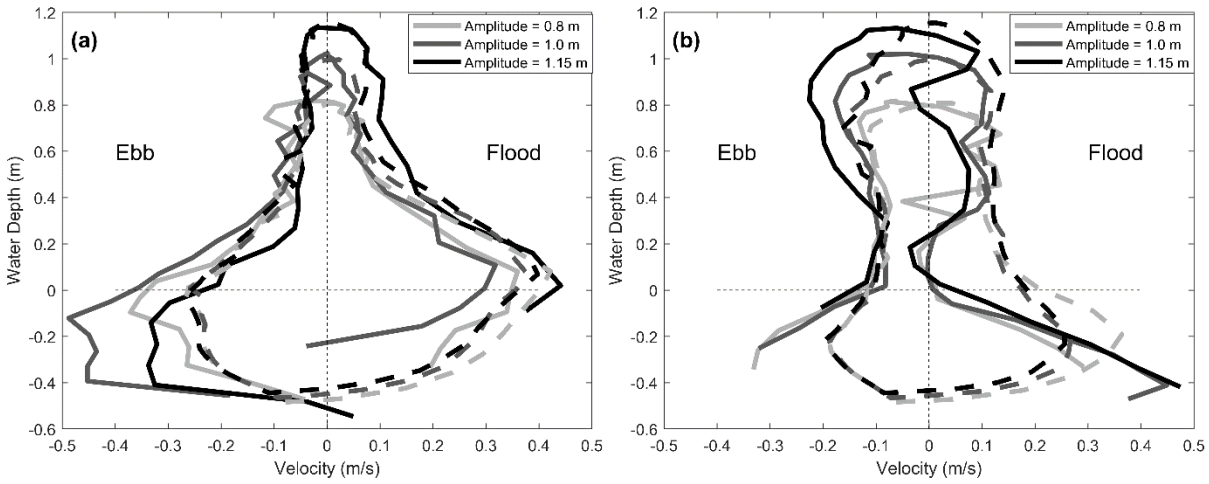

Figure 4-7: (a) Tide stage plot at the western channel velocimeter (location identified in Figure 4-2a) for 3 tidal cycles of varying amplitude forcing (solid lines) and model forced with a water level boundary condition from corresponding tide cycles (dashed). (b) Tide stage plot at the eastern channel velocimeter (location identified in Figure 4-2a) for the same 3 tidal cycles as panel (a) comparing data (solid lines) and model results (dashed lines). Note that data are from non-consecutive tide cycles because segments of the timeseries were discarded because of biofouling.

Figure 4-8 displays modelled depth averaged water velocity (panel a), water flux per unit width (panel c), and sea surface elevation (panel e) as water enters the forest from the channels during a 1 m amplitude tide. Water flux Q is the product of depth averaged velocity u and water depth h: $Q = u\,h$. The deeply incised channels in Pahoia are ~1.2 m deeper than the mangrove flats (Figure 4-2b). With depth averaged channel velocities exceeding forest flow velocities, water flux through channels per unit width greatly exceeds water flux through the forest due to both the greater channel depth and larger velocities. Water velocity, water flux, and sea surface elevation are shown for a greater water depth later in the flood stage in Figure 4-8 b, d, and f respectively. At all flood stages, velocity in the channel is larger than velocity through the vegetation. Note that water flux earlier in the flood cycle (Figure 4-8c) is similar to flux later in the tidal cycle (Figure 4-8d) although sea surface gradients driving flow early in the tidal cycle are ~double gradients later in the flood tide (Figure 4-8e & Figure 4-8f).

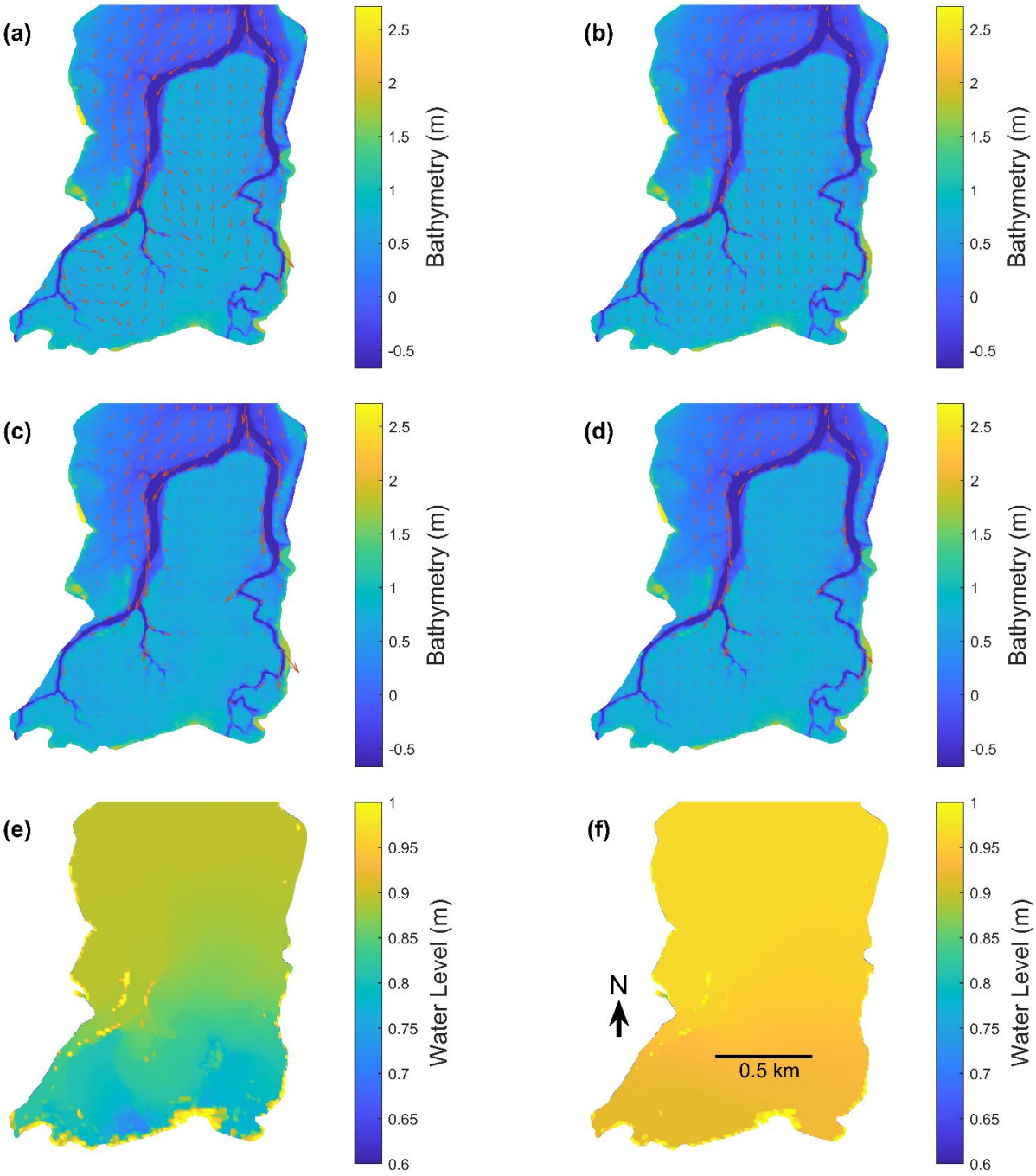

Figure 4-8: (a) Water velocity, (c) water flux, and (e) sea surface elevation as water first enters the mangrove forest, ~75 minutes before peak tide. (b) Water velocity, (d) water flux, and (f) sea surface elevation ~30 minutes before peak tide. Note that all subfigures have the same orientation and scale, shown in panel (f).

4.5.2 Idealized Model

To generalize the model into a "base case" for scenarios, we simplified the bathymetry by setting the vegetated areas to a fixed elevation of 0.6 m + MSL and extending the vegetation to the first channel bifurcation (see Figure 4-9). Vegetation was simplified by removing pneumatophores, to allow assigned vegetation properties to be constant with depth to not conflate variations in vertical distribution of vegetation with the influence of water depth on flow conveyance. Additionally, water level forcing at the open boundary was

simplified to the dominant tidal constituent, a 1m M2 tide, for simplicity and to allow for synthetic boundary conditions of varying amplitude to be easily developed.

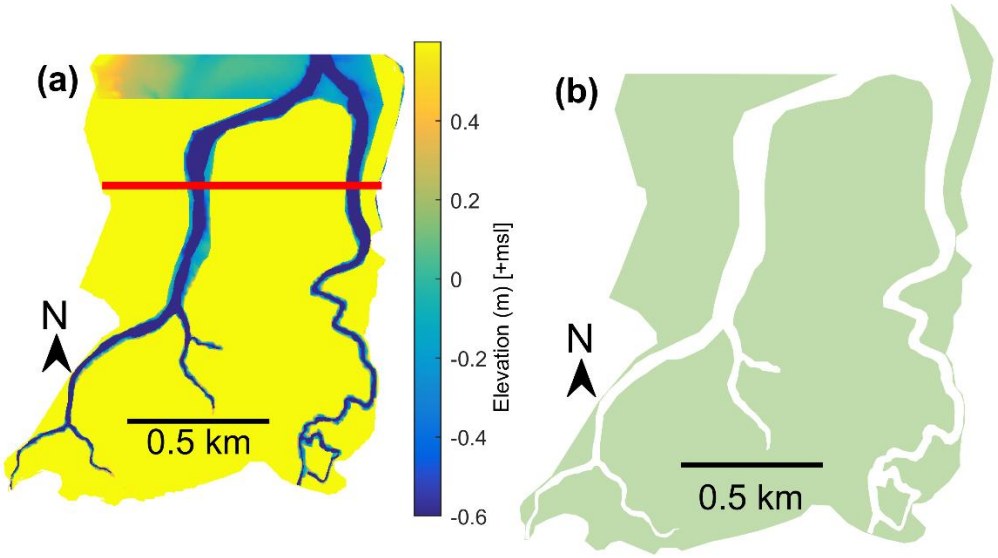

Figure 4-9: (a) Simplified bathymetry for idealized model. All vegetated regions are set to fixed elevation of 0.6m +msl. Transect for comparison of water velocity and transverse elevation in Figure 4-12 (red). (b) Vegetated regions (green) for idealized model.

To show that simplifications do not create substantial changes to model behaviour, a comparison of water level data from June 22, 2017 and the simplified model is presented in Figure 4-10 for the 8 sensor locations identified in Figure 4-2b. The open water boundary condition in the model was temporally aligned with the field data by setting peak water level to be concurrent. Note that although the model still reproduced the maximum tidal elevation, it does not reproduce the shape of the inundation patterns as accurately as the more complex model (presented in Figure 4-6). The average RMS error between the simplified model and observed water level for the 8 sensors is ~0.1 m, compared to ~0.06 m that for the more complex model. The rate of flood and ebb tide occurs too rapidly in the model, evident at instrument #C, #D, and #G in Figure 4-10 c, d, and g respectively, and is primarily attributed to the simplified M2 water level boundary condition. Additionally, the model predicts complex curvature of the inundation signal, particularly at channel instrument location #G – and locations #C and #F to a lesser extent. The complex curvature of the model water level signal is attributed to a combination of the simplified bathymetry (constant elevation mangrove platform at 0.6m +msl) and lack of pneumatophores that results in a rapid change in the rate of inundation as water enters the forest.

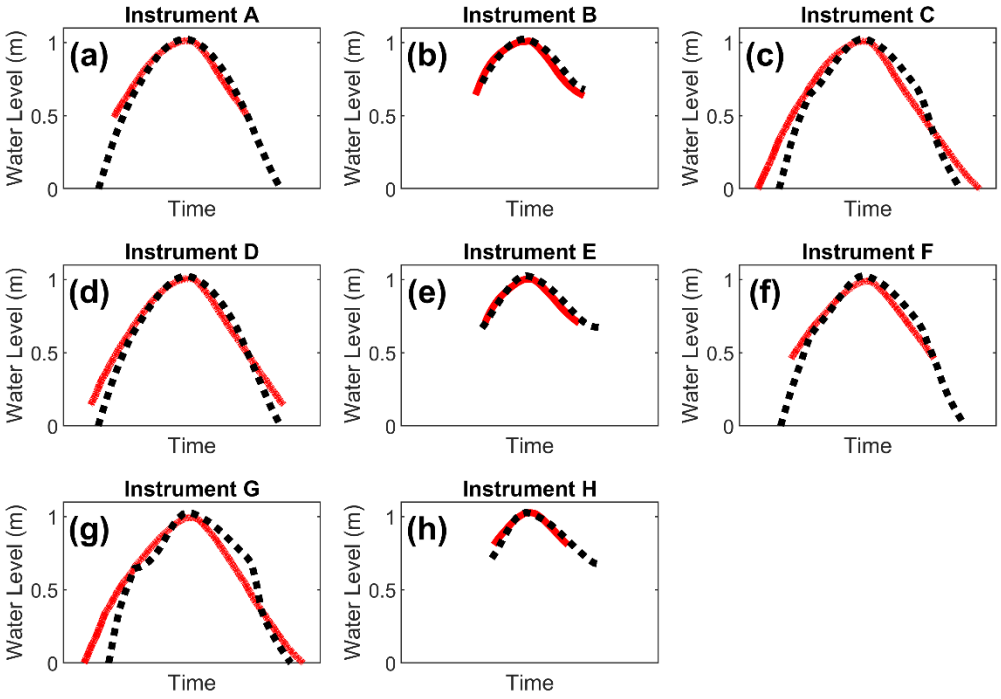

Figure 4-10: (a)-(h) Pahoia water level data (red line) and results from an idealized model (black dashed line) for instruments in west channel. Data is from a 1 m +MSL tide June 22, 2017. Model was forced with a 1 m M2 water level boundary. Instrument locations correspond to locations identified in Figure 4-2a.

Tide stage plots for the simplified model were compared to data collected during the 2017 field study for the E and W locations identified in Figure 4-2b (Figure 4-11). The model replicated the shape of the flood stage for the W location (Figure 4-11a), but less accurately replicated the ebb portion of the tide stage plot. The model predicted a large velocity as water drained off the flat vegetated platform (below 0.6 m) and under predicted velocities at water levels below mean sea level. At the E location (Figure 4-11b) the model generally reproduces the observed tide stage, although the model predicts the flood velocity peak to occur at a slightly higher water level than the data displays and does not capture the low velocity at water levels just above mean sea level. The model reproduces much of the ebb tide stage accurately but fails to capture the magnitude of the ebb flow below mean sea level.

The simplified model does not capture the water level and velocity data as accurately as the more complex model (Figure 4-6 and Figure 4-7 compared to Figure 4-10 and Figure 4-11). However, the simplified model does capture much of the important observed water level dynamics (no temporal delay in peak water level across the instrument locations and no reduction in peak water level) and key aspects of the flood tide stage plots. Therefore, we use perturbations to the simplified model to explore the importance of vegetation density, channelization, and sloped bathymetry on flooding through mangrove forests.

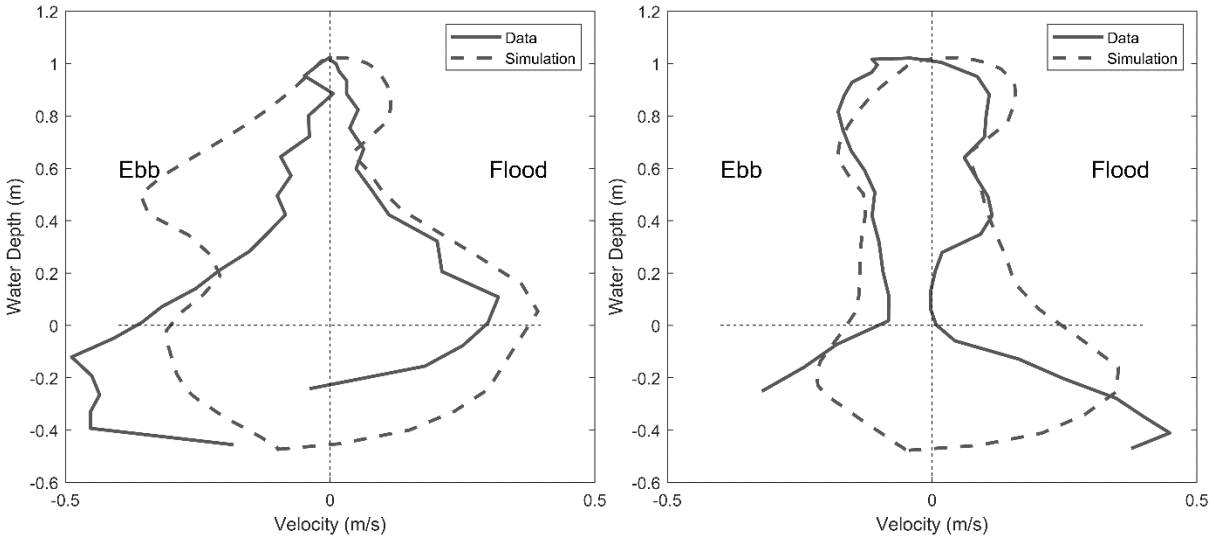

Figure 4-11: a) Tide stage plot at the western channel velocimeter (identified in Figure 4-2a) for 1 m amplitude tide with observations (solid line) and idealized model (dashed line). b) Tide stage plot at the eastern channel velocimeter (identified in Figure 4-2a) for 1 m amplitude tide with observations (solid line) and idealized model (dashed line).

4.5.3 Idealised Model Perturbations

The importance of vegetation density on flow routing and long wave attenuation in mangrove forests is investigated by increasing the tree frontal area density of the simplified model four-fold and forcing the model with a 1 m amplitude M2 tidal signal. Despite the large increase in vegetation density, no reduction in peak water elevation nor temporal delay in the inundation signal occurred across the domain (not shown). However, flow velocities in the forest were reduced for the increased vegetation density model (Figure 4-12a). Figure 4-12 shows flow at a transect given in Figure 4-9; the location was chosen because the channels are well within the mangroves, but the location is before complex bifurcations occur and sinuosity increases. In channel velocities were similar between the two models with widely varying vegetation density.

As water enters the forest, water surface elevation in the channels is higher than in the surrounding mangroves and further south in the domain, driving flow both along the channel and into the forest. At low water levels, sea surface gradients perpendicular to the channel into the forest are larger than later in the flood tide at higher water levels (Figure 4-12b). In flows dominated by vegetation resistance, velocities are independent of depth and are a function of sea surface gradient only (e.g. Eq. 4-1); therefore, large sea surface gradients in Figure 4-12b correspond to large flow velocities perpendicular to the channel in Figure 4-12c. As water depths increase, sea surface gradients and velocities decrease (Figure 4-12 b/c). However, water flux through the vegetation perpendicular to the channel is proportional to water depth and the decreased sea surface gradients and velocities do not necessarily mean a decrease in flow conveyance.

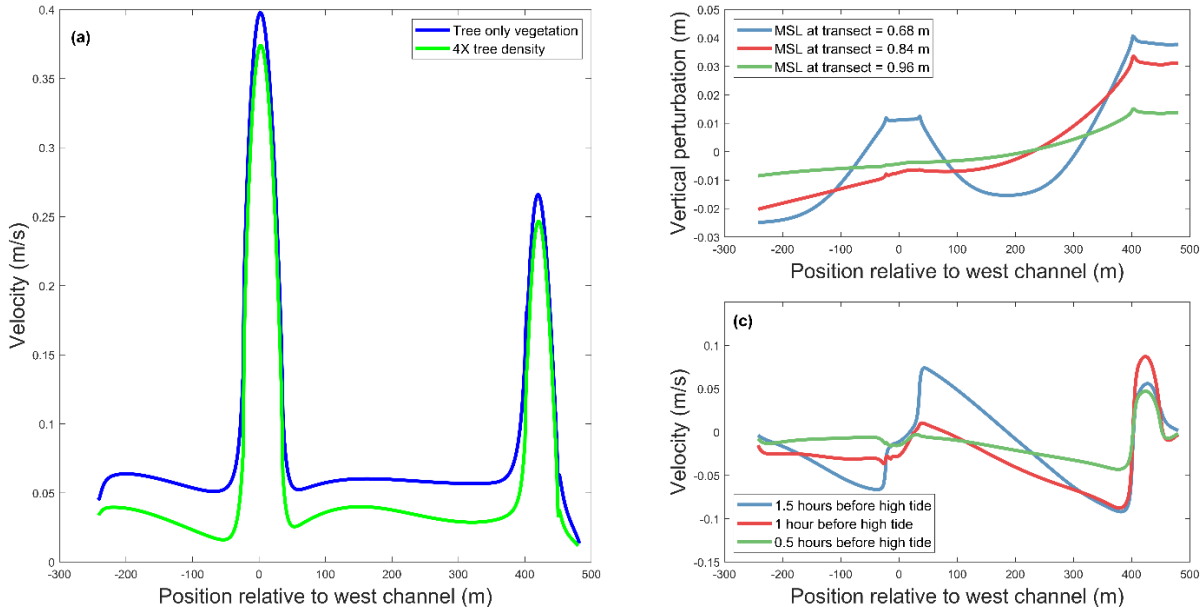

Figure 4-12: (a) Along channel flood velocity 1 hour before peak tide at transect location indicated in Figure 4-9a. The blue line represents the simplified model, the green line represents the simplified model but with the vegetation density increased four-fold. (b) Water surface elevation perturbation of simplified model from MSL along transect ~1.5 hours (blue), ~1 hour (red), and ~0.5 hours (green) before high tide. (c) Water velocity component perpendicular to the channel at transect location indicated in Figure 4-9a ~1.5 hours (blue), ~1 hour (red), and ~0.5 hours (green) before high tide. Note: water elevations in panel (b) and velocities detailed in panel (c) are for corresponding elevations/times.

To investigate the importance of channels on flow routing and long wave attenuation in mangrove forests, the simplified numerical model was modified to remove channels and forced with a 1 m amplitude M2 period wave, and results are shown in Figure 4-13a. In contrast to the simplified model with channels, attenuation of the peak water level occurred over the width of the mangrove forest. Without channels to convey fluid efficiently landward, all water entering the forest is forced to flow through the vegetation. Mangroves restrict

landward water flow delaying the inundation signal and reducing peak water level with distance into the forest (Figure 4-13a).

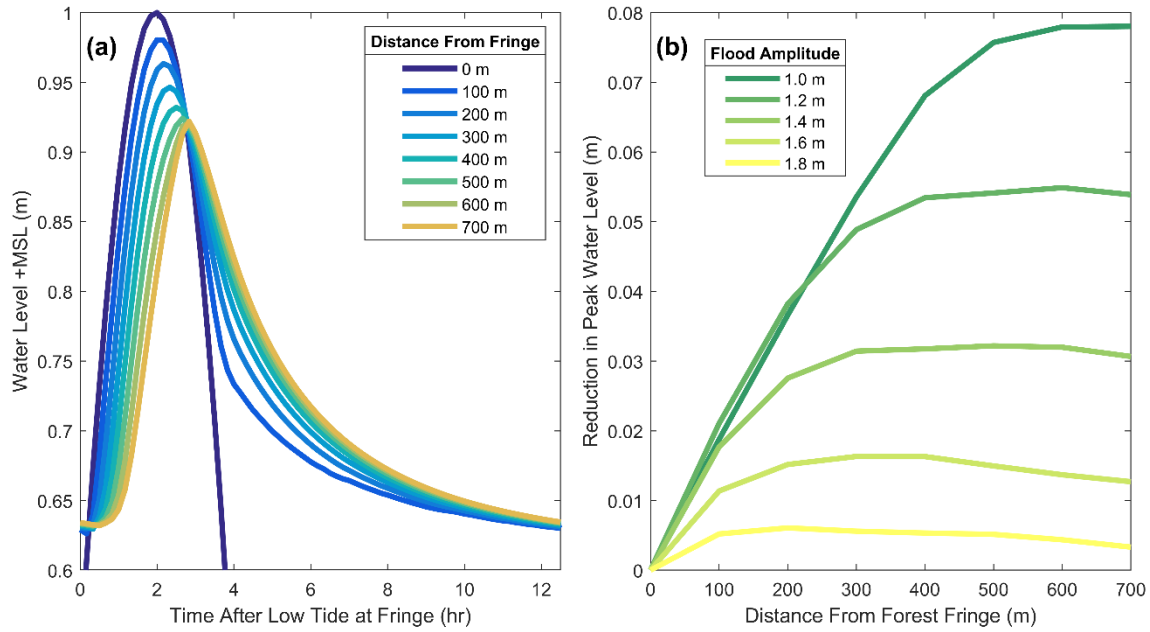

Figure 4-13: (a) Time series of water elevations for unchannelized mangrove forest forced with a +1 +MSL M2 tide.at 100 m distance intervals into the vegetation. (b) Water level attenuation with distance into an unchannelized mangrove forest with varying amplitude M2 period forcing.

With bathymetry modified to remove channels, a series of varying amplitude (1 m, 1.2 m, 1.4 m, 1.6 m and 1.8 m +MSL) M2 period waves were modelled, to test whether peak water depth plays a role in controlling attenuation. The forcing amplitudes were selected to represent a tide with storm surge, the maximum storm surge that has ever been detected in Tauranga Harbour is 0.7 m. Figure 4-13b displays peak water level with distance into the mangrove forest for each of the amplitude waves investigated. With increased amplitude signal, less attenuation and temporal delay of the wave occurred. The Pahoia mangrove area is surrounded by relatively steep topography on the landward boundaries resulting in little increase in water surface area with increasing water depth. Therefore, during a large amplitude flood event, the increase in water entering the forest is approximately linearly proportional to water depth.

We created a series of sloped bathymetry idealized models, to test the role of forest water storage capacity on attenuation. The numerical models are similar to the unchannelized model above (utilize the same computational grid, vegetation density, solution time step , etc.) ; however, the vegetated area slopes from 0.6 m +MSL at the forest fringe to 0.9 m, 0.8 m, and 0.7 m +MSL at the landward side of the ~1 km wide mangrove forest (corresponding to bottom slopes of 1:10000, 1:5000, and 1:3333). The models were forced with a 1 m amplitude M2 tide at the open boundary. Figure 4-14 displays peak water level with distance into the forest for each of the forest slopes. A clear trend is evident in that steeper bottom slopes result in less flood dissipation. Forests with greater bottom slopes have less water storage and therefore less water flows through the vegetation resulting in the

flow impeding effect of vegetation having a diminished effect. Although the greater forest slope results in shallower water through the forest and therefore less hydraulic conductivity, this effect is less significant than the reduction in water transported through the vegetation due to the smaller tidal prism.

The trend of increasing flood attenuation with flatter bathymetry is not maintained for the no slope model (black solid line in Figure 4-14). This deviation from the trend is attributed to the finite length of the forest. In the model, a no flow boundary condition exists at the back of the forest. With a flat bathymetry, landward water storage was limited by the boundary condition not the forest slope. However, the influence of greater water depths in the seaward portion of the forest, relative to sloped bathymetry scenarios, persisted. Therefore, the reduced peak water level attenuation present in the no slope bathymetry is attributed to lack of tidal prism landward of the back of the forest relative to the other scenarios displayed in Figure 4-14. Note that for all bottom slopes the rate of water attenuation is non-linear with maximum attenuation occurring at the forest fringe and no attenuation in the landward portion of the forest.

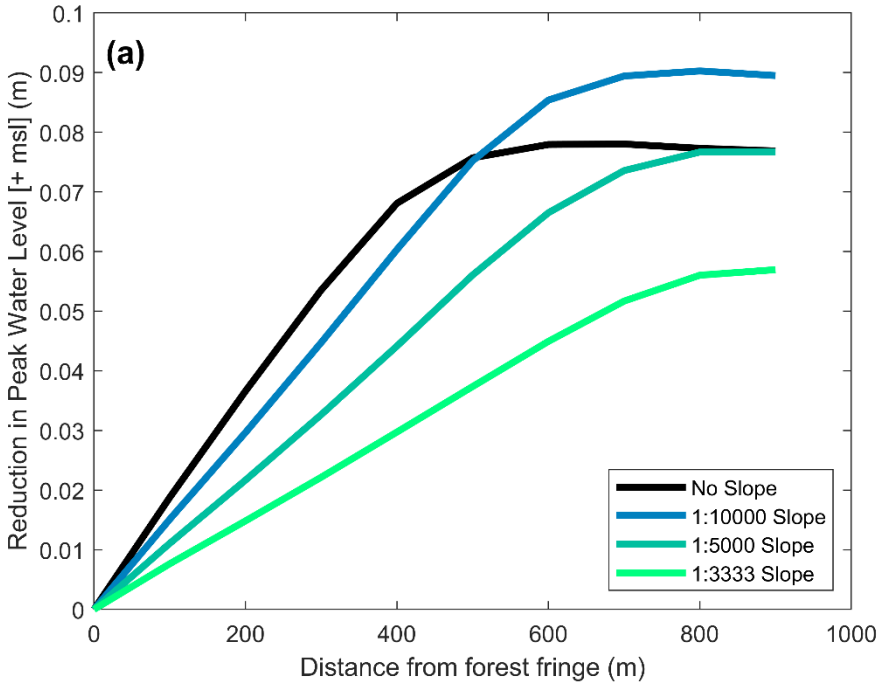

Figure 4-14: Peak water level attenuation with distance into an unchannelized mangrove forest with varying bottom slope for 1 m M2 period forcing.

4.6 Discussion

Mangroves have been shown to provide coastal flood protection by impeding the landward flow of water and acting as a water storage mechanism (*Montgomery et al.*, 2019). Our modelling study shows that large scale flow routing due to channelization of the mangrove forest is more important to flow dynamics than vegetation density. In heterogeneously vegetated river environments, flow has been shown to be deflected away from vegetation patches, showing that large patch-scale vegetation geometry is more important to flow resistance than vegetation density (*Nepf*, 2012). Similarly, here we found

that channels influence water flow resistance more than vegetation density. A delay in the inundation wave and reduction in peak water levels occurred in the unchannelized environment in which all landward flow of water was transported through the vegetation. Increasing vegetation density four-fold with channels present did not result in peak water level attenuation nor temporal delay in the flood wave. However, a large reduction in velocities in the forest occurred with the increased vegetation density indicating that if the channel network was insufficient to transport water landward, vegetation properties may ultimately become important to flood attenuation rates. If channel widths were insufficient to provide efficient landward water transport, an intermediate condition may exist with increased flow through the forest and some reduction of peak water level relative to a forest with wider and/or deeper channels.

The diffusion coefficient (Eq. 4-3) relates sea surface gradient to the temporal rate of change of water depth. A large diffusion coefficient represents greater water flux for a given sea surface gradient. For both channels and emergent vegetation, the diffusion coefficient is related to water depth (Eq. 4-4 & Eq. 4-5). Increased depth results in more rapid transfer of water for a fixed sea surface gradient and/or lesser surface gradients required to convey an amount of fluid. In flow through emergent vegetation, the diffusion coefficient is linearly related to water depth. The linear relationship between diffusion coefficient and water depth in vegetated flows is due to the additional depth over which water is conveyed. Therefore, if depth is doubled, flow velocity is halved to maintain similar water flux. For flow in unvegetated areas with resistance parameterized by bottom friction, the diffusion coefficient increases with depth more rapidly than for vegetated flows and is proportional to water depth to the 1.5 power (Eq. 4-5). The relationship between diffusion coefficient and water depth for unvegetated flows occurs both because of the increased water depth over which flow occurs and the non-linear velocity profile associated with bottom friction. Transport efficiency in channels increases more rapidly with depth than flow through vegetation resulting in channels dominating flow conveyance per unit width irrespective of water depth. In a basin with steep topography landward of the mangrove forest as in Pahoia, increased magnitude inundation results in increased fluid conveyance and reduced water level attenuation (as shown in Figure 4-13b). However, many mangrove forests are in regions with little topographic gradient (the Gulf of Mexico in the United States for example). In low gradient regions, increases in flood amplitude largely increase water surface area and results in increased water flux through the forest. The capacity of a mangrove forest to reduce peak flood levels is likely a balance between improved hydraulic efficiency due to greater water depths and the capacity to restrict the increased flow due to greater landward fluid storage. Stop-banking behind the forest will limit storage capacity. Additional research is needed to fully describe the importance of complex topography on mangrove flood attenuation rates.

The importance of vegetation distribution to flow resistance in tidally dominated mangrove forests is due to both the lack of flow impeding elements in channels and the elevation difference between the mangrove forested areas and channels. Mangrove channels are formed by the scour of daily tidal flows. Vegetation drag reduces velocities in the forest and concentrates flow, enhancing channelization and channel scour. Additionally, mangroves decrease bed erodibility, increase production of organic matter, and reduce in forest flow

velocities promoting sedimentation and accretion (*van Maanen et al.*, 2015). Due to daily tidal flows scouring channels, an unusually large flood event would be needed to force a large volume of water into (and landward of) the mangrove forest for the vegetation to provide effective coastal flood protection.

The extent of channelization in mangrove forests is highly variable. Mazda et al. (1995) notes that the ratio of forest area to creek area varies from ~3 to ~45 for the nine mangrove creeks analysed in that work. Here, the ratio of forest area to creek is ~7.5. Although velocities and water flux per unit width are much greater in channels than the forest, the relatively large surface area of some forests can make water flux through vegetation a non-negligible influence on landward water flow.

Existing models investigating the interaction of coastal flooding and mangrove forests has been done at regional scales parameterizing mangrove flow resistance using a bottom friction parameterization, Manning's coefficient (*Xu et al.*, 2010; *Zhang et al.*, 2012). Appropriately calibrated bottom friction parameterization may accurately capture the flow resistance properties of a complex mangrove forest within the limits of the calibrated conditions. However, the bottom friction parameterization is unlikely to accurately capture the flow/vegetation interaction beyond the calibrated condition. Here we have gone to some lengths to correctly characterise the drag associated with complex tree structures, which our modelling has clearly showed is unnecessary. Instead effort should be made to characterise the geometry of conveyancing channels. Nevertheless, our results show vegetation becomes increasingly important in larger amplitude events, when the flood protective benefits of mangrove forests are likely to be underestimated with bottom-friction parameterization of vegetation flow resistance. Moreover, our method can be applied to cases where little channelization exists, and the frictional effect of vegetation dominates (for example, the Firth of Thames, Aotearoa New Zealand, Montgomery et al., 2019). Applying a frontal area vegetation drag parameterization uniformly across a mangrove forest with complex creek/channel features is problematic and likely to overestimate the protective benefit of mangroves in extreme floods. Computational grid resolution that accurately captures channelization often requires a discretization that may be computationally problematic at regional scales. We are not suggesting a simple solution to accurately capture mangrove flow interaction in complex environments, care must be used when applying simplifications to modelling complex environments especially when extrapolating results beyond calibrated limits.

A number of studies have focused on the interaction of salt marsh and storm surge. In a review article, Shepard et al. (2011) summarized that marshes provide some coastal flood protection by absorbing water and forcing sheet flow towards the coast. Similar to much existing work on flood protection of mangrove forests, the protective benefit of marshes is often quoted as a rate of dissipation per length of marsh, ranging from 0.27-1.12 m/km (*Batker et al.*, 2010). Loder et al. (2009) examined the importance of marsh continuity (channelization), marsh elevation, and variations in friction on storm surge attenuation in an idealized numerical model parameterizing flow resistance with increased bottom roughness (increased manning's coefficient). The research concluded that marshes can have a

protective effect on coastal flooding, particularly for small to moderate surge levels. Additionally, decreased continuity (increased channelization) was found to result in less flood protection. Observations of varying amplitude inundation events in a large tidal marsh revealed maximum attenuation occurring at water levels that flooded the vegetation with 0.5-1.0 m of water (*Stark et al.*, 2015). The marsh provided less flood protection to larger flood events. Many similarities exist between the flood protection provided by mangroves and salt marshes. However, the parameterization of marsh flow resistance with bottom friction may be more appropriate than for taller vegetation such as mangroves that are often emergent even at extreme flood levels. Extrapolating models calibrated at low/moderate water levels to extreme events may accurately capture the flow resistance of marshes but under predict the protective benefits of mangroves.

4.7 Conclusions

Mangroves have been shown to be effective coastal flood protection provided vegetation reduces the landward flow of water. Flow through mangroves and in shallow channels is reasonably approximated as a balance between friction and pressure gradient and can be expressed as a diffusion equation. Here, we have shown that incised channels through mangrove forests are an efficient mechanism to transport water landward both because of the greater water depth and lack of flow impediments. The result is less flood attenuation compared to a forest lacking channels.

Sea surface gradients drive flow along channels and into vegetation. Greater water depths increase the efficiency of water conveyance and result in smaller sea surface gradients between channels and the adjacent forest. Increases in vegetation density provide additional flow concentration in channels and a decrease in flow rates through the forest. However, for the site studied an increase in vegetation density of four-fold resulted in no peak water level reduction across the forest, causing even more flow to route through channels. Elimination of channels forces all flow through mangroves and results in more rapid peak water level attenuation compared to channelized forests. Vegetation density and flow restriction are only important provided water flux through the forest is an important water transport mechanism. Increased water levels increase the water conveyance capacity of the area. However, large amplitude floods may be attenuated effectively by mangrove forests if the topography of the environment results in increased water flux through the forest that exceed the transport capacity of the forest/channels.

Our study highlights the importance of understanding the local characteristics of sites before generalising on the role of mangrove in surge attenuation. As sea-levels rise, more low-lying coastal land will become inundated. The overall storage will change, combined with the vegetation characteristics, depending on whether the intertidal has space to migrate inland, or is ‘squeezed’ by landward modifications.

5 General Conclusions

The interaction of storm surge and mangrove forests was explored using a simplified analytic solution, observations of water level in contrasting (channelized and unchannelized) forests, and with numerical experiments based on a simplified two-dimensional model of a forest in Tauranga New Zealand. The methods of investigation all indicate that mangroves can be effective coastal flood protection if the vegetation is distributed to impede the landward flow of water. Flood attenuation rates have previously been shown to vary dramatically between mangrove forests/events (*Krauss et al.*, 2009; *McIvor et al.*, 2012; *Xu et al.*, 2010; *Zhang et al.*, 2012). Here we have demonstrated that mangrove coastal flood protection depends on characteristics of the flood, properties of the mangroves, and bathymetry/topography of the region. Each method of investigating the interaction of storm surge and mangroves provides insight into the coastal protection provided by the forests but also has limitations. The analytic solution enables a convenient mechanism to assess the importance of some mangrove properties and surge characteristics on flood protection but is only strictly appropriate for very simple environments. Observations allow for the validation of the other techniques as well as comparison between events and locations. However, limited observations are available due to difficulty in obtaining data during flood events which are inherently unpredictable. Additionally, it is difficult to isolate mechanisms that are responsible for variations in flood attenuation rates due to confounding variables between observed locations/flood events. A computational model offers the possibility to perform numerical experiments to explore the interaction of storm surge and mangrove forests. However, the output of a numerical model is dependent on the method in which forces are parameterized and on a large array of modelling decisions. As a model is perturbed from a calibrated condition, uncertainty in the output increases.

The analytic solution demonstrated that mangroves can be effective coastal flood protection if the forest is sufficiently wide/dense to restrict the landward flow of water by providing both flow resistance and water storage. The assumptions used in generating the one-dimensional solution included no flow through the landward boundary of the forest; therefore, all flow into the mangroves occurred because of water entering and remaining within the vegetated area. Water level dissipation was shown to be highly non-linear with most of the flood reduction occurring in the seaward portion of the forest (Figure 2-3c). However, if low elevation areas exist landward of the forest, a relatively narrow mangrove may provide flood protection due to vegetation restricting the increase in landward flow. Conversely, if local bathymetry does not have any low elevation areas landward of the vegetation, the mangroves only resist flow that enters the forest and are likely to provide less protection than in a scenario with flood prone areas landward of the forest. However, if no low elevation flood prone areas exist landward of mangroves, the protective benefit of the forest is irrelevant.

Observations of the unchannelized mangroves in the Firth of Thames demonstrated that vegetation could reduce inundation water levels. However, the comparison of water level attenuation in the channelized forest portrayed the importance of water conveyance on flood reduction. The channels in Pahoia, Tauranga provide an efficient flow path and prevent the

vegetation from limiting water exchange through the forest and therefore do not attenuate the flood. The existence of channels in the Pahoia forest is due to the flow of daily tides. A typical spring tide results in a water level of ~0.6m throughout the Pahoia forest (Figure 3-3b). Conversely, a spring tide in the Firth of Thames does not enter the forest and therefore no channel network exists to facilitate the flow of water into/out of the forest (Figure 3-3a). If channel networks are maintained by the daily flow of tides, an unusually large flood event is required for water to enter regions without a channel network and allow for the vegetation to reduce water conveyance and reduce peak water level. Therefore, forests may only limit the landward flow of water when the channel network is insufficient to convey water and therefore only provide flood protection during extreme events. Although channels reduce flood protection provided by mangroves, flow through channels efficiently delivers sediment to forests promoting accretion within mangroves. Breda et al. (2021) have suggested that channelized forests may be better able to keep pace with sea level rise than vegetation without channels.

The 2-dimensional model allowed for numerical experiments to be performed to identify the relative importance of various mangrove/bathymetry properties. Although it is unlikely that any "real world" scenario would exactly match one of the numerical experiments, systematically varying individual properties of the model can inform on the importance of the modified property. As demonstrated in both the analytic solution (an increase in depth increased the decay length scale, Eq. *(2-3)*) and the numerical model with varying forcing amplitudes (Figure 4-13b), increased flood levels allow for increased water conveyance and a reduction in mangrove flood protection. The greater the water depth in the forest, the less flow resistance exerted by the vegetation and consequently less flood protection. The numerical model experiment with sloped bathymetry resulted in less peak water level reduction with increased bottom slope. The reduction in attenuation is attributed to both a decrease in water storage (and therefore less flow through mangroves) and a reduction in water depth with distance into the forest.

Mangroves are most effective flood protection when the threat of flooding is most severe. Attenuation rates during extreme events are influenced by flooding areas that are not frequently inundated (increasing flow through mangroves) and do not have sufficient channels (often created by daily tidal scour) to transport water. Conversely, extreme events increase water depths in vegetated areas inundated during typical tidal cycles resulting in greater hydraulic conductivity. As flood attenuation rates are affected by these competing principles the rate at which attenuation occurs is impacted by the relative change between increased landward water transport and improved hydraulic conductivity with depth. Low slope topography results in a rapid increase in flood threatened areas with increases in depth compared to the improvement in hydraulic efficiency with depth. Therefore, mangroves provide increased coastal protection when low elevation environments are threatened, and the flood hazard is greatest.

Properties of the vegetation, flood, and bathymetry influence the flow impeding effect of vegetation and therefore effect the flood reduction across the forest. As demonstrated by the analytic solution, peak water level attenuation is highly non-linear in even the most

simplified interaction between mangroves and storm surge. Flood protection provided by mangroves is complex and constant attenuation rates, as previously suggested (*Krauss et al.*, 2009; *McIvor et al.*, 2012; *Xu et al.*, 2010; *Zhang et al.*, 2012) fail to capture the intricacies of the interaction. Similarly, Stark et al. (2015) found that flood attenuation in a tidal marsh were complex and highly nonlinear with high variability in flood attenuation rates depending on event depth and location within the marsh. The rate of flood attenuation in a mangrove forest is unique to a storm event and local environment; each scenario must be evaluated individually to assess the importance of the vegetation on coastal protection.

Mangroves provide a wide array of coastal protection services including reducing currents, stabilizing sediments, diminishing high winds, attenuating wind waves, reducing tsunamis, and lessening storm surge. As demonstrated here, the benefit of mangroves on coastal flood reduction is complex and is dependent on vegetation, storm characteristics, and morphology and no simple method is currently available to quantify the flood attenuation rate in mangroves. However, independent of quantifiable flood reduction in mangroves, the importance of a buffer between humans and the ocean is of critical importance both as protection from the sea and as productive habitat. Barrier islands, salt marshes, mangrove forests and other environments that occupy the land/sea interface are uniquely threatened both by direct human destruction/development/exploitation and climate change. In their natural state these fringe environments have a demonstrated capacity to adapt and maintain their place on the edge of the ocean as a buffer between land and sea. Human interaction interferes with these natural mechanisms that allow coastal environments to adapt. With increasing knowledge of the importance of natural coastlines, hopefully additional measures can be taken to protect these unique environments.

5.1 Limitations of this work and suggestions for further research

This thesis addressed the interaction of mangrove forests and storm surge by focusing on water level attenuation and the interaction of long waves and vegetation. The analysis presented here has focused solely on the interaction of tides/surges and mangroves. Tides and surges are frictionally dominated and reasonably described as a diffusive process. Other long waves, i.e. Tsunamis, have a sufficiently shorter period (order of minutes) relative to tides and surges that the relevant coastal processes cannot be described as diffusive and the analysis presented here is inappropriate. Unlike marshes, mangroves are generally emergent, and rigid. In the presented analysis, mangroves have been assumed to be emergent during flood events and drag coefficient independent of flow velocity (within a turbulent regime). If mangroves are fully submerged, the flow impeding influence of the vegetation is likely to be substantially reduced and flood attenuation lessened.

Mangroves interact with flooding in many aspects that are not fully understood and suggest further research. The protective benefit of mangroves with respect to the effect of wind on water levels and storm damage has not been fully explored. Das et al. (2013) devised a model to quantify the protection mangroves provide with respect to direct wind damage on infrastructure and calibrated the model with data from a cyclone in Odisha Indian during a 1999 cyclone. Wind setup can have a large influence on water levels, particularly in wide shallow basins (*Dean and Dalrymple*, 1991). Mangroves may have a substantive impact on

reducing wind shear stress on the water surface and therefore reduce surge levels when winds are onshore (and most damaging). The capacity of mangroves to reduce winds and therefore surge levels may be an additional protective mechanism provided by the vegetation.

Rain is an additional water source during many surge events. Mangroves reduce the exchange of water both landward and seaward. The presence of vegetation may cause ponding landward of forests during large rain events increasing water levels and associated damage. In areas with large fluvial inputs the combination of riverine flooding and coastal storm surge interaction with mangroves could be a topic of interest. Additional research should be conducted to quantify the influence of rain on coastal flooding and the impact of mangroves on limiting land drainage.

Practical considerations have limited the collection of water level observations in mangrove forests during extreme flood events. Additional observations are always beneficial to comment directly on the impact of forests on storm surge as well as inform modelling.

Mangrove density was quantified using a Strahler ordering scheme and assuming constant distribution of vegetation with depth. Alternative methods of assessing vertical variability of mangrove vegetation may inform on plant distribution and flow interaction. Structure from motion is an interesting technique to quantify tree complexity and flow resistance. Assessing the impact of flexible and semi-rigid vegetation (particularly the leafy canopy) is a direction of research that may be of value.

Local morphology influences flood protection provided by mangroves. Land use changes within catchments can influence sediment supply and therefore alter forest morphology. The influence of sediment supply on aggradation within mangroves is a topic of interest that could better inform land management and improve prediction of forest dynamics.

Sea level rise and the projected frequency and intensity of storms are expected to increasingly threaten coastal communities. Coastal vegetation may respond to sea level rise by vertical accretion and landward migration to maintain coastal protection ecosystem services. Uncertainty in relevant processes (sea level rise, storms, availability of sediment, vegetation response …) makes prediction of the future protection provided by mangroves challenging. However, due to the wide array of ecosystem services mangroves provide, allowing sufficient space for natural coastal environments to respond to environmental changes should be a priority both to maintain ecological benefits and for the protection mangroves provide to human infrastructure.

6 References

Airoldi, L., M. Abbiati, M. W. Beck, S. J. Hawkins, P. R. Jonsson, D. Martin, P. S. Moschella, A. Sundelöf, R. C. Thompson, and P. Åberg (2005), An ecological perspective on the deployment and design of low-crested and other hard coastal defence structures, *Coastal Engineering*, *52*(10-11), 1073-1087, doi:10.1016/j.coastaleng2005.09.007.

Alongi, D. M. (2008), Mangrove forests: resilience, protection from tsunamis, and responses to global climate change, *Estuarine, Coastal and Shelf Science*, *76*(1), 1-13, doi:10.1016/j.ecss.2007.08.024.

Alongi, D. M. (2009), *The Energetics of Mangrove Forests*, Springer Science & Business Media.

Arkema, K. K., G. Guannel, G. Verutes, S. A. Wood, A. Guerry, M. Ruckelshaus, P. Kareiva, M. Lacayo, and J. M. Silver (2013), Coastal habitats shield people and property from sea-level rise and storms, *Nature Climate Change*, *3*(10), 913-918, doi:10.1038/NCLIMTE1944.

Armanini, A., M. Righetti, and P. Grisenti (2005), Direct measurement of vegetation resistance in prototype scale, *Journal of Hydraulic Research*, *43*(5), 481-487, doi:10.1080/00221680509500146.

Aucan, J., and P. V. Ridd (2000), Tidal asymmetry in creeks surrounded by saltflats and mangroves with small swamp slopes, *Wetlands Ecology and Management*, *8*(4), 223-232, doi:10.1023/A:1008459814925.

Baptist, M. J., V. Babovic, J. Rodríguez Uthurburu, M. Keijzer, R. E. Uittenbogaard, A. Mynett, and A. Verwey (2007), On inducing equations for vegetation resistance, *Journal of Hydraulic Research*, *45*(4), 435-450, doi:10.1080/00221686.2007.9521778.

Batker, D., I. De La Torre, R. Costanza, P. Swedeen, J. Day, R. Boumans, and K. Bagstad (2010), Gaining ground: wetlands, hurricanes, and the economy: the value of restoring the Mississippi River Delta, *Envtl. L. Rep. News & Analysis*, *40*, 11106.

Bedient, P. B., and W. C. Huber (1992), *Hydrology and Floodplain Analysis*, 2nd ed., Addison-Wesley, Reading, MA.

Bell, R., D. Goring, and W. de Lange (2000), Sea-level change and storm surges in the context of climate change, *Transactions of the Institution of Professional Engineers New Zealand: General Section*, *27*(1), 1.

Bell, R., D. Goring, R. Gorman, M. Hicks, H. Hurran, and D. Ramsay (2006), Impacts of climate change on the coastal margins of the Bay of Plenty, *NIWA Client Report HAM2006–031, prepared for Environment Bay of Plenty*.

Breda, A., P. M. Saco, S. G. Sandi, N. Saintilan, G. Riccardi, and J. F. Rodríguez (2021), Accretion, retreat and transgression of coastal wetlands experiencing sea-level rise, *Hydrology and Earth System Sciences*, *25*(2), 769-786.

Bryan, K. R., W. Nardin, J. C. Mullarney, and S. Fagherazzi (2017), The role of cross-shore tidal dynamics in controlling intertidal sediment exchange in mangroves in Cù Lao Dung, Vietnam, *Continental Shelf Research*, *147*, 128-143, doi:10.1016/j.csr.2017.06.014.

Chen, R., and R. R. Twilley (1998), A gap dynamic model of mangrove forest development along gradients of soil salinity and nutrient resources, *Journal of Ecology*, *86*(1), 37-51, doi:10.1046/j.1365-2745.1998.00233.x.

Cheng, N.-S. (2013), Calculation of drag coefficient for arrays of emergent circular cylinders with pseudofluid model, *Journal of Hydraulic Engineering*, *139*(6), 602-611, doi:10.1061/(ASCE)HY.1943-7900.0000722.

Costanza, R., O. Pérez-Maqueo, M. L. Martinez, P. Sutton, S. J. Anderson, and K. Mulder (2008), The value of coastal wetlands for hurricane protection, *AMBIO: A Journal of the Human Environment*, *37*(4), 241-248, doi:10.1579/0044-7447(2008)37[241:TVOCWF]2.0.CO;2.

Das, S., and A.-S. Crépin (2013), Mangroves can provide protection against wind damage during storms, *Estuarine, Coastal and Shelf Science*, *134*, 98-107, doi:10.1016/j.ecss.2013.09.021.

Das, S., and J. R. Vincent (2009), Mangroves protected villages and reduced death toll during Indian super cyclone, *Proceedings of the National Academy of Sciences*, *106*(18), 7357-7360, doi:10.1073/pnas.0810440106.

de Lange, W. P., and J. G. Gibb (2000), Seasonal, interannual, and decadal variability of storm surges at Tauranga, New Zealand, *New Zealand Journal of Marine and Freshwater Research*, *34*(3), 419-434, doi:10.1080/00288330.2000.9516945.

de Langre, E. (2008), Effects of wind on plants, *Annu. Rev. Fluid Mech.*, *40*, 141-168, doi:10.1146/annurev.fluid.40.111406.102135.

de Ruiter, P. J., J. C. Mullarney, K. R. Bryan, and C. Winter (2017), The influence of entrance constriction on hydrodynamics and intertidal morphology within estuarine basins, paper presented at Coasts & Ports, Cairns.

Dean, R. G., and R. A. Dalrymple (1991), *Water Wave Mechanics for Engineers and Scientists*, World Scientific.

Dronkers, J. J. (2005), *Dynamics of Coastal Systems*, 519 pp., World Scientific Publishing Company, Hackensack

Duke, N. C., J.-O. Meynecke, S. Dittmann, A. M. Ellison, K. Anger, U. Berger, S. Cannicci, K. Diele, K. C. Ewel, and C. D. Field (2007), A world without mangroves?, *Science*, *317*(5834), 41-42.

Emanuel, K. (2005), Increasing destructiveness of tropical cyclones over the past 30 years, *Nature*, *436*(7051), 686-688, doi:10.1038/nature03906.

FAO (2007), The world's mangroves, 1980-2005, *Fao Forestry PaperFood and Agriculture Organization of the United Nations, Rome.*

Folkard, A. M. (2011), Vegetated flows in their environmental context: a review, *Proceedings of the Institution of Civil Engineers-Engineering and Computational Mechanics*, *164*(1), 3-24, doi:10.1680/eacm.8.00006.

Friedrichs, C. T., and D. G. Aubrey (1988), Nonlinear Tidal Distortion in Shallow Well-mixed Estuaries: a Synthesis, *Estuarine, Coastal and Shelf Science*, *27*, 521-545.

Friedrichs, C. T., and O. S. Madsen (1992), Nonlinear Diffusion of the Tidal Signal in Frictionally Dominated Embayments, *Journal of Geophysical Research*, *97*, 5637-5650, doi:10.1029/92jc00354.

Gioia, G., and F. Bombardelli (2001), Scaling and similarity in rough channel flows, *Physical Review Letters*, *88*(1), 014501, doi:10.1103/PhysRevLett.88.014501.

Giri, C., E. Ochieng, L. L. Tieszen, Z. Zhu, A. Singh, T. Loveland, J. Masek, and N. Duke (2011), Status and distribution of mangrove forests of the world using earth observation satellite data, *Global Ecology and Biogeography*, *20*(1), 154-159, doi:10.1111/j.1466-8238.2010.00584.x.

Green, J. C. (2005a), Comparison of blockage factors in modelling the resistance of channels containing submerged macrophytes, *River Research and Applications*, *21*(6), 671-686, doi:10.1002/rra.854.

Green, J. C. (2005b), Modelling flow resistance in vegetated streams: review and development of new theory, *Hydrological Processes: An International Journal*, *19*(6), 1245-1259, doi:10.1002/hyp.5564.

Guannel, G., P. Ruggiero, J. Faries, K. Arkema, M. Pinsky, G. Gelfenbaum, A. Guerry, and C.-K. Kim (2015), Integrated modeling framework to quantify the coastal protection services supplied by vegetation, *Journal of Geophysical Research: Oceans*, *120*(1), 324-345, doi:10.1002/2014jc009821.

Haughey, R. R. (2017), Modelling the hydrodynamics within the mangrove tidal flats in the Firth fo Thames, University of Waikato, Hamilton, New Zealand.

Healy, T. R., R. Cole, and W. de Lange (1996), Geomorphology and Ecology of New Zealand Shallow Estuaries and Shorelines, *Estuarine Shores. New York: John Wiley and Sons*.

Heath, R. (1985), A review of the physical oceanography of the seas around New Zealand—1982, *New Zealand Journal of Marine and Freshwater Research*, *19*(1), 79-124, doi:10.1080/00288330.1985.9516077.

Henderson, S. M., B. K. Norris, J. C. Mullarney, and K. R. Bryan (2017), Wave-frequency flows within a near-bed vegetation canopy, *Continental Shelf Research*, *147*, 91-101, doi:10.1016/j.csr.2017.06.003.

Horstman, E. M., K. R. Bryan, and J. C. Mullarney (2021), Drag variations, tidal asymmetry and tidal range changes in a mangrove creek system, *Earth Surface Processes and Landforms*, doi:10.1002/esp.5124.

Horstman, E. M., K. R. Bryan, J. C. Mullarney, C. A. Pilditch, and C. A. Eager (2018a), Are flow-vegetation interactions well represented by mimics? A case study of mangrove pneumatophores, *Advances in Water Resources*, *111*, 360-371, doi:10.1016/j.advwatres.2017.11.018.

Horstman, E. M., C. M. Dohmen-Janssen, T. J. Bouma, and S. J. M. H. Hulscher (2015), Tidal-scale flow routing and sedimentation in mangrove forests: Combining field data and numerical modelling, *Geomorphology*, *228*, 244-262, doi:10.1016/j.geomorph.2014.08.011.

Horstman, E. M., C. M. Dohmen-Janssen, and S. J. M. H. Hulscher (2013), Modeling tidal dynamics on a mangrove creek catchment in Delft3D, in *Coastal Dynamics*, edited by P. Bonneton and T. Garlan, pp. 833-844, EPOC, Arcachon, France.

Horstman, E. M., C. J. Lundquist, K. R. Bryan, R. H. Bulmer, J. C. Mullarney, and D. J. Stokes (2018b), The Dynamics of Expanding Mangroves in New Zealand, in *Threats to Mangrove Forests*, edited, pp. 23-51, Springer, doi:10.1007/978-3-319-73016-5_2.

House Document (1965), United States Army Corps of Engineers, Morgan City and vicintiy, Louisiana: letter from the Secretary of the Army. , edited by A. C. o. Engineers, United States Congress Serial Set, 1965-1966, Washington.

Jalonen, J., and J. Järvelä (2014), Estimation of drag forces caused by natural woody vegetation of different scales, *Journal of Hydrodynamics, Ser. B*, *26*(4), 608-623, doi:10.1016/S1001-6058(14)60068-8.

James, C., A. Birkhead, A. Jordanova, and J. O'sullivan (2004), Flow resistance of emergent vegetation, *Journal of Hydraulic Research*, *42*(4), 390-398.

Järvelä, J. (2004), Determination of flow resistance caused by non-submerged woody vegetation, *International Journal of River Basin Management*, *2*(1), 61-70.

Klaassen, G., and J. Van der Zwaard (1974), Roughness coefficients of vegetated flood plains, *Journal of Hydraulic Research*, *12*(1), 43-63, doi:10.1080/00221687409499757.

Krauss, K. W., T. W. Doyle, T. J. Doyle, C. M. Swarzenski, A. S. From, R. H. Day, and W. H. Conner (2009), Water level observations in mangrove swamps during two hurricanes in Florida, *Wetlands*, *29*(1), 142-149, doi:10.1672/07-232.1.

Kroeker, K. J., B. G. Reguero, P. Rittelmeyer, and M. W. Beckd (2016), 4| Ecosystem Service and Coastal Engineering Tools for Coastal Protection and Risk Reduction, *Managing Coasts with Natural Solutions*, 75.

Lanzoni, S., and G. Seminara (1998), On tide propagation in convergent estuaries, *Journal of Geophysical Research: Oceans*, *103*(C13), 30793-30812, doi:10.1029/1998jc900015.

LeBlond, P. H. (1978), On tidal propagation in shallow rivers, *Journal of Geophysical Research*, *83*(C9), 4717, doi:10.1029/JC083iC09p04717.

Loder, N., J. L. Irish, M. Cialone, and T. Wamsley (2009), Sensitivity of hurricane surge to morphological parameters of coastal wetlands, *Estuarine, Coastal and Shelf Science*, *84*(4), 625-636, doi:10.1016/j.ecss.2009.07.036.

Lovelock, C., I. Feller, K. McKee, B. Engelbrecht, and M. Ball (2004), The effect of nutrient enrichment on growth, photosynthesis and hydraulic conductance of dwarf mangroves in Panama, *Functional Ecology*, *18*(1), 25-33, doi:10.1046/j.0269-8463.2004.00805.x.

Lovelock, C., B. Sorrell, N. Hancock, Q. Hua, and A. Swales (2010), Mangrove Forest and Soil Development on a Rapidly Accreting Shore in New Zealand, *Ecosystems*, *13*(3), 437-451, doi:10.1007/s10021-010-9329-2.

Luhar, M., J. Rominger, and H. Nepf (2008), Interaction between flow, transport and vegetation spatial structure, *Environmental Fluid Mechanics*, *8*(5-6), 423, doi:10.1007/s10652-008-9080-9.

Massel, S., K. Furukawa, and R. Brinkman (1999), Surface wave propagation in mangrove forests, *Fluid Dynamics Research*, *24*(4), 219-249, doi:10.1016/S0169-5983(98)00024-0.

Mazda, Y., N. Kanazawa, and E. Wolanski (1995), Tidal asymmetry in mangrove creeks, *Hydrobiologia*, *295*(1-3), 51-58, doi:10.1007/bf00029110.

Mazda, Y., D. Kobashi, and S. Okada (2005), Tidal-scale hydrodynamics within mangrove swamps, *Wetlands Ecology and Management*, *13*(6), 647-655, doi:10.1007/s11273-005-0613-4.

Mazda, Y., E. Wolanski, B. King, A. Sase, D. Ohtsuka, and M. Magi (1997), Drag force due to vegetation in mangrove swamps, *Mangroves and Salt Marshes*, *1*(3), 193-199, doi:10.1023/A:1009949411068.

McIvor, A., T. Spencer, I. Möller, and M. Spalding (2012), Storm surge reduction by mangroves *Rep.*, The Nature Conservancy and Wetlands International, Cambridge, UK.

McIvor, A., T. Spencer, I. Möller, and M. Spalding (2016), 2| Coastal Defense Services Provided by Mangroves, *Managing Coasts with Natural Solutions*, 24.

McLeod, E., G. L. Chmura, S. Bouillon, R. Salm, M. Björk, C. M. Duarte, C. E. Lovelock, W. H. Schlesinger, and B. R. Silliman (2011), A blueprint for blue carbon: toward an improved understanding of the role of vegetated coastal habitats in sequestering CO2, *Frontiers in Ecology and the Environment*, *9*(10), 552-560, doi:10.1890/110004.

McMahon, T. A. (1975), The mechanical design of trees, *Scientific American*, *233*(1), 92-103.

McMahon, T. A., and R. E. Kronauer (1976), Tree structures: deducing the principle of mechanical design, *Journal of Theoretical Biology*, *59*(2), 443-466, doi:10.1016/0022-5193(76)90182-X.

Montgomery, J., K. Bryan, J. Mullarney, and E. Horstman (2019), Attenuation of Storm Surges by Coastal Mangroves, *Geophysical Research Letters*, doi:10.1029/2018GL081636.

Montgomery, J., K. R. Bryan, E. M. Horstman, and J. C. Mullarney (2018), Attenuation of Tides and Surges by Mangroves: Contrasting Case Studies from New Zealand, *Water*, *10*(9), 1119, doi:10.3390/w10091119.

Mullarney, J. C., and S. M. Henderson (2018), Flows Within Marine Vegetaion Canopies in *Advances in Coastal Hydraulics*, edited by V. Panchange and J. Kaihatu, pp. 1-46, World Scientific Publishing Ltd, doi:10.1142/9789813231283_0001.

Mullarney, J. C., S. M. Henderson, J. H. Reyns, B. K. Norris, and K. R. Bryan (2017), Spatially varying drag within a wave-exposed mangrove forest and on the adjacent tidal flat, *Continental Shelf Research*, *147*, 102-113, doi:10.1016/j.csr.2017.06.019.

Needham, H. F., B. D. Keim, and D. Sathiaraj (2015), A review of tropical cyclone-generated storm surges: Global data sources, observations, and impacts, *Reviews of Geophysics*, *53(2)*, 545-591, doi:10.1002/2014RG000477.

Nepf, H. (1999), Drag, turbulence, and diffusion in flow through emergent vegetation, *Water Resources Research*, *35*(2), 479-489, doi:10.1029/1998WR900069.

Nepf, H. (2004), Vegetated flow dynamics, *The Ecogeomorphology of Tidal Marshes*, 137-163, doi:10.1029/59CE09.

Nepf, H. (2012), Hydrodynamics of vegetated channels, *Journal of Hydraulic Research*, *50*(3), 262-279, doi:10.1080/00221686.2012.696559.

Nicholls, R. J., and A. Cazenave (2010), Sea-level rise and its impact on coastal zones, *Science*, *328*(5985), 1517-1520, doi:10.1126/science.1185782.

Nikora, V., S. Larned, N. Nikora, K. Debnath, G. Cooper, and M. Reid (2008), Hydraulic resistance due to aquatic vegetation in small streams: field study, *Journal of Hydraulic Engineering*, *134*(9), 1326-1332, doi:10.1061/(ASCE)0733-9429(2008)134:9(1326).

Norberg, R. A. (1988), Theory of growth geometry of plants and self-thinning of plant populations: geometric similarity, elastic similarity, and different growth modes of plant parts, *The American Naturalist*, *131*(2), 220-256, doi:10.1086/284787.

Norris, B. K., J. C. Mullarney, K. R. Bryan, and S. M. Henderson (2017), The effect of pneumatophore density on turbulence: A field study in a Sonneratia-dominated mangrove forest, Vietnam, *Continental Shelf Research*, *147*, 114-127, doi:10.1016/j.csr.2017.06.002.

Park, S. G. (2004), *Aspects of mangrove distribution and abundance in Tauranga Harbour*, Environment Bay of Plenty.

Parker, B. B. (1984), Frictional Effects on the Tidal Dynamics of a Shallow Estuary, 292 pp, Johns Hopkins Univ., Balitmore, MD.

Paulik, R., S. A. Stephens, R. G. Bell, S. Wadhwa, and B. Popovich (2020), National-Scale Built-Environment Exposure to 100-year Extreme Sea Levels and Sea-Level Rise, *Sustainability*, *12*(4), 1513, doi:10.3390/su12041513.

Peters, R., A. G. Vovides, S. Luna, U. Grüters, and U. Berger (2014), Changes in allometric relations of mangrove trees due to resource availability–A new mechanistic modelling approach, *Ecological Modelling*, *283*, 53-61, doi:10.1016/j.ecolmodel.2014.04.001.

Plant, N. G., and G. B. Griggs (1992), Interactions between nearshore processes and beach morphology near a seawall, *Journal of Coastal Research*, 183-200.

Pool, D. J., S. C. Snedaker, and A. E. Lugo (1977), Structure of mangrove forests in Florida, Puerto Rico, Mexico, and Costa Rica, *Biotropica*, 195-212, doi:10.2307/2387881.

Rodríguez, J. F., P. M. Saco, S. Sandi, N. Saintilan, and G. Riccardi (2017), Potential increase in coastal wetland vulnerability to sea-level rise suggested by considering hydrodynamic attenuation effects, *Nature Communications*, *8*, 16094, doi:10.1038/ncomms16094.

Shepard, C. C., C. M. Crain, and M. W. Beck (2011), The protective role of coastal marshes: a systematic review and meta-analysis, *Plos One*, *6*(11), e27374, doi:10.1371/journal.pone.0027374.

Small, C., and R. J. Nicholls (2003), A global analysis of human settlement in coastal zones, *Journal of Coastal Research*, 584-599.

Stark, J., T. Oyen, P. Meire, and S. Temmerman (2015), Observations of tidal and storm surge attenuation in a large tidal marsh, *Limnology and Oceanography*, *60*(4), 1371-1381, doi:10.1002/lno.10104.

Strahler, A. N. (1957), Quantitative analysis of watershed geomorphology, *Eos, Transactions American Geophysical Union*, *38*(6), 913-920, doi:10.1029/TR038i006p00913.

Swales, A., S. J. Bentley, C. Lovelock, and R. G. Bell (2007), Sediment processes and mangrove-habitat expansion on a rapidly-prograding muddy coast, New Zealand, in *Coastal Sediments' 07*, edited, pp. 1441-1454, doi:10.1061/40926(239)111.

Swales, A., S. J. Bentley, and C. E. Lovelock (2015), Mangrove-forest evolution in a sediment-rich estuarine system: opportunists or agents of geomorphic change?, *Earth Surface Processes and Landforms*, *40*(12), 1672-1687, doi:10.1002/esp.3759.

Tay, H. W., K. R. Bryan, W. P. de Lange, and C. A. Pilditch (2013), The hydrodynamics of the southern basin of Tauranga Harbour, *New Zealand Journal of Marine and Freshwater Research*, *47*(2), 249-274, doi:10.1080/00288330.2013.778300.

Temmerman, S., P. Meire, T. J. Bouma, P. Herman, T. Ysebaert, and H. J. De Vriend (2013), Ecosystem-based coastal defence in the face of global change, *Nature*, *504*(7478), 79, doi:10.1038/nature12859.

van Maanen, B., G. Coco, and K. R. Bryan (2015), On the ecogeomorphological feedbacks that control tidal channel network evolution in a sandy mangrove setting, *Proc Math Phys Eng Sci*, *471*(2180), 20150115, doi:10.1098/rspa.2015.0115.

Västilä, K., and J. Järvelä (2014), Modeling the flow resistance of woody vegetation using physically based properties of the foliage and stem, *Water Resources Research*, *50*(1), 229-245, doi:10.1002/2013WR013819.

Wahl, T., I. Haigh, R. Nicholls, A. Arns, S. Dangendorf, J. Hinkel, and A. Slangen (2017), Understanding extreme sea levels for broad-scale coastal impact and adaptation analysis, *Nature Communications*, *8*, 16075, doi:10.1038/ncomms16075.

Williamson, C. (1992), The natural and forced formation of spot-like 'vortex dislocations' in the transition of a wake, *Journal of Fluid Mechanics*, *243*, 393-441, doi:10.1017/S0022112092002763.

Wilson, C., J. Hoyt, and I. Schnauder (2008), Impact of foliage on the drag force of vegetation in aquatic flows, *Journal of Hydraulic Engineering*, *134*(7), 885-891.

Woodruff, J. D., J. L. Irish, and S. J. Camargo (2013), Coastal flooding by tropical cyclones and sea-level rise, *Nature*, *504*(7478), 44, doi:10.1038/nature12855.

Xu, H., K. Zhang, J. Shen, and Y. Li (2010), Storm surge simulation along the US East and Gulf Coasts using a multi-scale numerical model approach, *Ocean Dynamics*, *60*(6), 1597-1619, doi:10.1007/s10236-010-0321-3.

Zhang, K., H. Liu, Y. Li, H. Xu, J. Shen, J. Rhome, and T. J. Smith (2012), The role of mangroves in attenuating storm surges, *Estuarine, Coastal and Shelf Science*, *102-103*, 11-23, doi:10.1016/j.ecss.2012.02.021.